

# Two-Phase Heat Transfer Mechanisms within Plate Heat Exchangers: Experiments, Modeling and Simulations

THÈSE N° 6856 (2016)

PRÉSENTÉE LE 8 JANVIER 2016

À LA FACULTÉ DES SCIENCES ET TECHNIQUES DE L'INGÉNIEUR  
LABORATOIRE DE TRANSFERT DE CHALEUR ET DE MASSE  
PROGRAMME DOCTORAL EN ENERGIE

ÉCOLE POLYTECHNIQUE FÉDÉRALE DE LAUSANNE

POUR L'OBTENTION DU GRADE DE DOCTEUR ÈS SCIENCES

PAR

**Raffaele Luca AMALFI**

acceptée sur proposition du jury:

Prof. S. Haussener, présidente du jury  
Prof. J. R. Thome, directeur de thèse  
Prof. J. M. Corberan, rapporteur  
Dr R. Christensen, rapporteur  
Prof. J. A. Schiffmann, rapporteur



ÉCOLE POLYTECHNIQUE  
FÉDÉRALE DE LAUSANNE

Suisse  
2015



*Dedicata ai miei genitori Antonio e Lucia*





## Acknowledgements

The present project has been carried out at Laboratory of Heat and Mass Transfer (LTCM) at École Polytechnique Fédérale de Lausanne (EPFL) under the supervision of Prof. John R. Thome. The financial support has been provided by U.S. Office of Naval Research & Technology through Award Number N000141210398.

I would first like to express my gratitude to my unique supervisor Prof. John R. Thome for providing the opportunity to achieve the PhD degree at his prestigious laboratory. I am grateful to him for his constructive advice, guidance and confidence from the beginning till the end of this research study.

I would like to thank Dr. Farzad Vakili-Farahani for his willingness to share knowledge and insight during my first year of PhD. Thanks to Dr. Ricardo Lima, Dr. Chin Lee Ong and Dr. Nicolas Lamaison for the constructive discussions and collaborations. My sincere thanks go to Dr. Giulia Spinato and Houxue Huang for being a trustworthy friends, precious colleagues and for all the unforgettable moments spent together during the whole PhD.

I would like to thank the members of my committee, Prof. J.M. Corberan (University of Valencia), Dr. R. Christensen (Alfa Laval), Prof. S. Haussener (École Polytechnique Fédérale de Lausanne) and Prof. Schiffmann (École Polytechnique Fédérale de Lausanne), for their valuable efforts evaluating my thesis and their constructive remarks that improved the quality of the present manuscript.

I would also like to thank Dr. Navid Borhani (First Assistant of the LTCM), Chiara Falsetti, Filippo Cataldo and Albert Beisel for the great time spent together, generating a friendly scientific and social environment at LTCM.

I would like to thank the entire staff of the ATME workshop for the technical support on the test facility. I would also like to thank Cécile Taverney and Nathalie Matthey-De-l'Endroit for taking care of the administrative work.

Last but not the least, I would like to thank my parents: Antonio Amalfi and Lucia Elefante for their endurance, encouragement and smiles during all these years.



## Abstract

Plate heat exchangers are recently adopted in many domestic and industrial applications, such as ventilation, air conditioning, evaporation or condensation process, heat pumps and cooling of hydrodynamic circuits in engines. Plate heat exchangers provide higher heat transfer performance, compactness and flexibility, compared to the conventional tube-in-tube and shell-and-tube heat exchangers. In the present thesis an experimental work to characterize thermal and hydraulic performance of a compact plate heat exchanger has been carried out. Upward single-phase flow and flow boiling heat transfer of low pressure liquid refrigerants were investigated within a plate heat exchanger prototype fabricated with 1 mm pressing depth and chevron angle of  $65^\circ$ . High spatial and temporal resolution infrared measurements were implemented to obtain local (pixel-by-pixel) heat transfer coefficients and frictional pressure drops. The technique developed to reduce the experimental data was also discussed in detail. Single-phase experiments were carried out for Reynolds numbers ranging from 34 to 1615 and Prandtl numbers from 4.9 until 6.5, and the associated effect of the main involved parameters on the thermal and hydraulic performance was analyzed in detail. In addition, the Fanning friction factor was found to be strongly dependent on the Reynolds number, while the Nusselt number was correlated to the Reynolds and Prandtl numbers, as common in tubular flow. Single-phase local heat transfer coefficients have been evaluated and the main trends against plate length, mass flux, heat flux, fluid temperature and type of refrigerants were investigated. Several of the most quoted prediction methods available in the literature were statistically evaluated against the present heat transfer and pressure drop database and a new models were proposed to predict mean thermal and hydraulic performance of the present compact plate heat exchanger. A local heat transfer prediction method that captured 94% of the experimental data within a bandwidth of  $\pm 30\%$  was also provided. On the other hand, two-phase experiments were carried out for a mass flux ranging from  $10 \text{ kgm}^{-2}\text{s}^{-1}$  to  $85 \text{ kgm}^{-2}\text{s}^{-1}$ , imposed heat flux from  $225 \text{ Wm}^{-2}$  to  $4100 \text{ Wm}^{-2}$ , saturation temperature from  $19^\circ\text{C}$  to  $35^\circ\text{C}$  and vapor quality from 0.05 to 0.90. The heat transfer coefficient increased with mass flux, heat flux and saturation temperature (system pressure). On the other hand, the frictional pressure drop raised with mass flux and vapor quality and decreased with saturation temperature. Based on local infrared measurements, the effect of

outlet port pressure drop on the hydraulic performance was properly characterized and new correlation for predicting local frictional pressure gradient through the test section was also suggested. This model captured the entire pressure drop database within a bandwidth of  $\pm 30\%$ , providing a mean absolute error of 10% and mean error of 0.2%. Next, a wide experimental databank was culled from thirteen literature research studies, which investigated flow boiling heat transfer and two-phase frictional pressure drop within chevron plate heat exchangers. The database was first adopted to validate the predicted capabilities of 29 literature models, and then utilized to provide the new prediction methods to evaluate local heat transfer coefficients and frictional pressure gradient. These new models were developed from 1903 heat transfer and 1513 frictional pressure drop data points (3416 total) and were proved to work better over a very wide range of operating conditions, plate designs and fluids (including ammonia). The general flow boiling prediction methods have been involved in a simulation code to analyze local thermal and hydraulic performance of the plate heat exchangers in a large range of test conditions. The simulation results were then validated against independent experimental database from literature resulting in very good agreement between each other. The present simulation code represents a powerful tool to be used for practical applications by the thermal engineers in order to design and rate commercial plate heat exchangers.

Keywords: Adiabatic two-phase pressure drops, compact plate heat exchanger, general prediction methods, local heat transfer coefficient, local infrared measurements, modeling, numerical simulations.



## Sommario

Gli scambiatori di calore a piastre sono recentemente impiegati in molti settori domestici e industriali: ventilazione, sistemi di raffreddamento e riscaldamento domestici, processi di evaporazione e condensazione, pompe di calore e raffreddamento dei circuiti idrodinamici all'interno dei motori. Gli scambiatori di calore a piastre forniscono elevate prestazioni in termini di trasmissione del calore, compattezza e flessibilità rispetto ai convenzionali scambiatori di calore a tubi coassiali e tubi e mantello. La presente tesi è focalizzata nell'analisi delle prestazioni termiche e idrauliche di uno scambiatore di calore a piastre ad alto grado di compattezza. Il fenomeno di scambio termico monofase e bifase in direzione verticale ascendente, impiegando refrigeranti a bassa pressione, è stato studiato all'interno di un prototipo di scambiatore di calore a piastre. Tale sistema è stato fabbricato con 1 mm di spazio fra le due piastre contigue ed un angolo del profilo corrugato di  $65^\circ$ . Misure ad infrarossi con un'elevata risoluzione spaziale e temporale sono state adoperate allo scopo di calcolare localmente i coefficienti di scambio termico e le perdite di carico. La tecnica di riduzione dei dati sperimentali è stata anche discussa. Gli esperimenti con refrigerante in monofase sono stati effettuati variando il numero di Reynolds da 34 a 1615, il numero di Prandtl da 4.9 a 6.5 e l'influenza dei principali parametri sulle prestazioni termiche ed idrauliche è stata analizzata in dettaglio. Il fattore di attrito era funzione del numero di Reynolds, mentre il numero di Nusselt è stato correlato con il numero di Reynolds ed il numero di Prandtl, come si verifica in flusso interno ai condotti. Il coefficiente di scambio termico monofase è stato valutato e confrontato con la lunghezza della piastra, il flusso di massa, il flusso termico, la temperatura del fluido ed il tipo di refrigerante. Differenti modelli predittivi disponibili in letteratura sono stati statisticamente confrontati rispetto ai dati sperimentali in termini di scambio termico e perdite di carico e nuovi modelli per predire le prestazioni medie termiche ed idrauliche del nuovo scambiatore di calore sono stati introdotti. Un modello predittivo per il coefficiente di scambio termico locale è stato sviluppato, il quale prediceva il 94% dei dati sperimentali in un intervallo di  $\pm 30\%$ . Viceversa, gli esperimenti con fluido in passaggio di fase sono stati eseguiti variando il flusso di massa da  $10 \text{ kg m}^{-2} \text{ s}^{-1}$  a  $85 \text{ kg m}^{-2} \text{ s}^{-1}$ , il flusso termico da un minimo di  $225 \text{ W m}^{-2}$  ad un massimo di  $4100 \text{ W m}^{-2}$ , la temperatura di saturazione da  $19^\circ\text{C}$  a  $35^\circ\text{C}$  and il titolo da 0.05 a 0.95. Il coefficiente di

scambio termico bifase cresceva col flusso di massa, flusso termico e temperatura di saturazione (pressione del sistema). Viceversa le perdite di carico aumentavano con il flusso di massa e titolo, mentre diminuivano con la temperatura di saturazione. Con le misure ad infrarossi locali, l'effetto della perdita di pressione in uscita è stata ricavata in relazione alle prestazioni idrauliche del sistema ed un nuovo modello per predire la perdita di pressione locale lungo lo scambiatore di calore è stato anche sviluppato. Tale modello prediceva l'intero set di dati sperimentali in un range di  $\pm 30\%$ , con un errore medio assoluto di 10% ed un errore medio dello 0.2%. In aggiunta, un ampio set di dati sperimentali è stato collezionato da tredici studi presenti in letteratura che investigarono scambio termico e perdite di carico durante il processo di evaporazione. Tali dati sperimentali sono stati prima validati, confrontandoli con 29 modelli predittivi della letteratura, e dopo utilizzati per lo sviluppo di modelli predittivi dei coefficienti di scambio termico locali e delle perdite di carico locali. Tali modelli sono stati ricavati considerando 1903 dati sperimentali termici e 1513 dati sperimentali idraulici (in totale 3416), presentando migliori caratteristiche predittive, rispetto alle correlazioni esistenti in letteratura, su di un ampio campo di condizioni sperimentali, geometria delle piastre e fluidi di lavoro (incluso ammoniaca). I modelli predittivi generali per lo scambio termico locale e le perdite di carico locali in flusso bifase, sono stati introdotti in un codice simulativo per analizzare le prestazioni termiche ed idrauliche degli scambiatori di calore a piastre. I risultati simulativi sono stati validati rispetto a dati sperimentali ottenuti in altri centri di ricerca, risultando in ottimo accordo. Il presente codice simulativo rappresenta un importante supporto per ingegneri termici al fine di curare la progettazione e l'analisi di scambiatori di calore a piastre commerciali.

Parole chiave: Perdite di carico bifase in assenza di flusso termico, scambiatore di calore a piastre compatto, modelli predittivi generali, coefficienti di scambio termico locali, misure ad infrarossi locali, modellazione, simulazioni numeriche.





# Contents

<b>Acknowledgements .....</b>	<b>i</b>
<b>Abstract.....</b>	<b>iii</b>
<b>Sommario.....</b>	<b>vi</b>
<b>List of Figures.....</b>	<b>xiii</b>
<b>List of Tables .....</b>	<b>xix</b>
<b>Nomenclature .....</b>	<b>xxi</b>
 <b>CHAPTER 1 – Introduction .....</b>	 <b>1</b>
1.1 Overview of plate heat exchangers .....	1
1.2 Geometry specification .....	2
1.3 Objectives of the thesis .....	4
1.4 Thesis structure .....	6
 <b>CHAPTER 2 – Literature survey.....</b>	 <b>7</b>
2.1 Introduction.....	7
2.2 Review of experimental single-phase studies .....	7
2.3 Flow boiling heat transfer and two-phase pressure drop .....	11
2.4 Review of experimental flow boiling studies .....	14
2.5 Flow visualization and flow regimes .....	22
2.6 Conclusions.....	25
 <b>CHAPTER 3 – Experimental apparatus .....</b>	 <b>28</b>
3.1 Introduction.....	28
3.2 Test facility .....	28
3.3 Prototype plate heat exchanger .....	31
3.4 Experimental procedure .....	33
3.5 Uncertainty analysis.....	35
3.6 Data reduction technique .....	37

## Contents

---

3.7 Conclusions.....	40
<b>CHAPTER 4 – Single phase results .....</b>	<b>41</b>
4.1 Introduction.....	41
4.2 Infrared temperature measurements.....	41
4.3 Pressure drops .....	43
4.4 Energy Balance .....	45
4.5 Mean heat transfer coefficient .....	48
4.6 Local heat transfer coefficient .....	49
4.7 Conclusions.....	52
<b>CHAPTER 5 – Single phase prediction methods .....</b>	<b>54</b>
5.1 Introduction.....	54
5.2 Frictional pressure drop .....	54
5.3 Mean heat transfer coefficient .....	56
5.4 Local heat transfer coefficient .....	58
5.5 Conclusions.....	60
<b>CHAPTER 6 – Two phase results .....</b>	<b>61</b>
6.1 Introduction.....	61
6.2 Frictional pressure drop .....	61
6.3 Evaluation of local saturation pressure .....	62
6.4 Evaluation of outlet restriction pressure drop .....	68
6.5 Heat transfer coefficient.....	70
6.6 Conclusions.....	74
<b>CHAPTER 7 – Two phase prediction methods .....</b>	<b>75</b>
7.1 Introduction.....	75
7.2 Collection of experimental database .....	75
7.3 Dimensional analysis and new general pressure drop model .....	82
7.4 Dimensional analysis and new general heat transfer model .....	86
7.5 Comparison of general prediction methods to data .....	89
7.6 Conclusions.....	92

<b>CHAPTER 8 – Heat exchanger simulation code .....</b>	<b>93</b>
8.1 Introduction.....	93
8.2 Overview of the simulation code .....	93
8.3 Structure of the simulation code .....	94
8.4 Validation of the simulation code .....	100
8.5 Simulation results.....	102
8.6 Sensitivity analysis.....	113
8.7 Conclusions.....	115
 <b>CHAPTER 9 – Conclusions .....</b>	 <b>117</b>
9.1 Introduction.....	117
9.2 Main objectives and findings of the present study.....	117
9.3 Recommendations for future work .....	120
 <b>Bibliography .....</b>	 <b>121</b>
<b>Publications .....</b>	<b>129</b>
<b>Curriculum vitae.....</b>	<b>131</b>



## List of Figures

1.1: Brazed plate heat exchanger (courtesy Alfa Laval).....	2
1.2: Corrugation features of chevron plates: (a) geometrical description of sinusoidal pattern, (b) cross section of sinusoidal pattern with $\beta = 0^\circ$ and $\beta = 90^\circ$ , (c) different plate arrangements .....	4
2.1: Gas-liquid flow patterns observed by Tribbe and Müller-Steinhagen (2001c) within a plate heat exchanger: (a) regular bubbly flow, (b) irregular bubbly flow, (c) churn flow, (d) film flow, (e) partial film flow .....	23
3.1: Photograph of the front view of the experimental test facility .....	28
3.2: Photograph of the back view of the experimental test facility .....	29
3.3: Schematic of the flow loop .....	29
3.4: Drawing of the chevron plate prototype and the related geometrical parameters .....	31
3.5: Plate heat exchanger prototype: (a) chevron test plate before assembling, (b) after applying laser welded technique, (c) test section with inlet and outlet pipes .....	32
3.6: Photograph of the compact plate heat exchanger: (a) front view of the test section enclosed in a PVC support with the inlet and outlet pipes to be connected to the main loop, (b) back view of the evaporator with the two visible clamps before closing the supporting frame .....	33
4.1: Calibration applied to one pixel (row 240 and column 270) located in the third “window” counted from the bottom of the test section .....	42
4.2: Infrared camera measurements referred to one pixel (row 240 and column 270): (a) local and average pixel temperature, (b) standard deviation of the temperature .....	43
4.3: Single-phase pressure drop results: (a) effect of mass flux and type of refrigerant on the frictional pressure drop, (b) dimensionless pressure drop contributors against Reynolds number .....	44
4.4: Experimental Fanning friction factor versus Reynolds number for both tested fluids .....	45
4.5: Energy balance in the test section and the corresponding results: (a) heat loss due to the Joule effect, (b) heat loss due to the natural convection, (c) heat loss due to the radiation, (d) thermal efficiency of the plate heat exchanger against the effective power .....	46
4.6: Single-phase energy balance in the preheater and the associated results: (a) heat loss due to the natural convection, (b) heat loss due to the radiation .....	48

## List of Figures

---

4.7: Single-phase heat transfer results: (a) Nusselt number versus Reynolds number for the current fluids, (b) Nusselt number versus Reynolds number for two different Prandtl numbers .....	49
4.8: Local heat transfer results: (a) heat transfer coefficient map in laminar flow regime for the condition in which $G = 35 \text{ kgm}^{-2}\text{s}^{-1}$ , $Re = 160$ , $q = 350 \text{ Wm}^{-2}$ and R245fa, (b) heat transfer coefficient map in turbulent flow regime for the condition in which $G = 384 \text{ kgm}^{-2}\text{s}^{-1}$ , $Re = 1613$ , $q = 3500 \text{ Wm}^{-2}$ and R245fa, (c) and (d) the associated average lengthwise heat transfer coefficient versus the length of the plate at the same operating test conditions.....	50
4.9: Effect of the main experimental parameters on the quasi-local heat transfer coefficient: (a) effect of mass flux for $T_{in} = 24 \text{ }^{\circ}\text{C}$ , $q = 600 \text{ Wm}^{-2}$ and R245fa, (b) effect of heat flux for $T_{in} = 24 \text{ }^{\circ}\text{C}$ , $G = 30 \text{ kgm}^{-2}\text{s}^{-1}$ and R245a (c) effect of fluid temperature $G = 50 \text{ kgm}^{-2}\text{s}^{-1}$ , $q = 295 \text{ Wm}^{-2}$ and R236fa, (d) effect of type of refrigerant for $T_{in} = 24 \text{ }^{\circ}\text{C}$ , $G = 50 \text{ kgm}^{-2}\text{s}^{-1}$ and $q = 420 \text{ Wm}^{-2}$ .....	52
5.1: Single-phase experimental Fanning friction factor predicted by different prediction methods: (a) Focke et al. (1985), (b) Hayes et al. (2012a), (c) Martin (1996a), (d) proposed model.....	55
5.2: Single-phase experimental Nusselt number predicted by several prediction methods: (a) Jokar et al. (2006b), (b) Kovalenko-Maslov (1970), (c) Muley et al. (1999b), (d) proposed model.....	57
5.3: Local single-phase experimental Nusselt number predicted by different prediction methods: (a) Clark (1974), (b) Kakac et al. (1987), (c) Muley et al. (1999b), (d) proposed model.....	59
6.1: Adiabatic two-phase frictional pressure drop versus local vapor quality: (a) effect of mass flux at $T_{sat} = 30.5 \text{ }^{\circ}\text{C}$ and R245fa, (b) effect of saturation temperature at $G = 35 \text{ kgm}^{-2}\text{s}^{-1}$ and R245fa .....	61
6.2: Adiabatic two-phase pressure drop results for $G = 75 \text{ kgm}^{-2}\text{s}^{-1}$ , $T_{sat} = 30.5 \text{ }^{\circ}\text{C}$ , $x = 0.12$ and R245fa: (a) temperature measured by infrared camera, (b) corresponding absolute pressure map .....	62
6.3: Adiabatic two-phase pressure drop results for $G = 75 \text{ kgm}^{-2}\text{s}^{-1}$ , $T_{sat} = 30.5 \text{ }^{\circ}\text{C}$ , $x = 0.12$ and R245fa: (a) quasi-local temperature versus plate length, (b) quasi-local absolute pressure versus plate length.....	63
6.4: Two-phase experimental frictional pressure drop obtained by infrared measurements, predicted by four prediction methods: (a) Lee et al. (2014b), (b) Nilpueng and Wongwises (2010c), (c) Taboas et al. (2010d), (d) proposed model .....	64
6.5: Dimensionless local static, momentum and frictional pressure drop in which: (a) $G = 25 \text{ kgm}^{-2}\text{s}^{-1}$ , $T_{sat} = 30.5 \text{ }^{\circ}\text{C}$ , $q = 4000 \text{ Wm}^{-2}$ , $x_{out} = 0.33$ and R245fa, (b) $G = 85 \text{ kgm}^{-2}\text{s}^{-1}$ , $T_{sat} = 30.5 \text{ }^{\circ}\text{C}$ , $q = 4100 \text{ Wm}^{-2}$ , $x_{out} = 0.10$ and R245fa.....	66

6.6: Local fluid pressure and temperature predicted adopting linear scheme, Khan et al. (2014a, 2012c, 2012d) (prorated), Huang et al. (2012b) (prorated) and proposed model: (a) pressure profile, (b) temperature profile both for $G = 25 \text{ kgm}^{-2}\text{s}^{-1}$ , $T_{\text{sat}} = 30.5 \text{ }^{\circ}\text{C}$ , $q = 4000 \text{ Wm}^{-2}$ , $x_{\text{out}} = 0.33$ and R245fa, (c) pressure profile, (d) temperature profile both for $G = 85 \text{ kgm}^{-2}\text{s}^{-1}$ , $T_{\text{sat}} = 30.5 \text{ }^{\circ}\text{C}$ , $q = 4060 \text{ Wm}^{-2}$ , $x_{\text{out}} = 0.10$ and R245fa .....	67
6.7: Different pressure drop contributors against local vapor quality for $G = 25 \text{ kgm}^{-2}\text{s}^{-1}$ , $T_{\text{sat}} = 30.5 \text{ }^{\circ}\text{C}$ , $x = 0.33$ and R245fa: (a) frictional and outlet singularity measured by infrared camera, (b) static and pipe pressure drops .....	68
6.8: Effect of mass flux on the outlet singularity pressure drop in which $T_{\text{sat}} = 30.5 \text{ }^{\circ}\text{C}$ and R245fa.....	69
6.9: Predicted versus experimental outlet singularity pressure drop adopting the proposed prediction method .....	70
6.10: Local flow boiling heat transfer results for: (a) $\Delta T_{\text{in,sub}} < 1 \text{ }^{\circ}\text{C}$ , $G = 25 \text{ kgm}^{-2}\text{s}^{-1}$ , $T_{\text{sat}} = 30.5 \text{ }^{\circ}\text{C}$ , $q = 1000 \text{ Wm}^{-2}$ , $x_{\text{out}} = 0.05$ , (b) $\Delta T_{\text{in,sub}} < 1 \text{ }^{\circ}\text{C}$ , $G = 25 \text{ kgm}^{-2}\text{s}^{-1}$ , $T_{\text{sat}} = 30.5 \text{ }^{\circ}\text{C}$ , $q = 1750 \text{ Wm}^{-2}$ , $x_{\text{out}} = 0.33$ , (c) $\Delta T_{\text{in,sub}} < 1 \text{ }^{\circ}\text{C}$ , $G = 45 \text{ kgm}^{-2}\text{s}^{-1}$ , $T_{\text{sat}} = 30.5 \text{ }^{\circ}\text{C}$ , $q = 1750 \text{ Wm}^{-2}$ , $x_{\text{out}} = 0.08$ , (d) $x_{\text{in}} = 0.25$ , $G = 25 \text{ kgm}^{-2}\text{s}^{-1}$ , $T_{\text{sat}} = 30.5 \text{ }^{\circ}\text{C}$ , $q = 1750 \text{ Wm}^{-2}$ , $x_{\text{out}} = 0.45$ .....	71
6.11: Quasi-local flow boiling heat transfer coefficient versus local vapor quality: (a) effect of mass flux at $T_{\text{sat}} = 30 \text{ }^{\circ}\text{C}$ , $q = 3900 \text{ Wm}^{-2}$ and R245fa, (b) effect of heat flux at $T_{\text{sat}} = 30 \text{ }^{\circ}\text{C}$ , $G = 25 \text{ kgm}^{-2}\text{s}^{-1}$ and R245fa .....	73
6.12: Quasi-local flow boiling heat transfer coefficient versus local vapor quality: effect of saturation temperature at $G = 25 \text{ kgm}^{-2}\text{s}^{-1}$ , $q = 3090 \text{ Wm}^{-2}$ and R245fa .....	73
7.1: Distribution of data points related to: (a) chevron angle, (b) wavelength of surface corrugation, (c) hydraulic diameter, (d) working fluid, (e) saturation temperature, (f) mass flux .....	77
7.2: Flow boiling predicted Nusselt number against experimental Nusselt number using the correlations proposed by: (a) Danilova et al. (1981), Han et al. (2003b), (c) Huang et al. (2012b), (d) Donowski and Kandlikar (2000b), (e) and (f) Hsieh and Lin (2003c, 2002b) ....	80
7.3: Flow boiling predicted frictional pressure gradient against experimental pressure gradient using the correlations proposed by: (a) Ayub (2003a), (b) Huang et al. (2012b), (c) Khan et al. (2014a, 2012c, 2012d), (d) Taboas et al. (2012g), Han et al. (2003b) and Hsieh and Lin (2003c) .....	81
7.4: Prediction method for two-phase frictional pressure drops within plate heat exchangers: predicted against experimental frictional pressure gradient. ....	85
7.5: Flow boiling prediction methods for heat transfer within plate heat exchangers: predicted against experimental Nusselt number .....	89
7.6: Experimental frictional pressure drops versus vapor quality predicted by Khan et al. (2014a, 2012c, 2012d), and new method in case of: (a) Huang et al. data (2012b), (b) Khan et al. data (2014a, 2012c, 2012d), (c) Hsieh and Lin data (2003c), (d) Yan and Lin (1999c) .....	90

## List of Figures

---

7.7: Experimental heat transfer coefficients versus vapor quality predicted by Danilova et al. (1981) and new methods in case of: (a) Vakili-Farahani et al. data (2014c, 2014d), (b) Khan et al. data (2014a, 2012c, 2012d), (c) Hsieh et al. (2002a), (d) Han et al. data (2003b) .....	91
8.1: Schematic of the plate heat exchanger simulation code and the related flow chart in case of parallel- and counter-flow arrangement, in which the subscripts $w$ and $r$ are referred to water and refrigerant streams .....	95
8.2: Local plate heat exchanger calculation and the associated flowchart for: (a) single-phase liquid or vapor flow of refrigerant side and single-phase liquid flow of water side, (b) evaporation or condensation of refrigerant side and single-phase liquid flow of water side ..	96
8.3: Validation of the single-phase water-to-water heat transfer coefficient prediction method: prediction and experimental data have been provided by Yan and Lin (1999c) and the Nusselt number were plotted against the Reynolds number .....	101
8.4: Validation of the present simulation code using the flow boiling databases provided by Yan and Lin (1999c): (a) local heat transfer coefficient versus local vapor quality, (b) local frictional pressure drop against local vapor quality. ....	101
8.5: Numerical simulation of a parallel-flow plate heat exchanger and local results plotted against the plate heat exchanger length: (a) fluid temperatures, (b) fluid pressures, (c) interface (wall) temperature, (d) wall thermal conductivity, (e) vapor qualities, (f) heat transfer coefficients .....	104
8.6: Numerical simulation of a parallel-flow plate heat exchanger and local results plotted against the plate heat exchanger length: (a) thermal power, (b) heat flux, (c) convergence of the thermal power, (d) systematic error of the thermal power, (e) overall heat transfer coefficient, (f) normalized thermal resistances .....	106
8.7: Numerical simulation of a parallel-flow plate heat exchanger and local results plotted against the plate heat exchanger length: (a) Reynolds numbers, (b) static pressure drops, (c) momentum pressure drops, (d) frictional pressure drops, (e) normalized pressure drops for water side, (f) normalized pressure drops for refrigerant side .....	108
8.8: Numerical simulation of a counter-flow plate heat exchanger and local results plotted against the plate heat exchanger length: (a) fluid temperatures, (b) fluid pressures, (c) interface (wall) temperature, (d) wall thermal conductivity, (e) vapor qualities, (f) heat transfer coefficients .....	109
8.9: Numerical simulation of a counter-flow plate heat exchanger and local results plotted against the plate heat exchanger length: (a) thermal power, (b) heat flux, (c) convergence of the thermal power, (d) systematic error of the thermal power, (e) overall heat transfer coefficient, (f) normalized thermal resistances .....	110
8.10: Numerical simulation of a counter-flow plate heat exchanger and local results plotted against the plate heat exchanger length: (a) Reynolds numbers, (b) static pressure drops, (c) momentum pressure drops, (d) frictional pressure drops, (e) normalized pressure drops for water side, (f) normalized pressure drops for refrigerant side .....	111



8.11: Numerical simulation of a counter-flow plate heat exchanger: (a) iterate inlet temperature of the water side versus the number of iterations, (b) systematic error of the inlet temperature against the number of iterations .....	112
8.12: Sensitivity analysis on the effect of the chevron angle on the local thermal and hydraulic performance plotted against the plate heat exchanger length: (a) thermal power, (b) overall heat transfer coefficient, (c) total frictional pressure drop (water plus refrigerant), (d) performance index .....	113
8.13: Sensitivity analysis on the effect of the corrugation aspect ratio on the local thermal and hydraulic performance plotted against the plate heat exchanger length: (a) thermal power, (b) overall heat transfer coefficient, (c) total frictional pressure drop (water plus refrigerant), (d) performance index .....	114



## List of Tables

3.1: Geometry of the plate prototype .....	32
3.2: Experimental single-phase operating conditions .....	34
3.3: Experimental two-phase operating conditions.....	34
3.4: Summary of the measured parameters accuracy.....	35
3.5: Estimated uncertainty of the final single-phase results .....	36
3.6: Estimated uncertainty of the final two-phase results .....	36
4.1: Key features of the infrared camera (Flir SC645) .....	42
5.1: Predicted single-phase Fanning friction factor against the frictional pressure drop database.....	54
5.2: Predicted single-phase Nusselt number against the heat transfer database .....	56
5.3: Predicted quasi-local single-phase Nusselt number against the heat transfer database....	58
6.1: Predicted two-phase frictional pressure drop against the present measured pressure drop database.....	64
7.1: Range of dimensionless numbers for flow boiling pressure drop database.....	83
7.2: Range of dimensionless numbers for macroscale flow boiling heat transfer database ....	88
7.3: Range of dimensionless numbers for microscale flow boiling heat transfer database .....	88
8.1: Simulation conditions for parallel- and counter-flow thermal and hydraulic analysis...	102



# Nomenclature

## Roman symbols

a	amplitude of sinusoidal surface corrugation	[m]
A	surface area	[m <sup>2</sup> ]
b	pressing depth	[m]
B	fixed error	[-]
Bo	boiling number	[-]
Bd	Bond number	[-]
C	heat capacity rate	[WK <sup>-1</sup> ]
C'	leading coefficient for prediction methods	[-]
c <sub>p</sub>	specific heat at constant pressure	[Jkg <sup>-1</sup> K <sup>-1</sup> ]
d	diameter	[m]
D	random error	[-]
E	uncertainty	[-]
f	Fanning friction factor	[-]
F	enhancement factor for convective boiling	[-]
g	acceleration due to the gravity	[m <sup>2</sup> s <sup>-1</sup> ]
G	mass flux	[kgm <sup>-2</sup> s <sup>-1</sup> ]
h	heat transfer coefficient	[Wm <sup>-2</sup> K <sup>-1</sup> ]
h'	coefficient for heat transfer correlation	[Wm <sup>-2</sup> K <sup>-1</sup> ]
i <sub>lv</sub>	latent heat of vaporization	[Jkg <sup>-1</sup> ]
I	electrical current	[A]
k	thermal conductivity	[Wm <sup>-1</sup> K <sup>-1</sup> ]
KE	kinetic energy	[J]
L	length	[m]
L*	dimensionless length	[-]
m	mass flow rate	[kgs <sup>-1</sup> ]
M	molar mass	[gmol <sup>-1</sup> ]
n	number of data points	[-]
N <sub>cell</sub>	Number of cells	[-]
N <sub>pass</sub>	number of passages of the heat exchanger	[-]
Nu	Nusselt number	[-]
p	pressure	[Pa]
Pr	Prandtl number	[-]

## Nomenclature

---

Q	thermal power	[W]
q	heat flux	[Wm <sup>-2</sup> ]
R	variable for uncertainty analysis	[-]
Re	Reynolds number	[-]
S	suppression factor for nucleate boiling	[-]
t	thickness	[m]
T	temperature	[K]
u	superficial velocity	[ms <sup>-1</sup> ]
U	overall heat transfer coefficient	[Wm <sup>-2</sup> K <sup>-1</sup> ]
V	voltage	[V]
W	width	[m]
We	Weber number	[-]
x	vapor quality	[-]
X	Lockhart-Martinelli parameter	[-]
y	transverse coordinate of the plate	[m]
Y	variable for uncertainty analysis	[-]
z	axial coordinate of the plate	[m]
z <sup>*</sup>	dimensionless axial coordinate of the plate	[-]
Z	dimensionless corrugation parameter	[-]

## Greek symbols

β	chevron angle	[°]
β <sup>*</sup>	dimensionless chevron angle	[-]
γ	corrugation aspect ratio	[-]
δ	mean absolute error	[-]
δ	mean error	[-]
Δ	difference	[-]
ε	effectiveness	[-]
ζ	pressure loss coefficient	[-]
θ	standard deviation	[-]
λ	percentage predicted within ± 50%	[-]
Λ	wavelength of surface corrugation	[m]
μ	dynamic viscosity	[Pa·s]
ξ	percentage predicted within ± 20%	[-]
Π	dimensionless group	[-]
ρ	density	[kgm <sup>-3</sup> ]
ρ <sup>*</sup>	dimensionless density	[-]
γ	corrugation aspect ratio	[-]

$\sigma$	surface tension	$[\text{Nm}^{-1}]$
$\tau$	shear stress	$[\text{Nm}^{-2}]$
$\Upsilon$	percentage predicted within $\pm 30\%$	$[-]$
$\varphi$	surface enlargement factor	$[-]$
$\phi^2$	two-phase multiplier	$[-]$
$\chi$	performance index	$[\text{WPa}^{-1}]$
$\Psi$	dimensionless group	$[-]$
$\omega$	coverage factor	$[-]$

### **Subscripts**

a	ambient
c	cross section
cb	convective boiling
ch	channel
conv	convection
curr	current
cr	critical
eff	effective
eq	equivalent
f	fluid
fri	frictional
guess	guess
h	hydraulic
ht	heat transfer
id	ideal
in	inlet
input	input
IR	infrared
l	liquid
lo	liquid only
lat	latent heat
loc	local
loss	loss
m	average or homogeneous
max	maximum
min	minimum
meas	measured
mom	momentum

## Nomenclature

---

nb	nucleate boiling
out	outlet
output	output
pipe	pipe
p	port
pl	plate
preh	preheater
pro	prolonged
r	refrigerant
rad	radiation
sat	saturation
sub	subcooling
tot	total
sta	static
tp	two-phase
tt	turbulent-turbulent
v	vapor
vo	vapor only
w	water
wall	wall

## Acronyms

GUI	Graphic User Interface
IR	Infrared
NTU	Number of Transfer Units





# CHAPTER 1 – Introduction

## 1.1 Overview of plate heat exchangers

In this thesis, single- and two-phase thermal and hydraulic performances of a prototype chevron plate heat exchanger have been experimentally investigated, modelled and simulated in detail. In fact, plate heat exchangers are an important type of compact heat exchanger widely used for many applications: refrigeration, heating, cooling, chemical processing, etc. Generally, plate heat exchangers consist of thin, rectangular, pressed steel plates (most often stainless steel) that are stacked together, such that hot and cold fluid streams alternate through the inter-plate passages. The plates are stamped with corrugated patterns, providing a larger effective heat transfer surface area and additionally modify the flow field in order to promote enhanced thermal-hydraulic performance. Their most important feature is the larger heat transfer surface area per unit volume compared to shell-and-tube and tube-in-tube units and thus plate heat exchangers have increasingly become the preferred solution in many industrial and domestic applications in the small to medium size range.

Several types of plate heat exchangers are utilized, depending on the application. Mainly, there are four types of plate heat exchangers: Gasketed, brazed, welded and semi-welded and shell and plate. The brazed type shown in Figure 1.1 is that of interest here. In the present study, a new much more compact version is proposed and tested, whose corrugation depth is only 1 mm (so about 3-5 time more compact than those industrially available with corrugation depths of 3-5 mm) combined with a much thinner stainless steel plate (with a 60% materials saving). Notably, the present plates were fabricated in 2010, before the recent patent of August 2015 was issued to Christensen et al. (2015d) of Alfa Laval for small corrugation depths. Thus, as no experimental or prediction methods are suitable for the thermal/hydraulic simulation of this new compact version, the present thesis will investigate, both the single-phase liquid and two-phase evaporation heat transfer and pressure drops. These results will then be utilized to propose new prediction methods, suitable not only for the present test section but predicting a large database culled from the literature, i.e. to propose new generally applicable methods for all size ranges of corrugations for their heat transfer coefficients and pressure drops. As temperature approaches in refrigeration

evaporators are going to 1 K (or less) between the refrigerant and chilled water to obtain higher COP's and reduced energy consumption for driving their compressors, the new more compact plate heat exchanger that will be tested here is potentially a very interesting advance in technology and thus the extensive experimental and modeling study proposed here is one of the keys to enabling this process. Of particular note, a pixel-by-pixel self-calibrated IR camera will be introduced to measure local heat transfer coefficients (normally only mean values are measured for plate heat exchangers in other studies) and to deduce local two-phase pressure gradients during adiabatic tests for development of local (not mean) prediction methods.



Figure 1.1: Brazed plate heat exchanger (courtesy Alfa Laval).

## 1.2 Geometry specification

An approximately sinusoidal chevron corrugation geometry is the main pattern normally adopted to fabricate the plates for different commercial applications. The angle between the corrugation and the vertical axis is typically defined as the chevron angle,  $\beta$ , in the literature. In some publications, however, an inclination angle has been used, i.e. the angle between the furrows and the horizontal axis ( $90-\beta$ ), in place of the chevron angle. The first definition is used here for consistency with most of the literature (Figure 1.2a). Plates with different chevron angles, such as low and high chevron angles, can be stacked together in either a symmetric or mixed arrangements. In a mixed arrangement, plates of two different chevron values are employed alternately (Figure 1.2c). It should be noted that conventionally the

mixed-plate arrangement is usually designated by the average chevron angle of the two plates. The multiple metal-to-metal inter-plate contact points lend to their increased rigidity and mechanical support of the stack. A plate with a larger chevron angle provides higher thermal performance compared to that with lower corrugation angle, however, accompanied by a higher pressure drop penalty. The lateral and transversal cross sectional profiles of the channels are shown in Figure 1.2b for plates with chevron angles of  $\beta = 0^\circ$  and  $\beta = 90^\circ$ , respectively.

The severity of sinusoidal surface waviness can be essentially defined by two dimensionless parameters: the plate corrugation aspect ratio,  $\gamma$ , and the enlargement factor,  $\phi$ , defined below:

$$\gamma = \frac{4a}{\Lambda} = \frac{2b}{\Lambda} \quad (1.1)$$

$$\phi = \frac{\text{Effective area}}{\text{Projected area}} = \frac{\int_0^\Lambda \sqrt{1 + \left(\frac{\gamma\pi}{2}\right)^2 \cos^2\left(\frac{2\pi}{\Lambda}x\right)} dx}{\Lambda} \quad (1.2)$$

where  $a$  and  $\Lambda$  are the respective amplitude (depth of corrugation) and wavelength (pitch) of a sinusoidal surface corrugation. The enlargement factor can be approximated for a sinusoidal corrugation from a three-point integration formula, using the dimensionless corrugation parameter  $Z$ :

$$Z = \frac{2\pi a}{\Lambda} \quad (1.3)$$

$$\phi \approx \frac{1}{6} \left( 1 + \sqrt{1 + Z^2} + 4\sqrt{1 + Z^2/2} \right) \quad (1.4)$$

In general, both heat transfer coefficients and flow friction losses increase with increasing  $\beta$ ,  $\phi$ , and  $\gamma$ . The length scale or the equivalent diameter for the inter-plate spacing that confines the flow channel then becomes:

$$d_{eq} = 4a = 2b \quad (1.5)$$

and  $a$  is the amplitude of the corrugation, while  $b$  is the pitch between two plates ( $b = 2a$ ).

A modified length scale in the form of hydraulic diameter is defined as follow:

$$d_h = \frac{d_{eq}}{\phi} = \frac{4a}{\phi} = \frac{2b}{\phi} \quad (1.6)$$

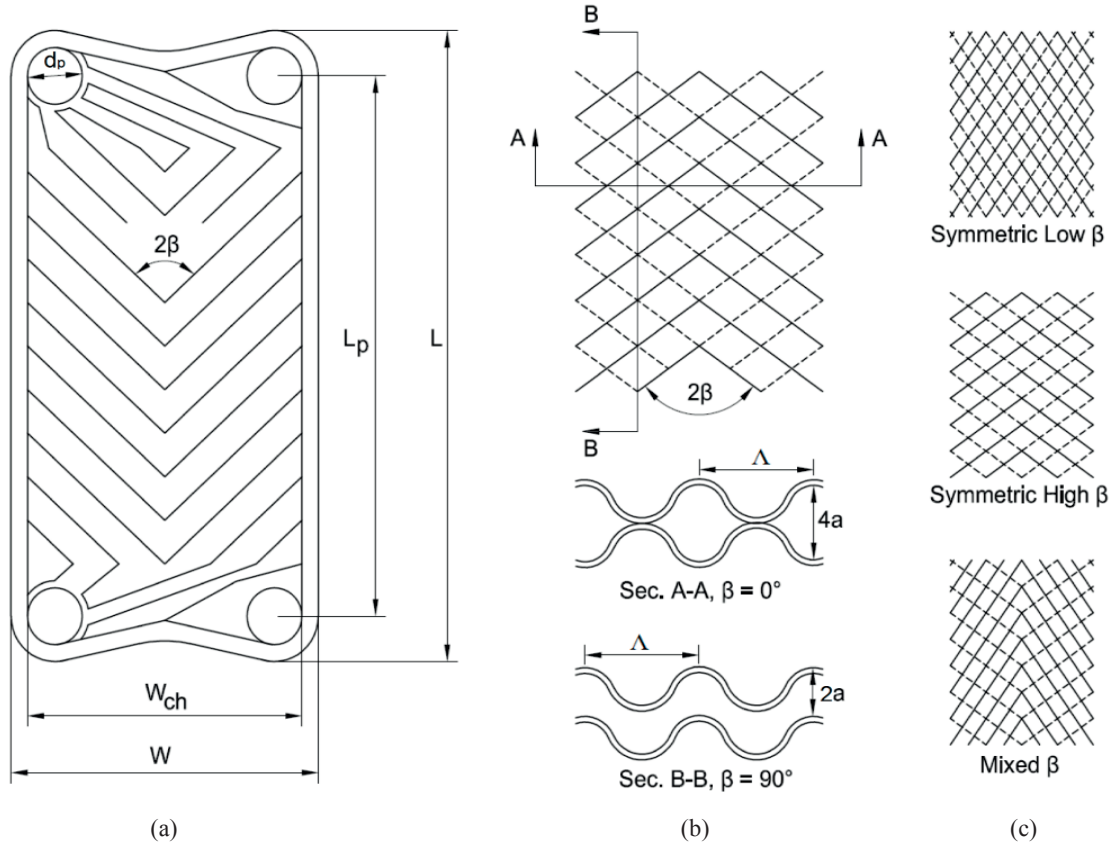


Figure 1.2: Corrugation features of chevron plates: (a) geometrical description of sinusoidal pattern, (b) cross section of sinusoidal pattern with  $\beta = 0^\circ$  and  $\beta = 90^\circ$ , (c) different plate arrangements.

### 1.3 Objectives of the thesis

In the present thesis, higher compactness and thermal performance will be gained by going to a smaller corrugation of the plates, from the conventional pressing depth of about 3 to 5 mm down to the current pressing depth of only 1 mm. The thickness of the stainless steel sheets has been reduced from a typical thickness of 0.4 mm down to 0.15 mm. As this represents a significant extrapolation of the present plate heat exchanger prediction methods, extensive experiments will undertake to determine single- and two phase pressure drops and local heat transfer coefficients for comparison to literature methods and development of new ones, especially for predicting local thermal performance.

So far, past research studies focused on single- and two- phase flow mechanisms within plate heat exchangers but provided mostly mean heat transfer data for the entire unit, rather

than local data; thus, assuming an average value of the heat transfer coefficient may be far from the reality, especially when considering the onset of dryout at high vapor qualities. In order to correctly design and optimize these systems, the overall thermal and hydraulic performance should be evaluated starting from a local calculation. These reasons emphasize the importance of the present work on the local heat transfer coefficients and pressure drops phenomena within a more compact plate heat exchanger. The main objectives of this Ph.D. thesis thus as follows:

- Provide an extensive literature survey of existing two-phase flow heat transfer and pressure drop knowledge in plate heat exchangers and extend the current understanding of two-phase flow phenomena within these heat exchangers.
- Fabricate a novel more compact corrugated plate heat exchanger, that yields higher thermal performance for its small pressing depth and wavelength of surface corrugation and large chevron angle.
- Build a new test facility able to host this new test section and automatize the data acquisition control system.
- Undertake a comprehensive experimental study of single-phase and flow boiling of low pressure liquid refrigerants, using a thermographic infrared camera to obtain high temporal and spatial resolution measurements.
- Compare and validate the present experimental heat transfer and pressure drop databases against the most quoted single- and two-phase prediction methods available in the open literature.
- Collect a wide, diversified and multi-lab database from literature and coordinate activities with Prof. Kim, who is the joint partner of the present Office of Naval Research project at University of Maryland (UMD) where experimental tests with another fluid was undertaken for a convention size plate design and more recently a replica of our present one.
- Propose more general and reliable prediction methods for local flow boiling heat transfer coefficients and two-phase frictional pressure drops to be employed for accurate thermal designs.
- Develop a simulation code for predicting local thermal and hydraulic performance of the commercial plate heat exchangers. This tool has to handle a wide range of operating

conditions, working fluids, flow arrangements and plate geometries (it is now a freely available “app” for use on the new *VIR2AL* institute’s website at [www.2phaseflow.org](http://www.2phaseflow.org), founded by the LTCM lab with now 19 international member labs).

### 1.4 Thesis structure

The present thesis is comprised of nine chapters. In chapter 2, a state-of-art review is reported and the main works that have been done in terms of flow boiling heat transfer, two-phase pressure drop and flow regime are listed and discussed. Chapter 3 describes the experimental apparatus and its operation, the new prototype corrugated plate heat exchanger, the uncertainty analysis and the data reduction technique in order to obtain local heat transfer coefficients and frictional pressure drops. In chapter 4 the validation of the single-phase experimental measurements, the technique to calibrate the infrared camera, the energy balance to characterize the thermal losses and the main trends of local heat transfer coefficient versus mass flux, heat flux, refrigerant temperature and axial plate location are discussed in detail. According to the experimental results presented earlier, in chapter 5, a new set of mean and local prediction methods to predict single-phase thermal/hydraulic performance and the associated statistical comparisons with literature methods are presented. Chapter 6 is divided into two sections; first, the two-phase frictional pressure drop results and a novel technique, based on infrared measurements, to obtain the local saturation temperature of the refrigerant along the evaporator are reported and second the mean and local flow boiling heat transfer results and the associated effects of mass flux, system pressure, imposed heat flux, vapor quality and axial plate length are investigated. Chapter 7 first includes the collection of a wide experimental flow boiling database from literature research studies, which then is adopted to develop a set of prediction methods in order to evaluate the local flow boiling heat transfer coefficient and local two-phase frictional pressure gradient within plate heat exchangers. In chapter 8, a selection of the previous mentioned methods are implemented in a simulation tool coded in MATLAB, for rating water to refrigerant and direct electrical heating plate heat exchangers for a wide range of operating conditions. A validation of the code, a sensitivity analysis and the new simulation data are also provided. Concluding remarks and recommendation for future work are reported in chapter 9.

## **CHAPTER 2 – Literature survey**

### **2.1 Introduction**

Chapter 2 of the current thesis presents a comprehensive overview of the single- and two-phase research studies available in the open plate heat exchanger literature. In this chapter the most quoted correlation schemes in order to evaluate the heat transfer coefficient as well as the frictional pressure drop have been introduced. Finally, the main flow regimes observed during heat transfer or two-phase adiabatic studies are also addressed.

### **2.2 Review of experimental single-phase studies**

Single-phase thermal and hydraulic performance within plate heat exchangers have been widely investigated over the past years and the main experimental research studies are summarized below.

Ayub (2003a) provided an extensive literature review on single-phase heat transfer and pressure drop within plate heat exchangers. In his article, 28 prediction methods were summarized as well as the information regarding their experimental test conditions.

Focke et al. (1985) performed mass transfer measurements to evaluate the influence of chevron angle on the thermal and hydraulic performance of a plate heat exchanger. The chevron angle effect was examined over a large range from 0° to 90°. The authors concluded that the heat transfer coefficient and frictional pressure drop increased with chevron angle at a fixed Reynolds number. Furthermore, increasing the chevron angle, the transition from laminar to turbulent flow regime occurred earlier.

Han et al. (2003b) performed flow boiling experiments with refrigerants R410a and R22 in brazed plate heat exchangers with different chevron angles (45°, 55° and 70°) and corrugation pitches (7 mm, 5.2 mm, and 4.9 mm). In order to characterize the heat transfer coefficient on the water side, they performed some single-phase (water-to-water) heat transfer experiments. Based on their data, the Nusselt number was correlated in terms of the Reynolds number, Prandtl number and chevron angle. Hayes et al. (2011c, 2012a) studied condensation of CO<sub>2</sub> in three different brazed plate heat exchangers (two symmetric configurations



27°/27°, 60°/60° and one mixed arrangement (27°/27°). In order to characterize the two-phase performance, the author conducted preliminary water-to-water and dynalene-to-water experiments to evaluate the single-phase heat transfer and pressure drop. The Nusselt number was linked to the Reynolds number, Prandtl number and viscosity ratio (fluid to wall) and three different models were provided according to the chevron angle arrangement. In the same way, the Fanning friction factor was also correlated and linked to the Reynolds number. Finally, they observed that both the liquid heat transfer coefficient as well as the frictional pressure drop increased with chevron angle, which was identified with the vertical axis.

Heavner et al. (1993b) investigated the effect of mixed chevron angle on water's heat transfer coefficient and frictional pressure drop within a plate heat exchanger. The mean chevron angle between the two plates was included in the range from 23° to 67.5°, and the authors observed that, increasing the mean chevron angle, the heat transfer and the pressure drop rose. Furthermore, to correlate the Fanning friction factor and Nusselt number, the surface enlargement factor was also included.

Hsieh and Lin (2002a, 2003c, 2002b) performed experiments on single-phase and saturated flow boiling of R410A and R134a in the 60° corrugated plate heat exchanger. They observed that the single-phase Nusselt number increased with Reynolds number and working with R410A, the heat transfer coefficient was about 25% to 35% larger than R134a. The authors concluded that the larger heat transfer rate was due to the higher thermal conductivity of the R410A. Later, a correlation for the liquid Nusselt number was introduced adopting the Wilson plot technique.

Jokar et al. (2006b) analyzed the performance of three plate heat exchangers, different in number of flow passages and similar in plate geometry specifications. Their average heat transfer and pressure drop data for complete evaporation were dependent on the water side heat transfer coefficient. For this reason, they carried out experiments in which the water was streaming in one side, while 50% water-glycol mixture was flowing on the other side. Based on dimensional analysis coupled with the Wilson plot technique, the Nusselt number was linked to the Reynolds and Prandtl numbers. Finally, the power of the Prandtl number was found to be equal to 0.3 for cooling and 0.4 in case of heating process.

Kovalenko and Maslov (1970) studied the thermal and hydraulic performances of a 60° chevron plate heat exchanger. Based on their large experimental database, the authors correlated the single-phase Nusselt number and Fanning friction factor for the laminar and turbulent flow regimes and the transition was found to occur at a Reynolds number equal to about 200.

Kumar (1984b) undertook one of the first single-phase study in plate heat exchangers. In his article, water to water heat transfer was investigated over a wide range of Reynolds numbers and chevron angles (from 25° to 60°). The author observed that the heat transfer performance was enhanced with increasing chevron angle as well as Reynolds number. The author correlated the Fanning friction factor with the Reynolds number, while the Nusselt number was linked to the Reynolds number, Prandtl number and viscosity ratio.

Martin (1996a) provided a theoretical study to predict single-phase thermal and hydraulic performance of chevron-type plate heat exchangers. Based on the complex fluid phenomena which occur inside plate heat exchangers, the author proposed an analytical model to evaluate the pressure drops while the fanning friction factor was correlated with chevron angle and Reynolds number. According to developing thermal boundary layer in fully developed laminar and turbulent flow theory, a theoretical equation was also presented to characterize the heat transfer coefficient that was function of chevron angle, Reynolds number, Prandtl number, viscosity ratio and pressure drop.

Muley et al. (1999a, 1999b) developed prediction methods for the heat transfer coefficient and frictional pressure drop in case of laminar and turbulent flow within plate heat exchangers. Their correlations were obtained by fitting several databases in which the Reynolds number varied from 30 to more than 1000, chevron angle varied from 30° to 60° and surface enlargement factor changed from about 1 to 1.5. Furthermore, the frictional pressure drop was correlated with the chevron angle, surface enlargement factor and Reynolds number, while the heat transfer coefficient involved also the Prandtl number, viscosity ratio and the ratio between equivalent diameter and port-to-port length.

Yan and Lin (1999c) studied evaporation heat transfer and pressure drop of R134a in a plate heat exchanger of 60° chevron angle. In order to calculate the two-phase heat transfer coefficient on the water side, the authors first performed some single-phase (water-to-water) heat transfer experiments. Based on their data, the Nusselt number was correlated in terms of the Reynolds number, Prandtl number and viscosity ratio and a turbulent flow regime was already observed at Reynolds number close to 200. Furthermore, the authors showed that the single-phase heat transfer coefficient within their plate heat exchanger was 8 times greater than the one reached in a circular pipe at the same test conditions.

Freund and Kabelac (2010a) investigated local heat transfer coefficient of liquid water within a plate heat exchanger composed of two corrugated plates with a chevron angle of 63°. The wall temperature was measured using an infrared camera in response to a periodic heat flux (0.1 - 0.2 Hz) generated by a halogen spot array. They observed different heat transfer

patterns according to the Reynolds numbers. In particular, at low values of Reynolds numbers, a minimum in the heat transfer coefficient was observed at the crossing points, while the maximum heat transfer rate was achieved along the corrugations. The average Nusselt number was in good agreement with the literature methods. Increasing the Reynolds numbers, the heat transfer distribution became more uniform and the maximum heat transfer coefficient was about 3-4 times greater compare to the average value. Furthermore, at high fluid velocities, the lowest heat transfer coefficient, located downstream of the contact points, was periodically interrupted by local recirculation sites, that enhanced the thermal performances.

Gherasim et al. (2011a, 2011b) carried out an experimental study to investigate thermal and hydraulic fields in a 60° chevron plate heat exchanger. The test section was composed of three plates, providing two flow channels for the cold and hot water respectively. In order to measure the local wall temperature, 80 thermocouples were placed on the outside of the plates. The authors evaluated the Nusselt number and Fanning friction factor over a wide range of Reynolds numbers from laminar to turbulent flow conditions and compared their results with several prediction methods. Finally, due to the effect of the inlet/outlet ports, complex corrugated pattern and number of plates, the isotherms measured on the first and last plates were very irregular, meaning large temperature gradients along the axial and transverse coordinates of the two plates.

Solotych et al. (2015e) performed an experimental study to investigate steady-state, local heat transfer coefficients of single-phase flow of HFE7100 within a corrugated plate heat exchanger. The test section was composed of two calcium fluoride ( $\text{CaF}_2$ ) plates, which identified a single channel for the upward refrigerant flow. The plates were machined with a chevron angle of 60°, pressing depth equal to 2 mm and wavelength of the surface corrugation of 5.72 mm. Moreover, the authors manufactured their plate heat exchanger with inlet and outlet distributors to minimize flow maldistribution. In order to promote heat transfer between the plate prototype and refrigerant, the test section was electrically heated adopting a flexible film heater, which was able to handle heat fluxes up to  $8 \text{ kWm}^{-2}$ . A high resolution infrared camera was used to measure the local wall temperatures, while the fluid temperatures were directly measured by locating several thermocouples along the test section. Experiments were carried out over a wide range of Reynolds numbers covering laminar and turbulent flow regimes and the average Nusselt number was linked to the Reynolds and Prandtl numbers. Finally, the authors concluded that, the maximum heat transfer coefficient

occurred upstream of the contact points, where the fluid impacted on the wall, while the minimum heat transfer coefficient was at the contact points.

Stasiek et al. (1996b) analyzed heat transfer and pressure drop mechanisms within several compact chevron plate heat exchangers in order to provide more general prediction methods useful for thermal engineers. The authors adopted liquid crystal thermography to measure the local wall temperature and obtain local heat transfer data. The test section was composed of two corrugated plates, located in a wind tunnel, forming an inner-flow channel. The liquid crystal was attached on the upper surface, which was maintained at a constant temperature by using a water bath, while the bottom surface was exposed to a hot air flow. The authors observed that the average Nusselt number increased with chevron angle, Reynolds number and decreased with the ratio between the wavelength of the surface corrugation and pressing depth. The same behaviors have been discovered in terms of Fanning friction factor. In conclusion, the lowest heat transfer coefficient occurred downstream of the contact points between the two plates, while the highest Nusselt number was on the upstream surface (minimum cross-sectional area for the fluid flow), where the liquid collided with the wall.

## 2.3 Flow boiling heat transfer and two-phase pressure drop

Plate heat exchangers are increasingly adopted for many evaporation applications, such as steam generators, petrochemical reboilers and very often in small to medium size refrigeration systems. A survey shows that there has been much experimental work done on plate evaporators with refrigerants as the working fluid. However, most research work until now has only resulted in prediction methods of limited application, instead of refined general correlations for predicting the local heat transfer coefficients and pressure drops. The reason for this is probably due to the fact that the evaporation process is very complex and geometry dependent, and because typically only in-house data are included rather than larger data sets of independently measured data. Heat transfer mechanisms in plate heat exchangers are in fact a complex function of the flow regime, geometry of the system, properties of the fluids, heat flux and many other parameters.

While studies of evaporation inside tubes can give relevant fundamental knowledge, the actual details can be quite different for flow boiling in between two plates. In general, three fundamental heat transfer mechanisms govern the flow boiling process inside smooth tubes: nucleate boiling, two-phase convective boiling, and single-phase/mist flow heat transfer to

the vapor in the drywall and superheating region. The latter, which is also termed the post-dryout region, may or may not be reached during experimental campaigns, depending upon the magnitude of the heat flux and the outlet conditions. Even if dryout is reached before reaching complete evaporation, typically this aspect is ignored, or not known to have occurred, when reducing the test data. Therefore, in most cases, only the first two mechanisms are considered. Typically, the liquid velocity in the liquid film tends to suppress nucleate boiling. Therefore, the evaporation heat transfer is typically divided into: (i) a nucleate boiling dominated regime, (ii) a two-phase convective boiling dominated regime and (iii) a transition regime where both nucleate and two-phase convective boiling contribute. However, based on the literature, evaporation in confined corrugated channels of plate heat exchangers belongs mainly in the convective dominated regime as the heat fluxes in such applications are low as narrow temperature approaches between the evaporating fluid and the heating fluid (such as chilled water) are the norm, and getting even smaller for energetic reasons.

Most of the correlations in the literature for flow boiling heat transfer in tubes can be summarized in the following general form, taking into account the contributions made by the nucleate boiling and convective boiling components:

$$h = \left[ (h'_{nb})^j + (h'_{cb})^j \right]^{1/j} = \left[ (h_{nb} \cdot S_{nb})^j + (h_{cb} \cdot F_{cb})^j \right]^{1/j} \quad (2.1)$$

where  $h_{nb}$  and  $h_{cb}$  represent the nucleate boiling and convective boiling heat transfer coefficients.  $S_{nb}$  is the nucleate boiling correction factor that usually accounts for the partial or total suppression of nucleate boiling sites in two-phase flows and  $F_{cb}$  is the convective boiling correction factor that accounts for the enhancement of convection in a two-phase flow due to the higher velocity of the two-phase with respect to the only liquid flow. Although most of the original correlations were developed from evaporation tests in tubes, they are often adapted to plate heat exchangers by applying new empirical constants or by the modification of these correction factors. In such a case, it is logical to use single-phase correlations of plate heat exchangers instead of tubes for calculating the liquid convective heat transfer coefficient.

Basically, a correlation with the form presented above assures a smooth transition as the boiling mechanism changes from nucleate to convective dominated. The case  $j = 1$  represents a simple addition, that is termed superposition or a Chen-type model (1966) whilst  $j = \infty$  means the larger mechanism is predominant, which is actually the form of the Shah (1976) correlation, while the other values give an asymptotic power-law determination.

### 2.3 Flow boiling heat transfer and two-phase pressure drop

Measured pressure drops in two-phase flow consist of several components: the static (gravitational), acceleration (or deceleration) and frictional pressure drops inside the channels plus the pressure drops across the inlet and outlet ports and any flow distributor:

$$\Delta p_{tot} = \Delta p_{sta} + \Delta p_{mom} + \Delta p_{fri,tp} + \Delta p_p \quad (2.2)$$

The elevation and acceleration pressure losses may be evaluated theoretically by the homogeneous model, which gives:

$$\Delta p_{sta} = \rho_m \cdot g \cdot L_p \quad (2.3)$$

$$\Delta p_{mom} = G^2 \cdot \Delta x \cdot \left( \frac{1}{\rho_v} - \frac{1}{\rho_l} \right) \quad (2.4)$$

The pressure drops across the evaporator inlet and outlet ports are usually evaluated according to the correlation suggested by Shah and Focke (1988) assuming homogeneous flow:

$$\Delta p_p = 0.75 \cdot N_{pass} \cdot \left[ \left( \frac{G_p^2}{2 \cdot \rho} \right)_{in} + \left( \frac{G_p^2}{2 \cdot \rho} \right)_{out} \right] \quad (2.5)$$

Here,  $\rho_{in}$  and  $\rho_{out}$  are defined according to the state of the refrigerant at the inlet and outlet ports. For liquid-vapor flow, the two-phase mean density can be used. However, for prediction of two-phase frictional pressure drop,  $\Delta p_{fri,tp}$ , a survey in the literature indicates that a widely accepted method is to apply the Lockhart and Martinelli (1949) model. The Lockhart-Martinelli parameter,  $X$ , and the two-phase friction multiplier,  $\phi_l^2$ , for the liquid are respectively defined as:

$$X^2 = \frac{\Delta p_{fri,l}}{\Delta p_{fri,v}} \quad (2.6)$$

$$\phi_l^2 = \frac{\Delta p_{fri,tp}}{\Delta p_{fri,l}} \quad (2.7)$$

$$\Delta p_{fri,tp} = \phi_l^2 \cdot \Delta p_{fri,l} \quad (2.8)$$

where  $\Delta p_{fri,l}$  is the liquid phase frictional pressure drop calculated as if the liquid phase was flowing alone,  $\Delta p_{fri,v}$  is the vapor phase frictional pressure drop calculated as if the vapor phase was flowing alone and  $\Delta p_{fri,tp}$  is the resulting two-phase frictional pressure drop. The

relationship between the Lockhart-Martinelli parameter and two-phase friction multiplier for liquid was originally illustrated graphically by Lockhart and Martinelli (1949). In practice, this model is often represented by the following correlation suggested by Chisholm (1967):

$$\phi_l^2 = 1 + \frac{C}{X} + \frac{1}{X^2} \quad (2.9)$$

The value of constant C is usually determined from experimental data and depends on the flow regime (laminar or turbulent) of liquid and vapor phase. Normally, no specific aspects of the two-phase flow structure (i.e. flow pattern) are taken into account.

The second type of model presented in the literature to calculate frictional pressure drop in plate heat exchangers is based on the kinetic energy KE per unit volume, which is expressed as:

$$\Delta p_{fri,tp} = \zeta \cdot \frac{\text{KE}}{\text{Volume}} = \zeta \cdot \frac{G^2}{2 \cdot \rho_m} \quad (2.10)$$

The average two-phase density between the inlet and outlet of the plate heat exchanger are calculated by the homogeneous model at the average vapor quality  $x_m$  between inlet and outlet:

$$\frac{1}{\rho_m} = \frac{x_m}{\rho_v} + \frac{1-x_m}{\rho_l} \quad (2.11)$$

This type of method is not able to predict local pressures along the plate heat exchanger for calculating local saturation temperatures, the latter required for incremental heat exchanger design simulations.

In the third type of model reported in the literature, the frictional pressure drop is calculated with a two-phase Fanning friction factor usually correlated in terms of equivalent Reynolds number:

$$\Delta p_{fri,tp} = 2 \cdot f_{tp} \cdot \frac{L_p \cdot G^2}{d_h \cdot \rho_m} \quad (2.12)$$

## 2.4 Review of experimental flow boiling studies

Danilova et al. (1981) undertook one of the first and most extensive flow boiling studies on plate heat exchangers, testing refrigerants R12, R22, R113 and ammonia. It was observed that

the evaporation heat transfer coefficient increased almost linearly with vapor quality and refrigerant mass flux. The authors correlated the Nusselt number with the Bond number, which the latter takes into account the ratio between the gravitational and the surface tension forces, and is also a parameter commonly used now in two-phase heat transfer applications to establish the transition from macro-to-microscale thermal performance. They also stated that the level of the heat flux provided an enhancement in the heat transfer rate but the effect was less dominant compared to vapor quality and mass flux.

Engelhorn and Reinhart (1990a) tested a plate evaporator of 0.522 m height, 0.115 m width, and a total heat transfer surface area of 3.02 m<sup>2</sup> with R22 as the working fluid. They found that the heat transfer coefficient increased with increasing heat flux and mass flux, but decreased with increasing saturation temperature. Also, they tested the plates with and without a flow distributor at the inlet. Based on their tests, they concluded that with the distributor the evaporation heat transfer coefficient increased significantly and no adverse influence on the evaporation temperature was observed. This indicates that mal-distribution has a considerable effect on the evaporation performance of plate heat exchangers if not addressed correctly.

Kumar (1992) tested several plate heat exchangers, using R22 and ammonia as test fluids, and reported that the heat transfer coefficient increased with increasing outlet vapor quality. However, a significant drop in heat transfer coefficient was observed when the exit quality exceeded 0.7, similar to trends for flow boiling in tubes after the onset of partial dryout.

Thonon et al. (1995b) gave a review of the status of research on single-and two-phase flows in plate heat exchangers at that time. For evaporation, they suggested that the annular flow pattern dominated over a large range of test conditions in the corrugated channels, except at low vapor qualities, providing higher heat transfer coefficients. As in tubes, the total heat transfer in evaporation was assumed to be attained from the contributions of nucleate and convective boiling components. Furthermore, a criterion based on the multiplication of the Lockhart-Martinelli parameter and the boiling number was suggested for distinguishing whether the flow was nucleated boiling dominated ( $Bo \cdot X_{tt} < 0.00015$ ) or two-phase convective boiling dominated ( $Bo \cdot X_{tt} > 0.00015$ ). They suggested the Gorenflo (1993a) fluid specific nucleate pool boiling correlation to be used directly in the nucleate boiling dominated region (without correction for any influence of the flow) and an enhancement factor method for the convective boiling dominated region, where the liquid heat transfer coefficient assuming all the fluid flows as liquid is calculated using the specific correlation



for the specific plate heat exchanger. Finally, the evaporation heat transfer coefficient should then be chosen as the larger value of the nucleate boiling term and the two-phase convective boiling term, rather than combining them using some type of asymptotic model. They also indicated that the corrugations influenced the critical vapor quality (i.e. meaning in fact the onset of dryout, not critical heat flux), at which the heat transfer coefficient dropped. This onset value was noted to be lower than for tubes.

The group of Lin (2003c, 2002b, 1999c) performed experiments on saturated flow boiling with R134a and R410A in a vertical plate heat exchanger of 60° chevron angle. The effects of vapor quality, mass flow rate, heat flux and system pressure on the evaporation heat transfer and pressure drop were investigated in detail. They suggested two distinct correlations, in terms of the boiling number and an equivalent Reynolds number, to predict their experimental heat transfer coefficient data with R134a and R410A, respectively. However, a Chen-type correlation was suggested later by Hsieh and Lin (2003c) in order to predict the saturated flow boiling data of R410A, where the liquid only and pool boiling heat transfer coefficient are respectively given by the Dittus-Boelter (1930) equation and Cooper (1984a) pool boiling correlation. Hsieh et al. (2002a) also investigated subcooled flow boiling heat transfer characteristics of refrigerant R134a and demonstrated in detail the effects of heat flux, refrigerant mass flux and system pressure. They proposed a correlation for subcooled flow boiling of R134a in their plate heat exchanger as a function of the Froude, boiling, and Jakob numbers. The liquid only heat transfer coefficient was determined from an empirical correlation obtained through single-phase water-to-water tests. However, one can see that the subcooled boiling condition was not established for some of their experimental results presented in their graphs as the local wall temperature was not superheated.

Donowski and Kandlikar (2000b) analyzed their experimental data as well as the evaporation heat transfer data of Yan and Lin (1999c), concluding that there is a large discrepancy between either the single-phase or two-phase original experimental data and the corresponding values predicted by the Yan and Lin (1999c) correlation; strangely, the correlation underpredicted all the original database. Therefore, they used Yan and Lin data and developed a new correlation for single-phase heat transfer coefficients of water-to-water and two correlations for two-phase evaporation heat transfer coefficients of refrigerant R134a. Regarding the latter two, the first scheme retained the basic form of the Kandlikar (1991a) in tube flow boiling prediction method while the second proposed a simplified format to fit to the same database, and the single-phase heat transfer coefficient was modified for its use within the above correlations.

Longo et al. (2012e, 2012f, 2007b, 2007c, 2007d, 2004a) conducted extensive experiments with complete evaporation, obtaining mean heat transfer coefficients in a plate heat exchanger. Numerous refrigerants were tested: R134a, R410A, R236fa, R600a (isobutane), R290 (propane), R1270 (propylene) and R1234yf. Longo and Gasparella (2007b) concluded that their heat transfer coefficients showed a weak sensitivity to saturation pressure and a great sensitivity to heat flux, outlet conditions (outlet vapor qualities of around 0.8-1.0 or vapor superheating up to around 5-10 K). The Cooper (1984a) and Gorenflo (1993a) correlations were able to reproduce the majority of the saturated boiling heat transfer coefficient data, although not of course typical trends as a function of local vapor quality. Longo et al. (2004a) investigated the application of a “cross-grooved” surface to R22 vaporization and condensation inside a brazed plate heat exchanger with a herringbone macro-scale corrugation. The results indicated this surface gave an increase in the heat transfer coefficient from 30% to 40% in boiling and up to 60% in condensation with respect to a smooth surface. In terms of pressure drop, they reported a linear relationship between their frictional pressure drop data and the kinetic energy per unit volume of the refrigerant flow. This meant to be a constant value for the friction factor against the refrigerant mass flux and therefore the Reynolds number as it occurs for single-phase fully turbulent flow. They concluded for each plate corrugation and geometry that it is possible to determine a specific constant to correlate the frictional pressure drop and kinetic energy. However, multiple values ( $\xi = 1.835, 2.05, 2, 1.9, 1.875, 1.8$ ) were introduced by the authors in different studies for one plate heat exchanger and different fluids. Furthermore, no unique constant value was found for the same plate geometry or a method to predict these values.

Palm and Claesson (2006c) studied single-phase and flow boiling heat transfer and pressure drops within plate heat exchangers. They found that the heat transfer performance was well correlated by modifying the Cooper (1984a) nucleate pool boiling correlation scaled up with a constant factor of 1.5 to account for the plate heat exchanger enhancement.

Han et al. (2003b) performed flow boiling experiments with refrigerants R410a and R22 in brazed plate heat exchangers with different chevron angles (45°, 55° and 70°) and corrugation pitches (7 mm, 5.2 mm, and 4.9 mm). Based on their experimental data, the authors established an empirical correlation for two-phase heat transfer in terms of the equivalent Reynolds and boiling numbers, adding some geometric parameters. The prediction method was thus based on the equivalent mass flux, that was first proposed by Akers et al. (1959).

Palmer et al. (2000c) presented the average Nusselt numbers for pure refrigerants R22 and R290, and mixtures of R290/R600a and R32/R152a, undergoing complete evaporation at low heat and mass flux in a commercial brazed plate heat exchanger. They proposed one correlation to predict evaporation heat transfer data for R22, R290 and R290/R600a and a second prediction approach in the case of R32/R152a mixture. The need for the separate correlations was attributed to the use of different lubricants for the refrigerants.

Ammonia is an environment friendly natural refrigerant with attractive thermo-physical properties, but has been tested by only a few research groups. Khan and collaborators (2014a, 2012c, 2012d) investigated evaporation and pressure drops of commercial plate heat exchangers with symmetric 30°/30° and 60°/60° and mixed 30°/60° chevron plates. Empirical correlations for a two-phase Nusselt number and Fanning friction factor were suggested in terms of reduced pressure, equivalent Reynolds number and boiling number. Furthermore, they found that the pressure drop was strongly influenced by the equivalent Reynolds number, whereas the effect of saturation temperature was moderate. The authors provided three different empirical correlations depending on the chevron angle. As one can see, there was no attempt to integrate the two-phase friction factor correlations into one correlation such as accomplished for the two-phase Nusselt numbers. However, it has to be pointed out that, the friction factor correlation for  $\beta = 30^\circ$  is to be ignored since it does not reproduce the corresponding experimental data (2012c). Khan et al. (2010b) also performed water-to-water experiments to investigate single-phase heat transfer characteristics of the commercial plate heat exchanger with different chevron angles, corrugation depths and plate arrangements under turbulent flow conditions. They correlated the single-phase heat transfer coefficient in the range of chevron angles between 30° and 60°.

Ayub (2003a) presented an extensive literature survey, mostly concentrating on single-phase flow studies and their relevant correlations. He also proposed heat transfer and pressure drop correlations for refrigeration evaporators based on the performance data of various installed evaporators (mainly operating with ammonia as the working fluid). His correlations incorporate the principle of corresponding states as well as the effect of the chevron angle of the mating plates, but is independent of heat flux and vapor quality. The prediction methods can be applied to flooded, thermosyphon and direct expansion plate heat exchanger evaporators. The authors also correlated the evaporation pressure drop in terms of the Fanning friction factor, including the effect of chevron angle.

Jokar et al. (2006b) analyzed the performance of three plate heat exchangers, different in size (number of flow passages), but similar in plate geometry specifications. Their average

heat transfer and pressure drop data for complete evaporation were correlated using the dimensional analysis technique applied to both measured and calculated parameters. The authors provided the prediction methods for flow boiling of R134a and ammonia.

Jassim et al. (2006a) experimentally analyzed the frictional pressure drop in adiabatic two-phase flow of R134a through a plate heat exchanger with herringbone and bumpy corrugations. They found a linear dependence between their frictional pressure drop data at constant vapor qualities and the associated kinematic energy of refrigerant flow per unit of volume. They introduced a specific void fraction model, which was used within their model in order to predict two-phase frictional pressure drop data based on the kinetic energy of the flow.

Táboas et al. (2010d) conducted experimental work on the saturated flow boiling and the frictional pressure drops of ammonia/water mixtures flowing in a 60° chevron angle plate heat exchanger. Later, the authors (2012g) assessed several boiling heat transfer and pressure drop correlations. Based on that, a modified flow boiling correlation was proposed and a novel approach depending on the liquid and vapor superficial velocities was also suggested to establish which flow boiling mechanism had more influence on the heat transfer performance. As they explained in their first paper (2010d), the correlation of Kumar (1984b) was chosen to predict the single-phase heat transfer coefficients. Also, a correlation for the single phase Fanning friction factor was suggested. Additionally, they recommended the Chisholm (1967) correlation with  $C = 3$  in order to reproduce their two-phase pressure drop data. However, it has to be noted that their results covered only the low range of vapor qualities ( $x \leq 0.2$ ).

Djordjevic and Kabelac (2008) evaluated the evaporation of ammonia and R134a in chevron plate heat exchangers with angles of 27° and 63°. Their measurement technique enabled the obtaining of quasi-local heat transfer coefficients along the plate, as several thermocouples were welded on the plate wall to measure the surface temperatures. The results indicated that the heat transfer coefficient rose over the entire range of vapor quality for high values of mass flux but decreased for low mass fluxes after a maximum value at vapor qualities at about  $x = 0.5$ . From these results, they concluded the parallel flow case yields better overall performance than the counterflow case, and that plates with low chevron angle corrugations increased the evaporation heat transfer. The authors did not provide any correlation since it was observed some of the preexistent prediction methods, properly scaled, could well fit the experimental data.

Bogaert and Böles (1995a) analyzed the performance of a brazed plate heat exchanger in terms of the hydraulic diameter parameter over a wide range of Reynolds number, and developed only one equation predicting two-phase hydrodynamic and thermal characteristics.

Ouazia (2001a) carried out an experimental study to explore heat transfer coefficients and associated frictional pressure drops of R134a in a vertical plate heat exchanger. In this study, three plates with different chevron angles (0°, 30° and 60°) were tested. The desired test condition at the entrance of the test section was reached with an electrical preheater; two different inlet conditions of 4 K subcooling and 5-10% of vapor were tested. They found that the inlet condition slightly affected the thermal-hydraulic performance. The heat transfer coefficients and the associated pressure drops were slightly higher for the test condition of 5-10% vapor at the plate heat exchanger inlet.

The performance characteristics of industrial plate heat exchangers used as liquid over-feed evaporators were investigated experimentally by Huang et al. (2012b). The analysis was assisted by statistical regression, yielding correlations based on the non-dimensional groups that were found to be most appropriate. Based on their experimental data, correlations were developed for predicting the refrigerant flow boiling heat transfer coefficient and the associated frictional pressure drop covering R134a, R507A, ammonia and R12 within plate heat exchangers of 28°, 44° and 60° chevron angles. However, it has to be noted that one group in their method  $i_{lv} \cdot d_0 / \alpha^2$  is not dimensionless as claimed by the authors. Notably, the bubble departure diameter was used in place of the hydraulic diameter as the characteristic length to define the Nusselt number. The two-phase frictional pressure drop data of R134a and R507A were correlated using the homogenous approach, where two-phase viscosity was defined by the equation of Dukler et al. (1964) and the geometrical parameter was correlated as a function of the chevron angle.

Park and Kim (2004b) studied heat transfer and pressure drops of R134a boiling in an oblong shell and plate heat exchanger with a chevron angle of 45°. The effects of the mass flux, imposed heat flux, saturation temperature, and vapor quality on the measured data were experimentally examined. The authors noted that both, the evaporation heat transfer coefficients and frictional pressure drops for an oblong shell and plate heat exchanger were higher than those for a plate heat exchanger, where the rise in the evaporation heat transfer coefficient was more pronounced than the one in the pressure drop. Finally, empirical correlations were also provided for the measured heat transfer coefficients and pressure drops in terms of the Nusselt number and Fanning friction factor.

Garcia-Cascales et al. (2007a) studied the refrigeration cycles in which plate heat exchangers were used as either evaporators or condensers. Finally, the experimental results obtained for R22 and R290 were compared with several published two-phase heat transfer correlations with some success.

Boccardi et al. (2000a) have studied the thermal performance of two compact brazed plate heat exchangers using two pure refrigerants (R22 and R134a) and two mixtures (R407C and R410A). It was found that the thermal performance depended on the type of refrigerant, the thermal load, and the heat transfer process (evaporation or condensation). For evaporation, comparison showed that R410A had the highest and R407C the lowest heat transfer coefficients, respectively. Based on their results, the R22 replacement options in plate heat exchangers for air conditioning application were discussed. Furthermore, an analytical approach was explained to calculate the zeotropic mixture saturation temperature. However, no attempts were given to develop a correlation for the evaporation heat transfer coefficient.

Sterner and Sundén (2006d) considered the influence of an inlet flow distributor in several semi-welded, nickel-brazed plate heat exchangers on the evaporation performance of ammonia. They found that an integrated inlet flow distributor provided a higher performance compared to that without a flow distributor. Moreover, three discrete Nusselt and friction factor correlations were developed for different plate heat exchangers; notwithstanding, they concluded a more comprehensive database was needed to establish generalized correlations.

Lee et al. (2014b) investigated flow boiling of water at low mass flux within a plate heat exchanger. Their test section yielded local measurements by installing 9 thermocouples along the plate and thus local heat transfer coefficients and pressure drops were determined. Cartridge type heaters were inserted in the end plates made in aluminum alloy to provide the desired heat flux. The authors linked their experimental data points to the convective boiling regime and the effect of heat flux on the heat transfer and associated frictional pressure drop was negligible; the heat transfer coefficient decreased with increasing of vapor quality (opposite to most of the above studies) and decreasing of mass flux. Finally, a new correlation to estimate the frictional pressure drop was proposed as well as to evaluate the heat transfer coefficient in the pre- and post-dry-out conditions. The transition line for both regimes was expressed by the ratio between the vapor and liquid Reynolds numbers.

Vakili-Farahani et al. (2014c, 2014d) carried out a fine resolution experimental study of flow boiling within a very compact stainless steel plate heat exchanger. Two-extremely thin (0.15 mm thick) corrugated plates having a small pressing depth of only 1 mm and a large

chevron angle were assembled together to make a single flow channel for the fluid. Local heat transfer coefficients and pressure drops were measured by using an infrared camera, including the effects of inlet condition (subcooled or two-phase), heat flux, mass flux, vapor quality and system pressure (saturation temperature) on thermal and hydraulic performance. Subcooled, adiabatic two-phase and flow boiling data were obtained and a new models to predict two-phase Nusselt number and Fanning friction factor were proposed.

## **2.5 Flow visualization and flow regimes**

Tribbe and Müller-Steinhagen (2001c) carried out a two-phase flow visualization study on several commercial plate heat exchanger geometries. They visualized the air-water downflow in two replica plates fabricated from transparent polyester and constructed a simple flow pattern map for plate heat exchangers based on the superficial velocities and their flow observations. They identified five main flow patterns typically relevant to those of similarly small hydraulic diameter circular channels:

*Regular bubbly flow:* Individual bubbles of approximately 3-5 mm in diameter flow along the channels (Figure 2.1a). Due to the shear stress, small bubbles are forced towards the surface contact point and large bubbles are split when they approach the contact point. One part continues along the same furrow while the other goes to an opposite furrow and, therefore, changes direction. Similar to single-phase flow, the tendency towards crossing flow diminishes as the chevron angle increases and is overtaken by a longitudinal wavy flow character.

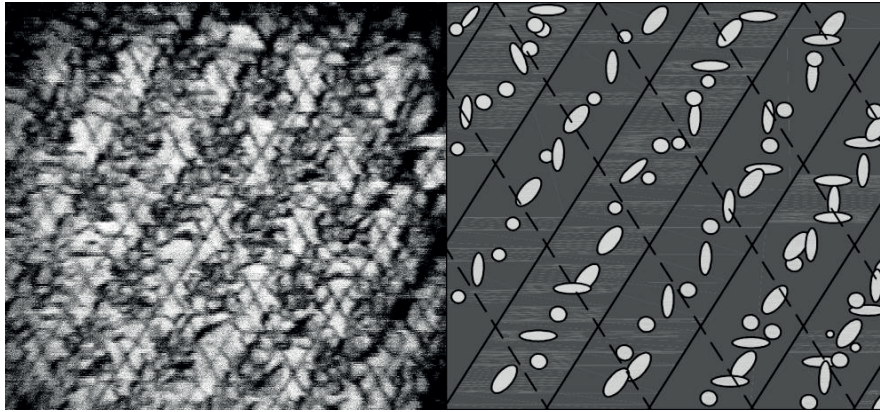
*Irregular bubbly flow:* As the gas flow rate increases, large irregularly shaped regions of gas appear among the regular bubble flow structure (Figure 2.1b). The bubbles spread over a number of furrows and exist over the entire depth of the channel. This is a meandering slug flow.

*Churn flow:* The appearance of high-velocity liquid slugs indicates the transition to churn flow (Figure 2.1c). Initially, they are sporadic and often short-lived. As the gas flow increases, the stability increases and they maintain their character along the length of the channel and occur with a regular frequency.

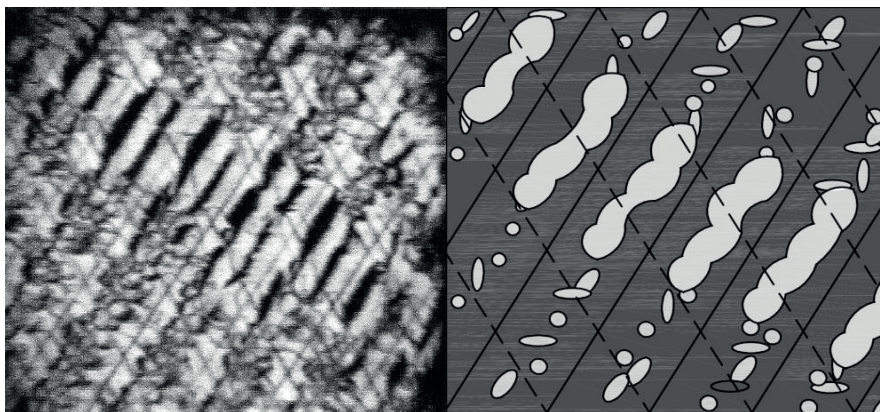
*Film flow:* The film flow pattern consists of a thin liquid film flowing along a furrow over which a fast-moving gas stream flows (Figure 2.1d). This is a sort of meandering annular flow, which follows the geometry of the corrugated channels.



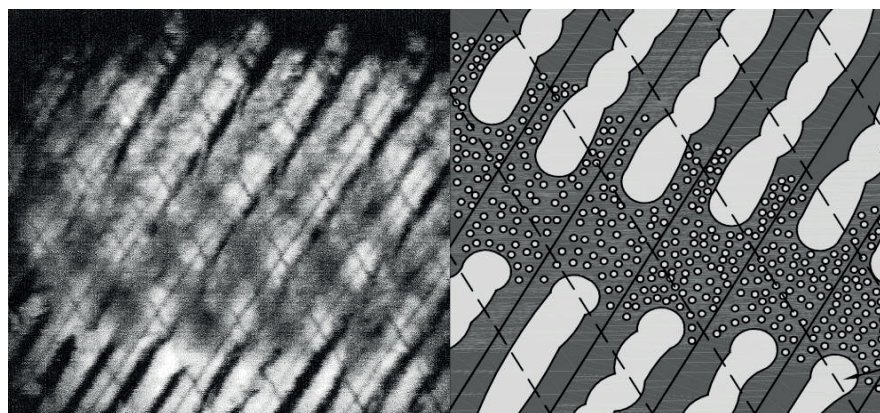
*Partial film flow:* At high vapor flow rates, the film no longer wets the entire surface and regions of dry surface appear (Figure 2.1e). Deposition of entrained liquid is observed at the gas/liquid interface, while liquid droplets are noted to appear on the dry edge.



(a)

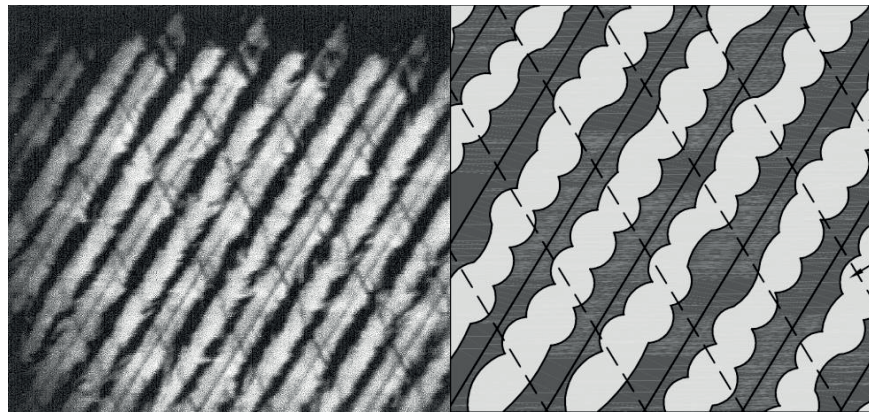


(b)

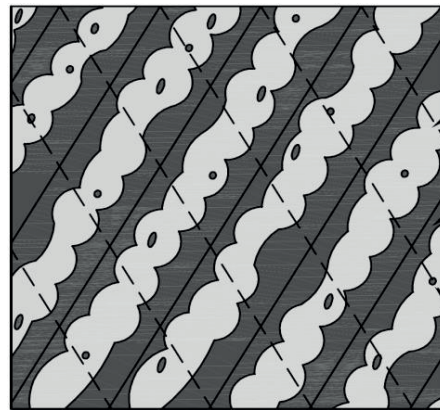


(c)





(d)



(e)

Figure 2.1: Gas-liquid flow patterns observed by Tribbe and Müller-Steinhagen (2001c) within a plate heat exchanger: (a) regular bubbly flow, (b) irregular bubbly flow, (c) churn flow, (d) film flow, (e) partial film flow.

Yan and Lin (1999c) also conducted flow visualizations through a transparent test plate which was fabricated with a chevron angle of  $60^\circ$ . The authors observed many nucleation sites close to the inlet port, but as soon as the vapor velocity downstream became sufficient, the heat transfer was dominated by the shear at the interface between both phases, whilst the geometry of the channel caused the liquid film thickness to be periodically interrupted and eventually turbulent mist flow regime was observed. No general equation was developed, even for two fluids in the same test section. This indicates the difficulty in reaching a general correlation for predicting the evaporation heat transfer coefficient and the associated frictional pressure drop for plate heat exchangers over all these regimes.

Nilpueng and Wongwises (2010c) investigated flow patterns and pressure drops of air-water two-phase flow in a plate heat exchanger. A non-symmetric pair of plates with chevron angles of  $55^\circ$  and  $10^\circ$  was tested together with a transparent plate on the other side, having

the same configuration as the stainless steel plate, in order to visualize the flow within the test section. The results of the study revealed that the two-phase flow direction caused different flow patterns. They observed bubbly flow, bubble recirculation flow, and annular-liquid bridge flow for the vertical upward direction, while there were slug flow, annular-liquid bridge/air-alone flow, and annular-liquid bridge flow for the vertical downward direction. It was found that annular-liquid bridge flow occurs in both flow directions. The bubbly flow pattern was found in vertical upward flow only. Similarly, slug flow appeared in vertical downward flow only. As only one combination of gas and liquid was tested, the flow patterns and their boundaries in plate heat exchangers are not resolved yet and new efforts have to be made in the future to add to their observations.

## 2.6 Conclusions

According to the above mentioned state-of-art, the main conclusions can be summarized for single-phase heat transfer and pressure drop within plate heat exchangers as follows:

- A significant enhancement in thermal performance was observed for plate heat exchangers relative to convectional pipes. Depending on the test conditions, the overall heat transfer coefficient was estimated to be 5-8 times larger, but on the other hand higher pressure drops have to be accommodated.
- Experimental studies proved that the frictional pressure drop increases with chevron angle and mass flux. The same behavior has been observed for the heat transfer coefficient and both parameters are regardless to the imposed heat flux.
- Most prediction methods available in the open literature correlated the Fanning friction factor with the Reynolds number, while the Nusselt number was linked to the Reynolds number, Prandtl number and viscosity ratio (fluid over wall). Furthermore, some authors recognized the influence of the corrugated sinusoidal pattern of the plate on the thermal and hydraulic performance and as a consequence the chevron angle and also the surface enlargement factor were introduced in their models.
- Experimental tests have been performed for a wide range of Reynolds numbers, Prandtl numbers and plate geometries and different models have been developed to characterize the average heat transfer coefficient and frictional pressure drop suitable for the laminar, transitional and turbulent flow regimes.

- So far only few local heat transfer studies were carried out and they proved that the flow distribution become more uniform with increasing the Reynolds number and in general, the lowest heat transfer coefficients were observed downstream of the contact points, while the highest thermal performances were found upstream along the corrugations.
- While most plate heat exchanger test data follow the same flow boiling trends seen inside tubes, but the convectional in-tube flow boiling prediction methods do not work well if one simply substitutes the tube internal diameter with the plate hydraulic diameter (this is not surprising as the tubular single-phase correlation used in many tubular flow boiling correlations as their starting point does not predict single-phase flow in a plate heat exchanger).
- Most plate heat exchanger prediction methods are based only on their own specific experimental data and one or two working fluids, without inclusion of independent data, and most are simple reformulations of intube prediction methods, without any mechanistic modeling of the process. No flow pattern effects are accounted for so far in the models
- Similar to in-tube flow boiling data from independent sources, flow boiling results for plate heat exchangers are difficult (perhaps even more difficult) to be correlated within reasonable accuracy because of the large discrepancy of the data sets. This large deviation is due the influences of: inlet/outlet flow distributors, oil in some studies, different data reduction procedures to get local saturation temperatures used to obtain heat transfer coefficients, etc. This complexity is more pronounced at low mass flow rates, since the corresponding experimental uncertainty becomes larger and heat flux dependency is greater.
- There are no proven transition criteria available to establish whether the evaporation process is nucleate boiling dominated or two-phase convective boiling dominated.
- Presently, there is no widely validated correlation available in the literature to predict the flow boiling heat transfer coefficient in plate heat exchangers.
- Similar to two-phase flows in tubes, the frictional two-phase pressure drop increases with rising vapor quality and rising mass flux but it decreases with increasing saturation temperature.
- From the experimental results in the literature obtained by Yan and Lin, Hsieh and Lin and Khan et al. (2003c, 2012d, 1999c), there are several additional trends they identified: (i)

- the two-phase friction factor decreases significantly at low vapor quality and (ii) that at high vapor quality values it tends to approach an asymptote.
- To explain such experimental trends, Jassim et al. (2006a), Táboas et al. (2010d) and Longo et al. (2012e, 2012f, 2007b, 2007c, 2007d, 2004a) noted that there is a linear relationship between the frictional pressure drop and kinetic energy of refrigerant flow, meaning that there is a constant value of the friction factor, explainable by the plateau or asymptotic trends at higher vapor qualities. However, it is not clear how the flow restriction (from the plate into its outlet) influences such test data trends.
- While the separated flow modeling approach of Lockhart-Martinelli was the most widely accepted method in the plate heat exchanger literature, Chisholm's parameter  $C$  changes significantly from one study to another, probably as the underlying databases include inlet/outlet header effects, inlet/outlet flow conditions (subcooled, two-phase or superheat), etc.

For more details regarding the structure of the heat transfer and pressure drop prediction methods and the test conditions in which these models have been developed, the reader could refer to Vakili-Farahani et al. (2015f) and Amalfi et al. (2015b, 2015c).

# CHAPTER 3 – Experimental apparatus

## 3.1 Introduction

In this chapter an overview of the experimental test facility and the equipment adopted during the experimental campaign are presented. The fabrication process and the geometrical specification of the new plate heat exchanger prototype are here illustrated. Next, the experimental procedure and uncertainty analysis are presented and then the data reduction techniques used to obtain local heat transfer coefficients and pressure drops are also detailed.

## 3.2 Test facility

As mentioned in Amalfi and Thome (2015a), a new test facility was built at LTCM (Laboratory of Heat and Mass Transfer at École Polytechnique Fédérale de Lausanne) to perform single- and two-phase experiments of refrigerants with high spatial and temporal resolution measurements for a more compact plate heat exchanger.



Figure 3.1: Photograph of the front view of the experimental test facility.



In Figure 3.1 and Figure 3.2 the pictures of the front and back views of the test facility are presented. The associated schematic of the flow loop is reported in Figure 3.3.

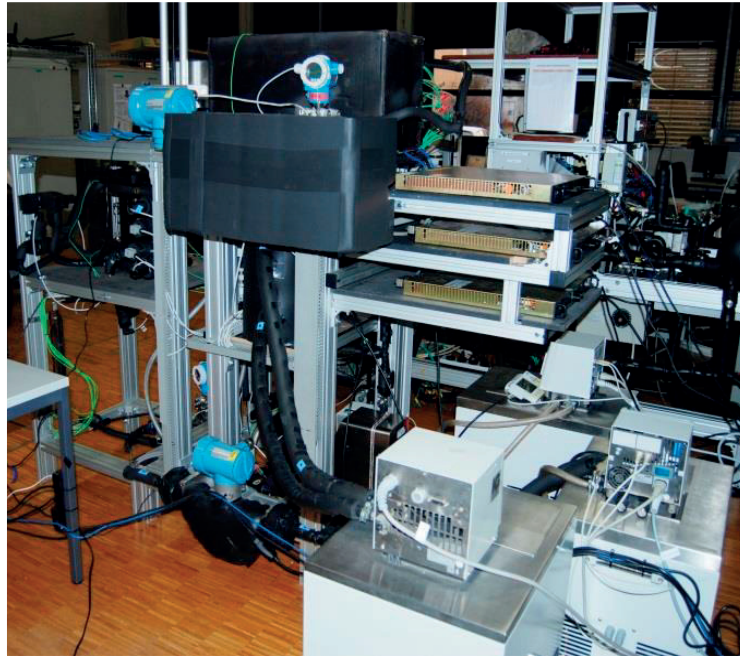


Figure 3.2: Photograph of the back view of the experimental test facility.

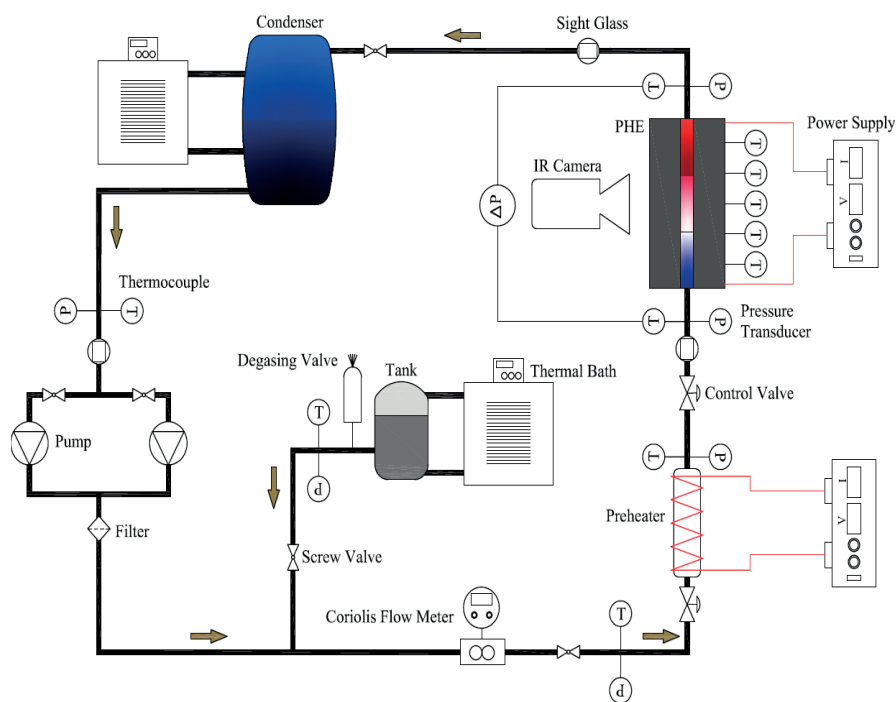


Figure 3.3: Schematic of the flow loop.

The main components of the present circuit are: gear pumps, condenser, preheater, Coriolis mass flow meter, infrared camera, absolute and differential pressure transducers, K-type thermocouples, transmitter, test section (compact plate heat exchanger), reservoir, thermal baths, power suppliers and data acquisition system. The test facility was able to carry out single-phase experiments in order to obtain local heat transfer coefficient and pressure drop in a prototype plate heat exchanger, although designed for two-phase tests.

The refrigerant was fully subcooled at the outlet of the condenser ( $\Delta T = 5\text{ }^{\circ}\text{C} - 10\text{ }^{\circ}\text{C}$ ) in order to avoid cavitation phenomena for the pump. The fluid was circulated within the loop by one of two oil-free magnetic gear pumps, which were magnetically coupled to a variable speed motor to ensure the desired mass flow rate, measured downstream using a Coriolis mass flow meter. A by-pass circuit was built to host two different pumps into the loop and choose the more suitable one according to the operating test conditions. An electrical preheater was installed to reach the desired inlet condition into the plate heat exchanger and its power was provided by a power supply. The inlet and outlet fluid temperatures of the preheater were measured as well as its local wall temperatures by placing three thermocouples along the surface. The thermal power in the plate heat exchanger was given by Joule effect using another power supply. A thermographic infrared camera was set up in front of the test plate in order to measure the local wall temperatures for one of the plates. At the exit, the refrigerant was again subcooled in another plate heat exchanger working in a counter-current flow configuration, before starting the same loop. It has to be pointed out that 2 thermal baths were employed in order to control the temperature of the cold water stream and the reservoir temperature (setting the system pressure of the entire test facility). At the inlet and outlet of the evaporator, 2 thermocouples and 3 pressure transducers were installed to measure respectively the refrigerant temperatures, absolute pressures and total pressure drop through the plate heat exchanger. Two needle valves were located upstream of the evaporator and preheater to ensure stable flow boiling over the entire experimental range by reducing back flow and instabilities phenomena. In order to have a reference for the measured values by the infrared camera, 15 thermocouples were attached on the back of the test plate. A high pressure safety valve, a micro-filter and a degassing valve were utilized for maintaining safe, clean and gas-free operations. A National Instrument data acquisition system was employed to record the measured parameters, such as the temperatures, pressures, flow rate, input powers and the signals from the infrared camera. Finally, the test facility was fully automated through a LabView control system.

### 3.3 Prototype plate heat exchanger

The test section was composed of two extremely thin corrugated stainless steel plates which yielded higher thermal performance (large chevron angle, small corrugation pitch and small pressing depth) compared to conventional plate geometries. Figure 3.4 depicts a schematic of the plate and its main geometrical parameters are defined in Table 3.1.

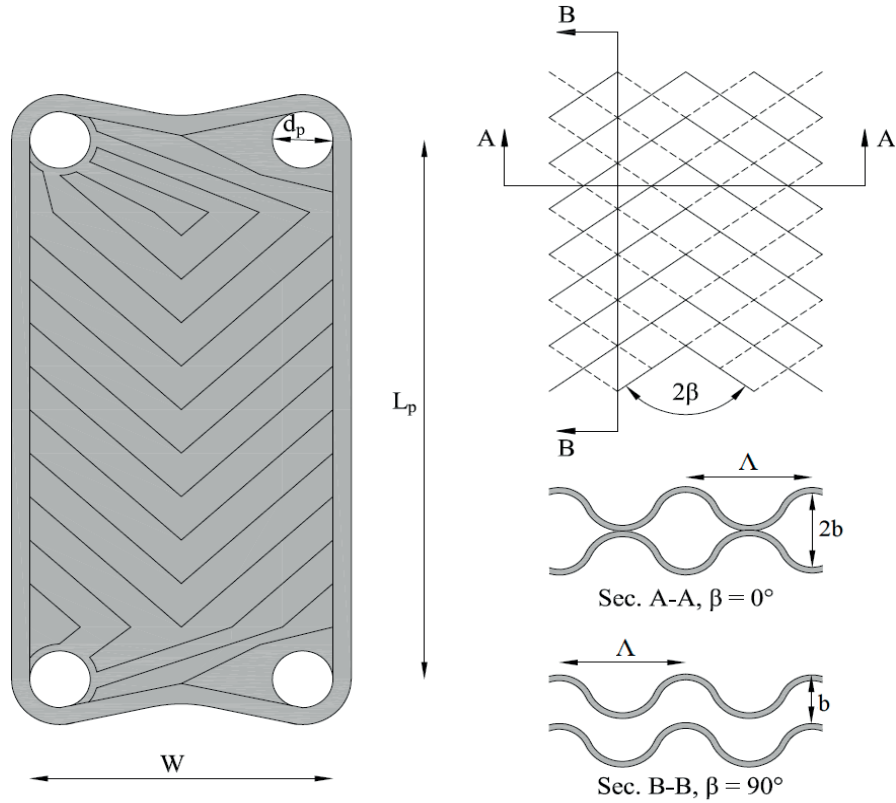


Figure 3.4: Drawing of the chevron plate prototype and the related geometrical parameters.

The goal of the present thesis is to investigate with high spatial and temporal resolution measurements local and mean heat transfer coefficient and frictional pressure drop of single-phase flow and flow boiling process of refrigerants using the direct electrical heating in a vertical more compact plate heat exchanger prototype.

Figure 3.5 illustrates the different steps as the fabrication of the plate heat exchanger was completed. The two corrugated stainless steel plates, were laser spot welded together around their common perimeter, and inlet and outlet pipes were also laser welded into their



### 3.3 Prototype plate heat exchanger

respective openings in one of the plates, creating a single flow passage between the two plates for the refrigerant flow.

Table 3.1: Geometry of the plate prototype.

Test section	Parameter	Value
Welded chevron plate heat exchanger with single channel for the refrigerant flow heated by electrical current (uniform heat flux). Plate material: SUS316	Chevron angle, $\beta$	65 (°)
	Corrugation pitch, $\Lambda$	3.71 (mm)
	Enlargement factor, $\phi$	1.17
	Equivalent diameter, $d_{eq}$	2 (mm)
	Flow cross sectional area, $A_c$	50 (mm <sup>2</sup> )
	Heat transfer area, $A_{ht}$	23400 (mm <sup>2</sup> )
	Hydraulic diameter, $d_h$	1.70 (mm)
	Length, $L$	258 (mm)
	Port diameter, $d_p$	6 (mm)
	Port to port length, $L_p$	228 (mm)
	Pressing depth, $b$	1 (mm)
	Width, $W$	50 (mm)
	Thickness, $t$	0.15 (mm)

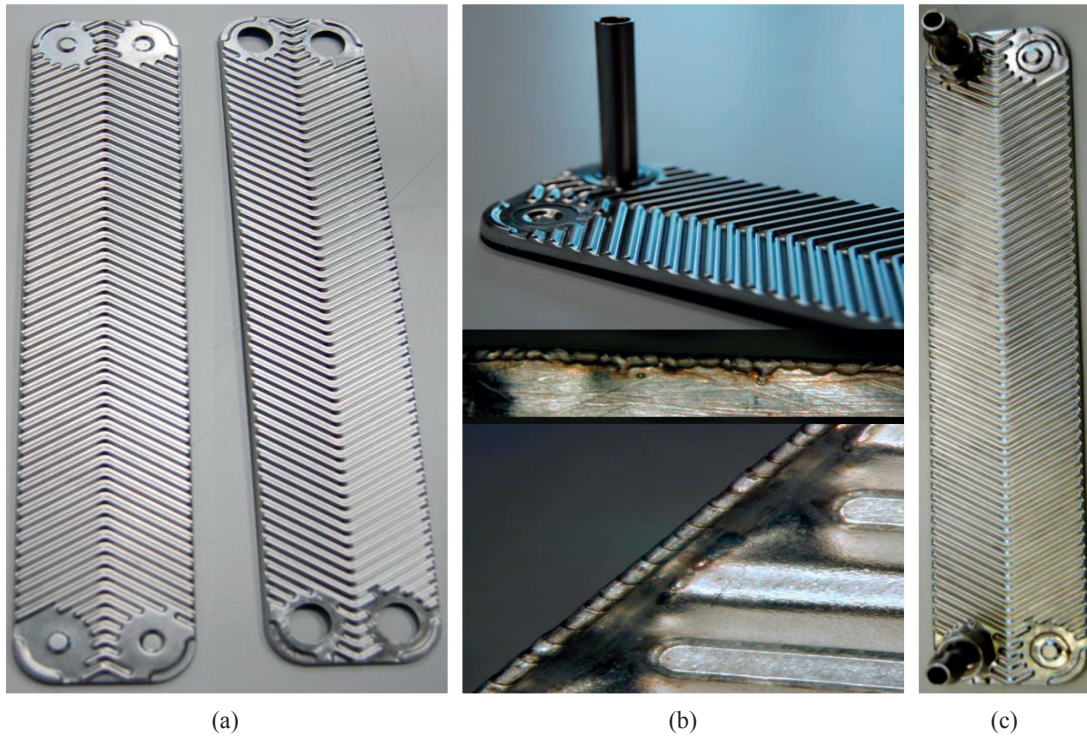


Figure 3.5: Plate heat exchanger prototype: (a) chevron test plate before assembling, (b) after applying laser welded technique, (c) test section with inlet and outlet pipes.

Figure 3.6a depicts the PVC supporting frame designed to enclose, support and insulate these two plates during the experimental tests. Six “windows” on the frame surface were machined to allow visual access for local thermal measurements by the infrared camera. Finally, the test section was coated with high emissivity black paint and then insert in a box in order to avoid any parasite radiation phenomena. Figure 3.6b shows the back view of the plate prototype, in which, the electrical current was applied directly into the plates using two clamps in order to create a uniform heat flux. The electric current is assumed to uniformly heat the two plates due to the electrical circuit between the two clamps as well as the small electrical resistance of the plates ( $< 1\Omega$ ), which required a high electrical current to provide the desired input power. The effect of the resistance of the welded perimeter of the two plates was assumed to be negligible with respect to the central windows.

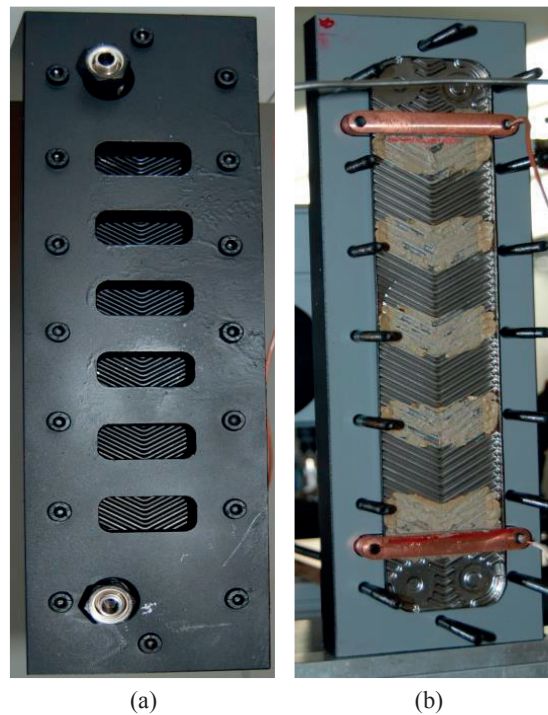


Figure 3.6: Photograph of the compact plate heat exchanger: (a) front view of the test section enclosed in a PVC support with the inlet and outlet pipes to be connected to the main loop, (b) back view of the evaporator with the two visible clamps before closing the supporting frame.

### 3.4 Experimental procedure

During the tests, the saturation temperature of the refrigerant at the inlet of the test section was maintained at a specified value setting the temperature of reservoir thermal bath, according to the pressure drops in the system. Depending on the test conditions, the desired

subcooling or vapor quality at the inlet of the test section was achieved by controlling the electrical power in the preheater. In the same way, the direct electrical heating was adopted to promote the boiling process of the refrigerant within the plate heat exchanger. In Table 3.2 and Table 3.3 a complete overview of the experimental parameters is reported in case of single- and two-phase flow respectively.

Table 3.2: Experimental single-phase operating conditions.

Parameter	Range
Fluid temperature	21 – 25.50 (°C)
Heat flux	74 – 3478 (Wm <sup>-2</sup> )
Mass flux	8 – 384 (kgm <sup>-2</sup> s <sup>-1</sup> )
Prandtl number	4.90 – 6.50
Refrigerant	R245fa, R236fa
Reynolds number	34 – 1615
Total heat transfer data points	85
Total pressure drop data points	146

Table 3.3: Experimental two-phase operating conditions.

Parameter	Range
Heat flux	225 – 4060 (Wm <sup>-2</sup> )
Inlet saturation temperature	19 – 35 (°C)
Inlet subcooling	0.5 – 1.0 (°C)
Inlet vapor quality	0.10 – 0.25
Mass flux	10 – 85 (kgm <sup>-2</sup> s <sup>-1</sup> )
Outlet vapor quality	0.05 – 0.90
Refrigerant	R245fa
Total heat transfer data	345
Total pressure drop data	650

Consequently, to carry out an experiment at a fix value of refrigerant mass flow rate, the speed of the pump was adjusted until the steady-state condition of the test facility was reached. Based on the type of experiment, a range between 10/20 minutes for single-phase and 60/90 minutes for two-phase flow was needed to reach statistically the steady state condition. Then, the data acquisition system started to scan all the data channels, in which 100 acquisitions were made in 0.1 seconds and the mean values of these measurements were calculating during the acquisition time and employed to process the data. For the present

experimental study, several tests have been carried out: single-phase heat transfer, single-phase pressure drop, saturated flow boiling, flow boiling and two-phase pressure drop.

### 3.5 Uncertainty analysis

In order to estimate the uncertainties of the experimental results, a summary of the accuracy of the measured parameters has to be specified and the details are reported in Table 3.4.

The accuracy was evaluated taking into consideration the fixed error (B) and random error (D), where the first is commonly defined during the calibration process, while the second is the precision coming from the measurements. Furthermore, the random error is experimentally evaluated as the multiplication of the coverage factor (for 95% level of confidence,  $\omega = 2$ ) and standard deviation.

Table 3.4: Summary of the measured parameters accuracy.

Parameter	Type of sensor	Range	Accuracy
Absolute Pressure	Pressure transducer	0 – 4 (bar)	$\pm 0.015\%$
Current	Power supply	10 – 69 (A)	$\pm 0.9\%$
Differential pressure	Pressure transducer	0 – 0.5 (bar)	$\pm 20$ (Pa)
Dimensions	Caliper	0.01– 300 (mm)	$\pm 0.005$ (mm)
Fluid temperature	Thermocouple	10 – 60 (°C)	$\pm 0.08$ (°C)
Mass flow rate	Coriolis flow meter	0.0004 – 0.00192 (kgs <sup>-1</sup> )	$\pm 0.5\%$
Voltage	Power supply	0.56 – 1.62 (V)	$\pm 0.05\%$
Wall temperature	IR camera (calibrated)	10 – 60 (°C)	$\pm 0.15$ (°C)

The uncertainties of the properties of the refrigerants determined by REFPROP 9.0 were defined as listed: 3% for liquid dynamic viscosity, 4% for vapor dynamic viscosity, 0.375% for enthalpy, 0.05% for density, 0.75% for specific heat at constant pressure and 5% for liquid thermal conductivity. The uncertainty was then calculated as the Euclidian norm of these two errors and expressed as follows:

$$\delta E_i = \sqrt{B_i^2 + D_i^2} = \sqrt{B_i^2 + (\omega \cdot \theta)^2} \quad (3.1)$$

The approach proposed by Kline and McClintock (1953) was applied to characterize the propagation of errors from the measured parameters until the final results. First, for each parameter (R), a function of several variables which influence the final calculation of R has to be defined:

### 3.5 Uncertainty analysis

$$R_i = R_i(X_1, X_2, \dots, X_n) \quad \text{for } i = 1, \dots, n \quad (3.2)$$

Secondly, the effect of the uncertainty of the single variable is the partial derivative of the parameter R with respect to that single variable. The global uncertainty of R was obtained by summing the single uncertainty ( $\delta U_i$ ) of the variable involved in the eq. 2, as follows:

$$\delta R_i = \sqrt{\left(\frac{\partial R}{\partial X_1} \cdot \delta E_1\right)^2 + \left(\frac{\partial R}{\partial X_2} \cdot \delta E_2\right)^2 + \dots + \left(\frac{\partial R}{\partial X_n} \cdot \delta E_n\right)^2} \quad \text{for } i = 1, \dots, n \quad (3.3)$$

Table 3.5: Estimated uncertainty of the final single-phase results.

Calculated parameter	Range	Accuracy
Fanning friction factor	1.60 – 19.50	$\pm 0.3 - 9.4\%$
Frictional pressure drop	232 – 58695 (Pa)	$\pm 0.08 - 9.4\%$
Heat flux	74 – 3478 ( $\text{Wm}^{-2}$ )	$\pm 3.2 - 4.4\%$
Heat transfer coefficient	65 – 1996 ( $\text{Wm}^{-2}\text{K}^{-1}$ )	$\pm 10.7 - 24.8\%$
Mass flux	8 – 384 ( $\text{kgm}^{-2}\text{s}^{-1}$ )	$\pm 0.70\%$
Nusselt number	1.30 – 39	$\pm 11.8 - 25.3\%$
Prandtl number	4.90 – 6.50	$\pm 5.9\%$
Reynolds number	34 – 1615	$\pm 3.1\%$
Temperature difference between wall and fluid	0.70 – 3.20 ( $^{\circ}\text{C}$ )	$\pm 10.1 - 24.6\%$
Thermal power	2 – 77 (W)	$\pm 4.1 - 5.7\%$

Table 3.6: Estimated uncertainty of the final two-phase results.

Calculated parameter	Range	Accuracy
Effective power in the test section	4.5 – 81.2 (W)	$\pm 1.2 - 1.4\%$
Fluid temperature	18.9 – 34.9 ( $^{\circ}\text{C}$ )	$\pm 0.19\%$
Fluid pressure measured by infrared camera	1.1 – 3.8 (bar)	$\pm 0.5\%$
Frictional pressure drop	2900 – 33677 (Pa)	$\pm 0.3 - 2.4\%$
Heat flux	225 – 4060 ( $\text{Wm}^{-2}$ )	$\pm 1.2 - 1.4\%$
Heat loss	1 – 30.6 (W)	$\pm 1.7 - 4.1\%$
Heat transfer coefficient	1250 – 4800 ( $\text{Wm}^{-2}\text{K}^{-1}$ )	$\pm 5.6 - 20.9\%$
Input power	5.5 – 111.8 (W)	$\pm 0.9\%$
Inlet vapor quality	-0.05 – 0.25	$\pm 0.1 - 21.9\%$
Mass flux	10 – 85 ( $\text{kgm}^{-2}\text{s}^{-1}$ )	$\pm 0.7\%$
Outlet vapor quality	0.05 – 0.90	$\pm 1.6 - 3.4\%$
Temperature difference wall and fluid	0.7 – 2.9 ( $^{\circ}\text{C}$ )	$\pm 5.5 - 20.8\%$

Finally, the minimum and maximum values of the total uncertainty of the all calculated parameters was expressed in percentage and reported in Table 3.5 for single-phase results and Table 3.6 for two-phase flow results respectively.

It has to be pointed out that, the previous equations are valid under the following assumptions:

- The uncertainties ( $\delta U_i$ ) of the single variables have to include, both, systematic and random errors.
- The distribution of the measurements has to follow a Gaussian trend, and normally this can be determined, when the experimental campaign includes more than 30 measurements.
- The uncertainties of each variables are independent of one other.
- In the evaluation of the accuracy of the equipment, the random error has to be calculated imposing the same level of confidence. In the present work, 95% of the confidence, at which corresponds a coverage factor equal to 2, was chosen.

### 3.6 Data reduction technique

In the current study, the hydraulic diameter, mass flux and heat transfer area are required. The equation adopted to calculate the heat transfer area took into account the two heated surfaces as well as the enhancement surface heat transfer, and thus the enlargement factor was also involved.

$$d_h = \frac{2 \cdot b}{\varphi} \quad (3.4)$$

$$G = \frac{m}{A_c} = \frac{m}{b \cdot W} \quad (3.5)$$

$$A_{ht} = 2 \cdot L_{ht} \cdot W_{pro} = 2 \cdot \varphi \cdot L_{ht} \cdot W \quad (3.6)$$

The total pressure drop measured by the pressure transducers across the plate heat exchanger, was the summation of pipes, ports, static, momentum and frictional pressure drop and it was expressed as follows:

$$\Delta p_{tot} = \Delta p_{pipe} + \Delta p_p + \Delta p_{sta} + \Delta p_{mom} + \Delta p_{fri} \quad (3.7)$$



The pipe term took into account the loss from the inlet and outlet pressure gauge to the test section and it was evaluated using homogeneous model for in-pipe flow. In case of single-phase flow, the liquid only Reynolds number was implemented, while for two-phase flow the Reynolds number, based on the Cicchitti et al. (1960a) two-phase viscosity, was adopted.

$$f_{pipe} = 16.000 \cdot \text{Re}^{-1} \quad \text{for } \text{Re} \leq 2000 \quad (3.8)$$

$$f_{pipe} = 0.079 \cdot \text{Re}^{-0.25} \quad \text{for } \text{Re} > 2000 \quad (3.9)$$

The port pressure drop took into consideration sudden contraction, flow division at the inlet as well as sudden expansion and flow merging at the outlet and it was calculated applying the approach suggested by Shah and Focke (1988).

$$\Delta p_p = \Delta p_{p,in} + \Delta p_{p,out} = 0.75 \cdot \left[ \frac{G_p^2}{2 \cdot \rho_{in}} + \frac{G_p^2}{2 \cdot \rho_{out}} \right] \quad (3.10)$$

The static pressure drop was due to the gravity effect for vertical refrigerant flow and was evaluated based on the liquid density for single-phase tests, while for two-phase experiments the definition of two-phase homogeneous density was adopted:

$$\Delta p_{sta} = \rho_m \cdot g \cdot L_p \quad (3.11)$$

$$\rho_m = \left[ \frac{x}{\rho_v} + \frac{1-x}{\rho_l} \right]^{-1} \quad (3.12)$$

The momentum pressure loss took into consideration the acceleration of the flow, due to the increasing of the vapor quality from the inlet to outlet of the plate heat exchanger. This term was quantified according to the homogeneous flow model scheme and was active only in case of flow boiling experiments:

$$\Delta p_{mom} = G^2 \cdot \left[ x_{out} \left( \frac{1}{\rho_{v,out}} - \frac{1}{\rho_{l,out}} \right) - x_{in} \left( \frac{1}{\rho_{v,in}} - \frac{1}{\rho_{l,in}} \right) \right] \quad (3.13)$$

Furthermore, the frictional pressure drop was determined by subtracting all the components mentioned in the eq. 4 from the total (measured) pressure drop and then, the two-phase Fanning friction factor was also defined:

$$f = \frac{\Delta p_{fri} \cdot d_h \cdot \rho_m}{2 \cdot L_p \cdot G^2} \quad (3.14)$$

During the single-phase heat transfer experiments, the input power was calculated performing an energy balance through the test section:

$$\dot{Q}_{eff} = \dot{q}_{eff} \cdot A_{ht} = \dot{m} \cdot c_p \cdot (T_{f,out} - T_{f,in}) \quad (3.15)$$

The effective power delivered to the refrigerant flow in the test section was evaluated by subtracting the heat loss from the electrical input power. Next, the heat flux in the test section was introduced, computing the ratio between the effective power and the heat transfer area:

$$\dot{Q}_{eff} = \dot{Q}_{in} - \dot{Q}_{loss} = V \cdot I - \dot{Q}_{loss} \quad (3.16)$$

$$\dot{q}_{eff} = \frac{\dot{Q}_{eff}}{A_{ht}} \quad (3.17)$$

In case of saturated boiling experiments, the inlet vapor quality was defined according to the measured inlet subcooling, while for flow boiling tests this was computed by performing an energy balance overall the preheater:

$$x_{in} = \frac{\dot{m} \cdot c_p \cdot (T_{f,in} - T_{sat,in})}{\dot{m} \cdot i_{lv}} \quad (3.18)$$

$$x_{in} = \frac{\dot{m} \cdot c_p \cdot (T_{f,in,preh} - T_{sat,in}) + \dot{Q}_{eff,preh}}{\dot{m} \cdot i_{lv}} \quad (3.19)$$

On the other hand, the outlet vapor quality was estimated performing an energy balance overall the plate heat exchanger:

$$x_{out} = x_{in} + \frac{\dot{Q}_{eff}}{\dot{m} \cdot i_{lv}} \quad (3.20)$$

The local surface temperatures of the plate was measured by a self-calibrated infrared camera and were each an average value from 1000 sequential frames, corresponding to 20 seconds of video at a fix acquisition frequency of 50 Hz. During the single-phase tests, the local fluid temperature was evaluated performing a local energy balance from inlet to the outlet of the test section:



$$T_{f,out}(z) = T_{f,in} + \frac{Q_{eff} \cdot z}{m \cdot c_p \cdot L_{eff}} \quad (3.21)$$

On the other hand, in two-phase flow scenario, the local fluid temperatures were determined according to the local refrigerant pressure, which was carried out through a set of adiabatic two-phase flow experiments. In this case, the wall temperatures were supposed to be equal to the fluid temperatures and using the saturation curve of the refrigerant the pressure field was obtained:

$$p_{f,out}(z) = p_{f,in}(z) - \Delta p_{fri,meas}(z) - \Delta p_{mom}(z) - \Delta p_{sta}(z) \quad (3.22)$$

The local saturation temperature of the refrigerant was dependent on the local absolute pressure:

$$T_f(z) \propto p_f(z) \quad (3.23)$$

Finally, according to the previous statements, the local heat transfer coefficient was evaluated as follow:

$$h(z) = \frac{q_{eff}}{T_w(z) - T_f(z)} \quad (3.24)$$

### 3.7 Conclusions

The test facility presented in this chapter was flexible and able to test refrigerants over a wide range of operating conditions (but not at high pressures due to the method of construction of the prototype). Several types of experiments have been carried out: single-phase, saturated boiling, flow boiling and two-phase pressure drop. The present plate heat exchanger prototype provided higher thermal performance and compactness (about 3-5 times) than convectional plate heat exchangers and was fabricated with high chevron angle, small pressing depth (mean spacing between two plates) and corrugation pitch. The single- and two-phase experimental campaigns have been listed and the associated uncertainties of the final results have been also provided. A complete data reduction technique was introduced in order to evaluate the local pixel-by-pixel heat transfer coefficient and pressure drops overall the plate heat exchanger.

## **CHAPTER 4 – Single phase results**

### **4.1 Introduction**

This chapter presents the test results obtained from the single-phase experiments. First of all, the infrared camera was pixel-by-pixel self-calibrated within the experimental range and the technique adopted is fully detailed. The pressure drop and heat transfer measurements have been validated and the mean trends against Reynolds and Prandtl numbers have been investigated. Next, the energy balance through the preheater and plate heat exchanger to characterize the heat losses is also described. Finally, the local pixel-by-pixel heat transfer coefficients and the quasi-local heat transfer coefficient results have been reported and the effect of mass flux, heat flux, inlet temperature, type of refrigerant and local plate coordinates on the thermal performance are here addressed.

### **4.2 Infrared temperature measurements**

As presented in chapter 3 of the present thesis, the surface temperatures of the plate have been measured with an infrared camera, which was self-calibrated. The infrared camera calibration process was performed in order to correct several factors which can affect the temperature measurements, such as: inclination angle between the infrared camera and the test section and its corrugations, variation of the local emissivity of the plate and surface roughness.

To perform these calibration tests, a set of adiabatic subcooled experiments was performed in which the temperature of the refrigerant at the inlet and outlet of the test section were measured by two calibrated thermocouples and the average value was considered the reference temperature in this process. To cover the whole experimental range, several conditions were tested where the liquid refrigerant inlet temperature was controlled by adjusting the input power of the preheater. The pixel-by-pixel plate temperatures were measured directly by the infrared camera. The turbulent flow regime was ensured during the entire calibration campaign to guarantee a uniform isothermal condition; very small temperature differences between the inlet and outlet reference temperatures were achieved

(less than 0.2 K). It has to be pointed out that the heat loss due to natural convection was negligible since the plate heat exchanger was insulated by a PVC frame box, and only six small “windows” were exposed to the ambient. Furthermore, the entire plate heat exchanger was also inserted into a closed box that reduced even more the losses due to the natural convection. The specifications of the infrared camera are listed in Table 4.1.

Table 4.1: Key features of the infrared camera (Flir SC645).

Parameter	Value
Acquisition frequency	50 (Hz)
Area of a pixel	0.333 x 0.331 (mm <sup>2</sup> )
Detector type	FPA, uncooled microbolometer
Distance to the test section	480 (mm)
Field of view	25 x 18.8 (°)
Infrared resolution	640 x 480 (pixels)
Number of frames	1000
Minimum focus length	400 (mm)

The infrared camera was self-calibrated over the range from 20 °C to 40 °C with an accuracy of 0.15 °C. During these tests, the fluid temperature was controlled to be greater than the room temperature in order to avoid condensing moisture on the surface of the plate heat exchanger. Figure 4.1 illustrates the experimental data and the calibration curve for one pixel located in the third “window”.

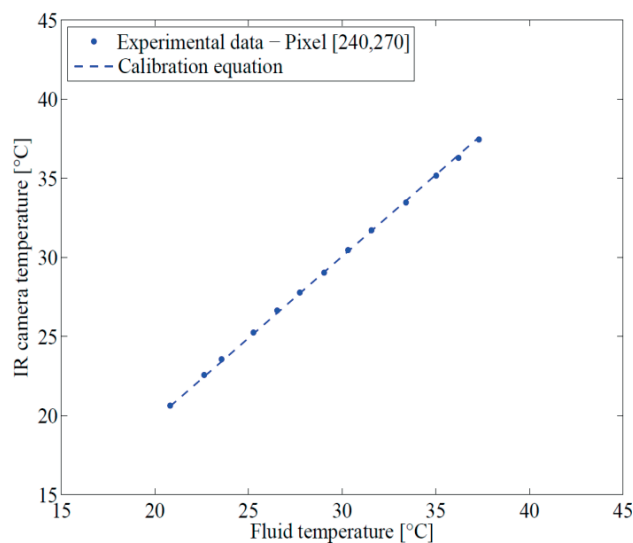


Figure 4.1: Calibration applied to one pixel (row 240 and column 270) located in the third “window” counted from the bottom of the test section.

The corresponding calibration equation in which the coefficients are respectively expressed in  $K^{-1}$  and  $K$  is:

$$T_{IR} = 1.031 \cdot T_f - 9.563 \quad (4.1)$$

In Figure 4.2 the local and average surface temperatures and corresponding standard deviations are plotted versus the number of frames for the same pixel mentioned above. The graphs identified the minimum number of frames needed to reach the steady-state condition. As can be seen 60 frames (1.2 seconds) or more are sufficient to characterize the steady-state conditions. In this study, 1000 frames equivalent to 20 seconds of video were recorded for each test condition and the corresponding average values were used to reduce the experimental data. Due to a very small temperature drop ( $\Delta T \approx 0.02 \text{ }^\circ\text{C}$ ) through the stainless steel thickness at the heat fluxes tested, the measured wall temperature was directly implemented for the heat transfer calculation.

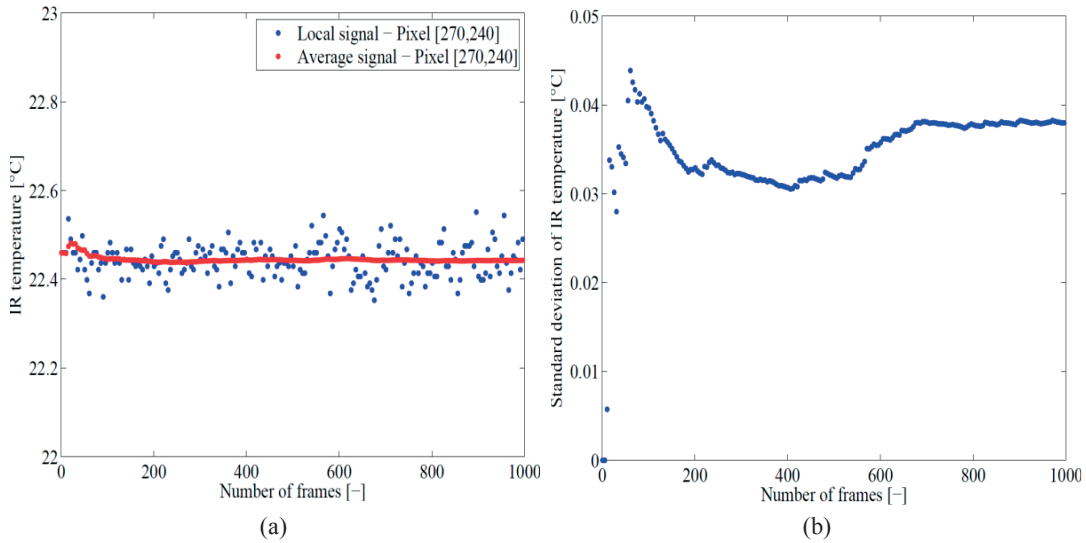


Figure 4.2: Infrared camera measurements referred to one pixel (row 240 and column 270): (a) local and average pixel temperature, (b) standard deviation of the temperature.

## 4.3 Pressure drops

In order to assess the pressure drop measurements, another set of single-phase tests was performed. In this case, subcooled flow of each of the two refrigerants at a defined inlet temperature flowed into the test section under adiabatic conditions. During the experimental

campaign, the mass flow rate was changed and as a consequence a wide range of Reynold numbers from laminar to turbulent flow for both fluids was covered.

Figure 4.3a depicts the trend of the frictional pressure drop versus mass flux for the two test fluids compared at the same conditions. The frictional pressure drop was evaluated by subtracting the pipe, port and static pressure drop from the total measured pressure drop. The pressure loss increased with mass flux and less pressure drop was discovered for R236fa due to the lower shear stress. Such a result may be explained because of the lower viscosity of the R236fa compared to that of R245fa. In Figure 4.3b, each component of pressure drop was normalized with respect to the total pressure drop measured across the plate heat exchanger and plotted against the Reynolds number. For the entire experimental range, the port and pipe pressure drop contributions were less than 1%, and thus can be neglected (these were estimated according to the equations 3.8, 3.9 and 3.10). The static pressure drop plays an important role only at low Reynolds numbers, while upon increasing the mass flux the frictional pressure drop became the major contributor. The reason was due to the fact that the static pressure drop was constant, while the frictional pressure drop increased with the square of the mass flux.

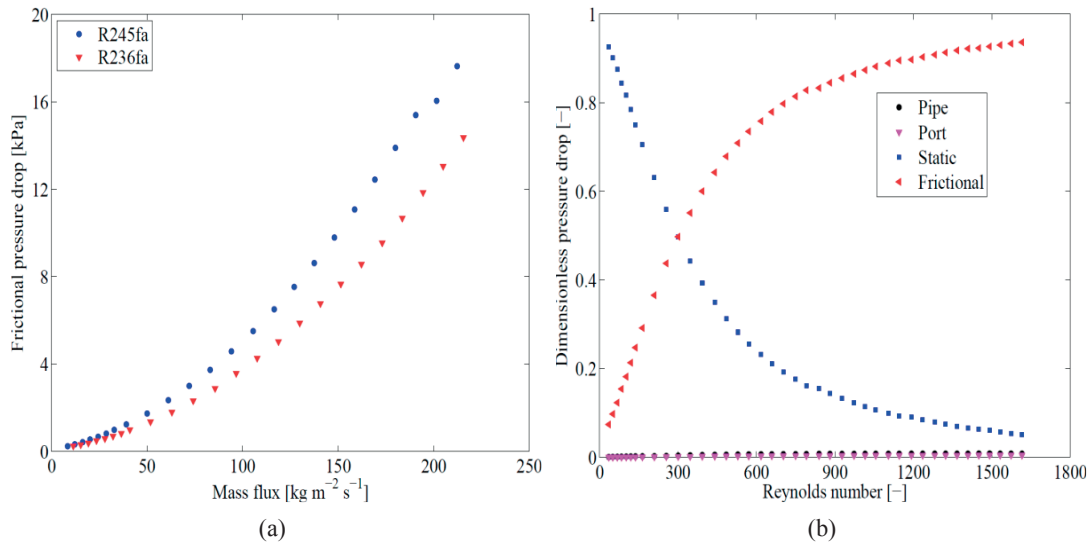


Figure 4.3: Single-phase pressure drop results: (a) effect of mass flux and type of refrigerant on the frictional pressure drop, (b) dimensionless pressure drop contributors against Reynolds number.

As can be seen from Figure 4.4, the Fanning friction decreased with Reynolds number and it was not influenced by the Prandtl number or by the imposed heat flux. Furthermore, the transition between no swirl flow and the swirl flow regime occurred at  $Re = 250$ , while the transition between swirl flow and the fully turbulent flow regime was observed for a

Reynolds number equal to about 1100. The reason for an early transition can be explained because of the complex geometry of the test plate and the V-shape plate corrugation, which promoted local cross flow. The transitions between the different flow regimes were also observed during the single-phase experimental campaign. In fact, at the transition points the mass flow rate as well as the absolute pressure measurements started to oscillate with higher amplitude compared to the conventional signal amplitude. The divergence in the values started at about  $Re = 250$  and this may be due to the onset of unsteady swirl flow. These data will be used in Chapter 5 to develop a friction factor equation that is then useful for characterizing the pressure drops in the short subcooled region in some of the two-phase test conditions in Chapter 6.

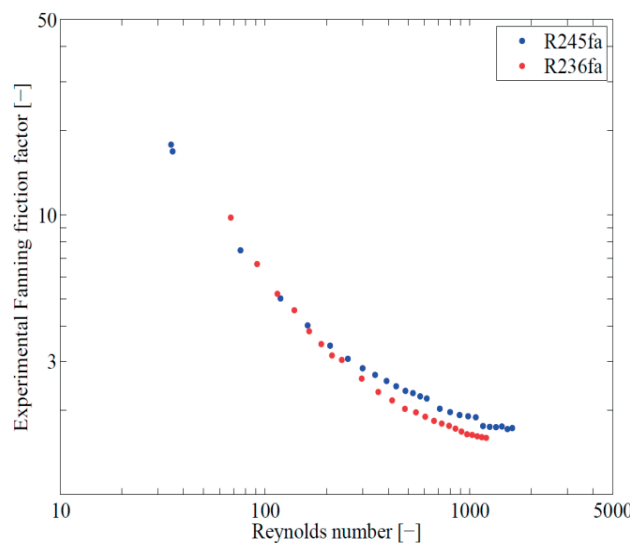


Figure 4.4: Experimental Fanning friction factor versus Reynolds number for both tested fluids.

## 4.4 Energy balance

For the present single-phase database, an energy balance over the test section was conducted in order to estimate the heat losses respectively from the test section and the preheater.

Most of the electrical heat provided by the DC-power supply was transferred to the refrigerant flow, providing an enthalpy increment. The difference between the input power and the effective power was realized as the total heat loss:

$$Q_{loss} = Q_{in} - Q_{eff} = Q_{in} - m \cdot c_p \cdot (T_{f,out} - T_{f,in}) \quad (4.2)$$

The main sources of the thermal losses have been classified as follows: loss through the electrical wires and connections, loss due to natural convection and radiation to the ambient.

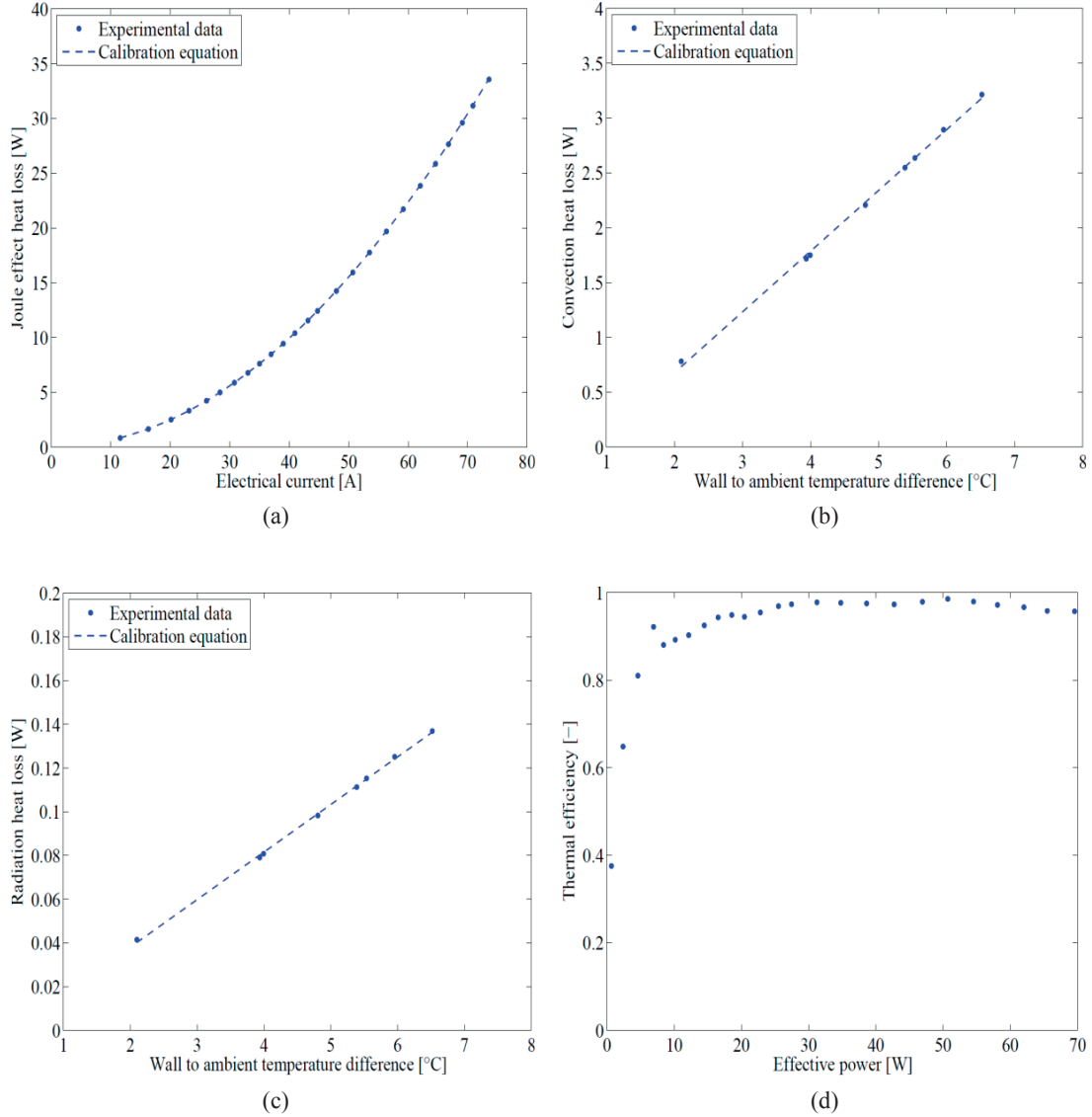


Figure 4.5: Energy balance in the test section and the corresponding results: (a) heat loss due to the Joule effect, (b) heat loss due to the natural convection, (c) heat loss due to the radiation, (d) thermal efficiency of the plate heat exchanger against the effective power.

Figure 4.5a reports the trend of the thermal loss due to the Joule effect against the electrical current. The heat loss due to the Joule effect was experimentally quantified, since the resistance of the cables was estimated by performing a voltage measurement before the test section. A quadratic dependence to the applied electrical current was observed and the calibration equation to predict this loss is also proposed. Moreover, it has to be pointed out

that, to increase the imposed heat flux into the evaporator, the electrical current has to be increased and the maximum value was fixed to  $4100 \text{ Wm}^{-2}$ , according to the maximum suitable temperature of the cabling which was equal to  $85^\circ\text{C}$ .

In Figure 4.5b and Figure 4.5c, the thermal losses due to the natural convection and radiation to the ambient are shown respectively. The first loss was characterized applying the natural convection heat transfer theory to the vertical plate with one heated surface, while the second loss was evaluated adopting the Stefan-Boltzmann radiation heat transfer equation assuming the test section as a black body (worst case). Furthermore, only the surfaces of the six “windows” ( $0.00324 \text{ m}^2$ ) were considered as effective heat transfer area for these two types of heat losses. A linear dependence of these losses versus the wall to ambient temperature difference was discovered and the associated calibration equations were also introduced to estimate such losses. Finally, the equations to predict the total heat loss are:

$$Q_{loss,curr} = 0.0062 \cdot I_{in}^2 \quad (4.3)$$

$$Q_{loss,conv} = 0.554 \cdot \Delta T_{w,a} - 0.430 \quad (4.4)$$

$$Q_{loss,rad} = 0.0218 \cdot \Delta T_{w,a} - 0.00553 \quad (4.5)$$

$$Q_{loss,tot} = Q_{loss,curr} + Q_{loss,conv} + Q_{loss,rad} = 0.0062 \cdot I_{in}^2 + 0.576 \cdot \Delta T_{w,a} - 0.436 \quad (4.6)$$

In Figure 4.5d the thermal efficiency of the test section is shown. Considering the entire experimental range, the major source of the heat loss was attributed to the Joule effect through the electrical wires and connections. On the other hand, the heat loss due to natural convection and radiation were not a function of the effective power and since, the electrical loss was properly involved in the energy balance, an overall thermal efficiency of 95% was achieved for test conditions used in heat transfer experiments in this study.

Following the same procedure, the heat losses from the preheater were quantified and correlated according to the temperature difference between wall and ambient. The results are shown in Figure 4.6a and Figure 4.6b. The major contributors were natural convection and radiation to the ambient, while the electrical Joule effect losses were negligible, giving these expressions:

$$Q_{loss,conv} = 1.770 \cdot \Delta T_{w,a} - 5.885 \quad (4.7)$$

$$Q_{loss,rad} = 0.0285 \cdot \Delta T_{w,a} - 0.00581 \quad (4.8)$$

$$Q_{loss,tot} = Q_{loss,conv} + Q_{loss,rad} = 1.799 \cdot \Delta T_{w,a} - 5.891 \quad (4.9)$$



Later, in the case of two-phase flow tests, the eq. 4.6 and 4.9, have been implemented during the post processing of the experimental data in order to quantify the real power delivered to the refrigerant and perform correctly the energy balance.

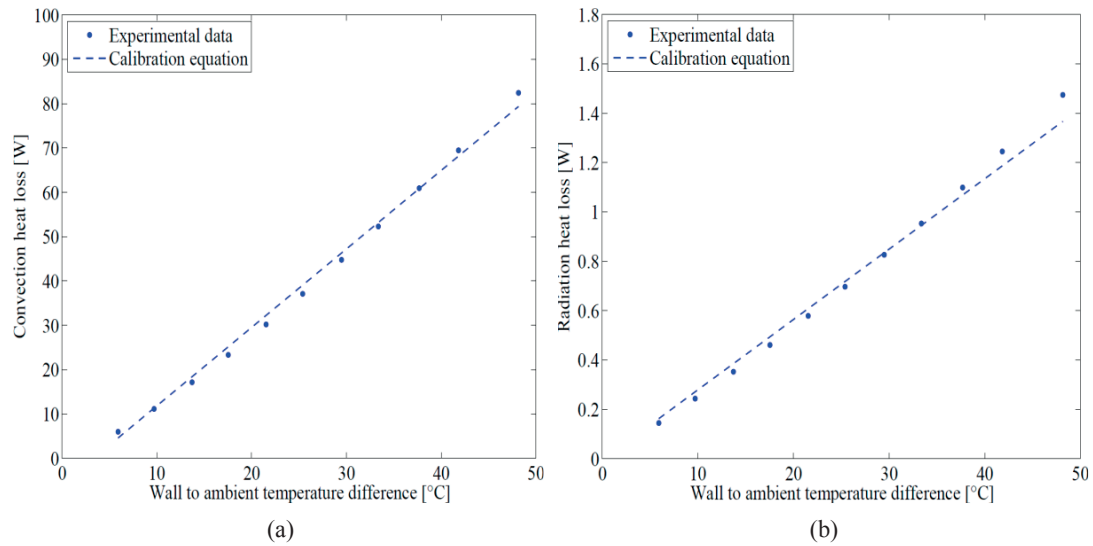


Figure 4.6: Single-phase energy balance in the preheater and the associated results: (a) heat loss due to the natural convection, (b) heat loss due to the radiation.

## 4.5 Mean heat transfer coefficient

To analyze the single-phase thermal performance of the present plate heat exchanger, most experiments have been carried out at a fixed value of the inlet fluid temperature for both refrigerants. In this case, the imposed heat flux as well as the mass flux were adjusted to ensure the same mean Prandtl number between inlet and outlet of the test section.

The mean heat transfer coefficients were obtained by applying Newton's law of cooling, where the heat flux was determined from the net heat transfer absorbed by the refrigerant divided by the area of the plate including its corrugations, while the temperature difference was obtained from the difference between the wall temperature (average over all the pixels temperatures in the six "windows" measured by the infrared camera) and the mean fluid temperature (average between inlet and outlet temperatures of the test section measured by the two thermocouples).

The effect of the Reynolds number is reported in Figure 4.7a, and as expected, the Nusselt number as well as the heat transfer coefficient increased with the Reynolds number. On the other hand, to take into account the effect of the fluid properties, the Prandtl number

was also varied and the results are shown in Figure 4.7b. The Nusselt number increased with a Prandtl number according to the thinner thermal boundary layer as expected, which provided less temperature difference between the surface and the fluid and consequently higher heat transfer performance can be achieved.

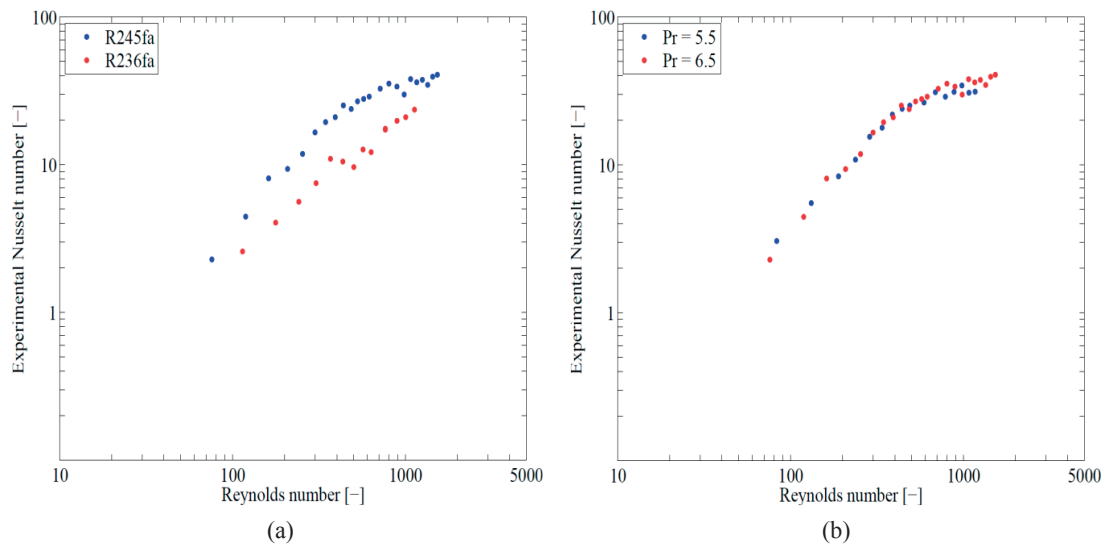


Figure 4.7: Single-phase heat transfer results: (a) Nusselt number versus Reynolds number for the current fluids, (b) Nusselt number versus Reynolds number for two different Prandtl numbers.

Furthermore, the heat transfer coefficient only depended on the mass flux and fluid properties but not the heat flux (all as typical of single-phase tests with small wall to fluid temperature differences). The present experimental database included both laminar and turbulent flows.

## 4.6 Local heat transfer coefficient

The local heat transfer coefficient was evaluated by performing local infrared measurements of the surface temperatures of the plate heat exchanger. In Figure 4.8a and Figure 4.8b, two examples of local (pixel-by-pixel) heat transfer coefficients are depicted.

The local thermal performances were determined for all the pixels contained in the six “windows”, and as can be seen, the heat transfer coefficient increased with respect to the mass flux. Moreover, it has to be pointed out that a large flow maldistribution was observed at low mass fluxes (the inlet and the outlet ports are at the left quadrant of the test section, but below and above the infrared images), which provided higher heat transfer coefficients at the left side of the test plate at the same side as the inlet and outlet ports. Finally, a decrease

in the heat transfer coefficient was discovered next to the inlet and outlet ports, due to the local flow phenomena.

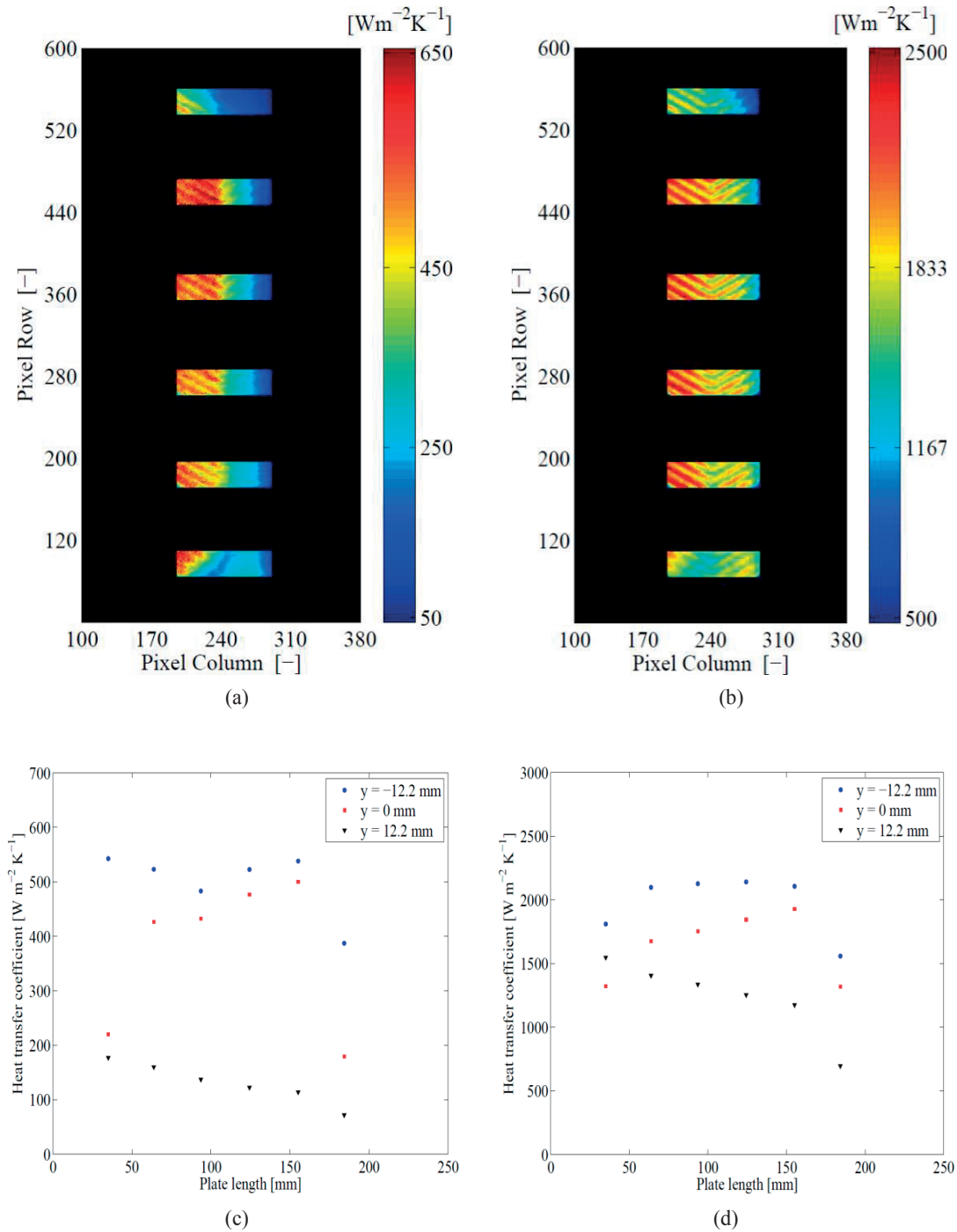


Figure 4.8: Local heat transfer results: (a) heat transfer coefficient map in laminar flow regime for the condition in which  $G = 35 \text{ kg m}^{-2} \text{ s}^{-1}$ ,  $Re = 160$ ,  $q = 350 \text{ W m}^{-2}$  and R245fa, (b) heat transfer coefficient map in turbulent flow regime for the condition in which  $G = 384 \text{ kg m}^{-2} \text{ s}^{-1}$ ,  $Re = 1613$ ,  $q = 3500 \text{ W m}^{-2}$  and R245fa, (c) and (d) the associated average lengthwise heat transfer coefficient versus the length of the plate at the same operating test conditions.

At the same conditions presented in Figure 4.8c, for each “window”, the lengthwise average heat transfer coefficient has been calculated in three different positions along the width of the plate heat exchanger. In particular, the middle of the plate was identified as 0 mm, while the right (far from the ports) and left side (close to the ports) of the plate were taken at  $\pm 12.2$  mm.

As can be observed in Figure 4.8d, the flow maldistribution became less important at higher values of the mass flux, since the refrigerant flow was able to uniformly follow the corrugated sinusoidal path. Furthermore, comparing these two scenarios, the maximum bandwidth in which the heat transfer coefficient varied, was about  $\pm 85\%$  in the first case and  $\pm 50\%$  in the second case. Hence, the general idea that plate heat exchangers provide uniform and ideal counter-current heat transfer is not true. In other single-phase studies usually only mean values are reported that ignore the inlet and outlet influences as being negligible.

Figure 4.9 illustrates the effect of plate length, mass flux, heat flux, fluid temperature and type of refrigerant on the quasi-local heat transfer coefficient. Particularly, for each “window” only one heat transfer coefficient was obtained, which represented an average value over all the pixels, and thus it was named the quasi-local heat transfer coefficient.

Figure 4.9a shows that with rising mass flux, the quasi-local heat transfer coefficient increased due to an enhancement of the convective heat transfer mechanism. Figure 4.9b proved that the quasi heat transfer coefficient is not sensitive to the average imposed heat flux, according to the single-phase heat transfer theory. In Figure 4.9c the quasi-local heat transfer coefficient versus plate length for two different fluid temperature is reported. Basically, the heat transfer coefficient increased with a decreasing of fluid temperature due to the smaller value of the refrigerant thermal conductivity. Furthermore, in Figure 4.9d the effect of the refrigerant is also depicted. As can be observed, the R245fa provided higher heat transfer coefficients because its thermal conductivity is about 20% greater than R236fa at the same conditions.

Finally, looking at the effect of plate length, conclusions similar to above were stated, because in all proposed cases, the quasi-local heat transfer coefficients were lower close to the inlet and outlet ports, while its value increased in the middle of the plate.

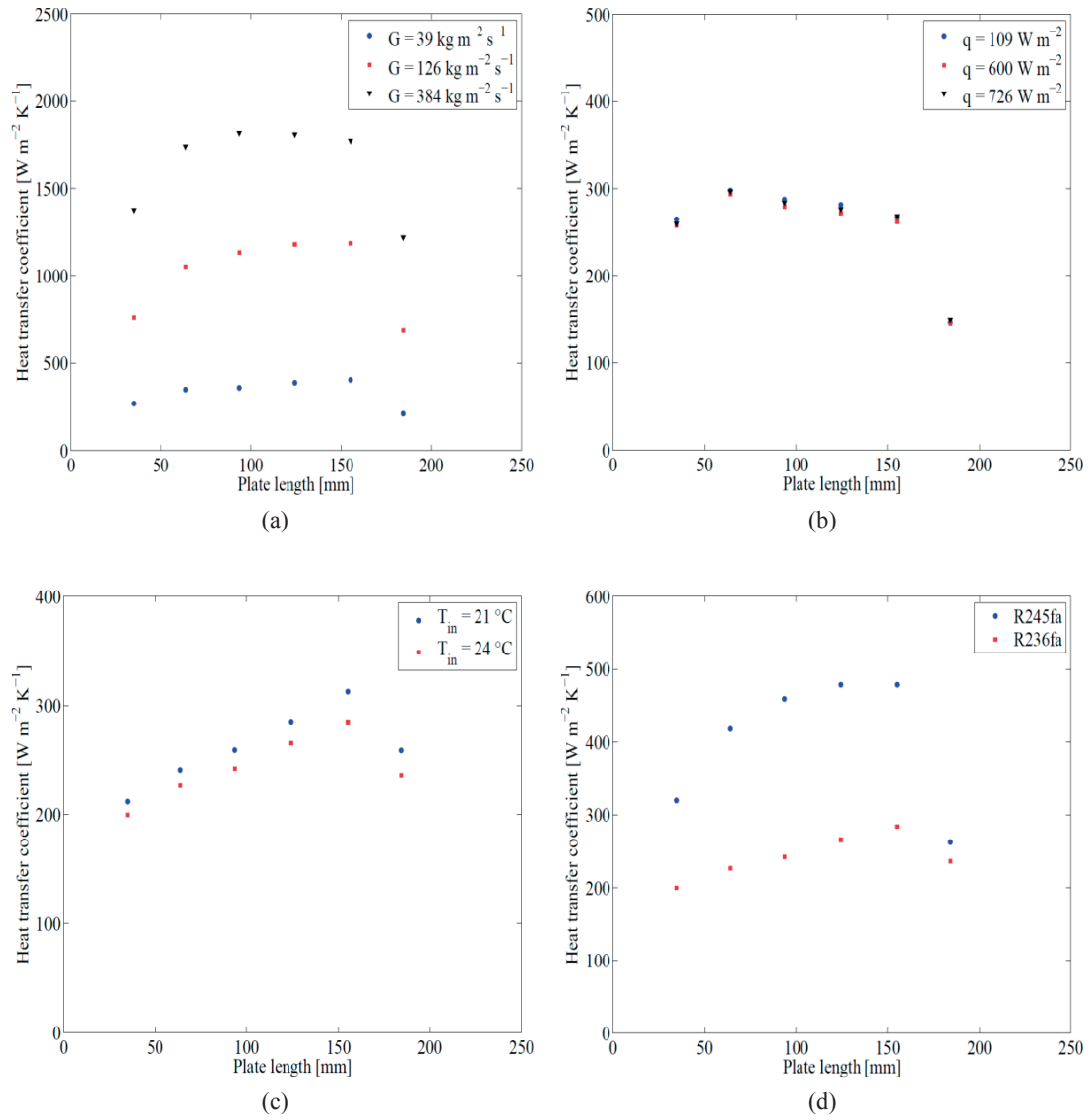


Figure 4.9: Effect of main experimental parameters on the quasi-local heat transfer coefficient: (a) effect of mass flux for  $T_{\text{in}} = 24^\circ\text{C}$ ,  $q = 600 \text{ W m}^{-2}$  and R245fa, (b) effect of heat flux for  $T_{\text{in}} = 24^\circ\text{C}$ ,  $G = 30 \text{ kg m}^{-2} \text{s}^{-1}$  and R245fa, (c) effect of fluid temperature  $G = 50 \text{ kg m}^{-2} \text{s}^{-1}$ ,  $q = 295 \text{ W m}^{-2}$  and R236fa, (d) effect of type of refrigerant for  $T_{\text{in}} = 24^\circ\text{C}$ ,  $G = 50 \text{ kg m}^{-2} \text{s}^{-1}$  and  $q = 420 \text{ W m}^{-2}$ .

## 4.7 Conclusions

Fine resolution infrared measurements of single-phase flow of refrigerant in a novel compact plate heat exchanger were implemented to analyze mean/local thermal and hydraulic performance. The frictional pressure drop rose with mass flux and when employing R245fa rather than R236fa. For the entire experimental range of Reynolds numbers, the major

pressure losses were due to the static and frictional terms, while the port and pipe contributions represented only 1% of the total measured pressure drop. The Fanning friction factor was only a function of Reynolds number, while it was not influenced by the Prandtl number or the imposed heat flux. In particular, the Fanning friction factor decreased with Reynolds number with different slopes according to three different flow regimes: undisturbed no swirl flow, steady swirl flow and fully turbulent flow. A complete single-phase characterization of the present experimental setup was provided, the thermal losses were identified and the calibration correlations were also developed, in order to calculate the effective power delivered to the refrigerant flow in the future two-phase tests. Basically, the heat loss due to Joule effect was linked with electrical current, while the heat transferred to the ambient by natural convection and radiation were correlated according to the temperature difference between the wall and ambient. The average heat transfer coefficients were taken over all the test section and the main trends were also presented. In particular, the Nusselt number increased with increasing Reynolds and Prandtl numbers, while it was insensitive to the imposed heat flux. Performing local infrared temperature measurements, the trends of the local heat transfer coefficient against the main involved parameters were also analyzed in this study. The local heat transfer coefficient increased with mass flux, decreased with inlet fluid temperature and it was not a function of the imposed heat flux. Higher heat transfer rates were achieved using R245fa instead of R236fa. Additionally, lower values of the local heat transfer coefficients were obtained close to the inlet and outlet ports due to the local flow phenomena.

## CHAPTER 5 – Single phase prediction methods

### 5.1 Introduction

In this chapter the experimental single-phase pressure drop and heat transfer database, presented in chapter 4, have been compared against 70 prediction methods available in the open literature. Next, the pressure and temperature measurements have been validated to ensure proper functioning of the experimental apparatus. Finally, a new set of correlations to predict mean and local thermal and hydraulic performance of the novel plate prototype have been also provided.

### 5.2 Frictional pressure drop

The following heat transfer and pressure drop comparisons, between the current experimental databank and the literature prediction methods from literature, are classified according to the definition of the mean error, the mean absolute error and the percentage of data predicted within a bandwidth of 20% and 30%.

The frictional pressure drop database has been validated against 23 literature correlations and the relevant results are summarized in Table 5.1.

$$\delta = \frac{100}{n} \sum_{i=1}^n \frac{\Upsilon_{i,pre} - \Upsilon_{i,exp}}{\Upsilon_{i,exp}}, \quad |\delta| = \frac{100}{n} \sum_{i=1}^n \left| \frac{\Upsilon_{i,pre} - \Upsilon_{i,exp}}{\Upsilon_{i,exp}} \right|, \quad \xi = n \pm 20\%, \quad \Upsilon = n \pm 30\% \quad (5.1)$$

Table 5.1: Predicted single-phase Fanning friction factor against the frictional pressure drop database.

Prediction method (n = 146)	\delta %	\delta%	\xi%	\Upsilon%
Focke et al. (1985)	29	-29	30.1	52.1
Hayes et al. (2012a)	23.7	-16.3	61	75.3
Leuliet et al. (1990b)	41.6	41.3	34.9	45.2
Martin (1996a)	32.2	30.5	35.6	46.2
Proposed model	8.2	-2.6	100	100

The correlations from the literature were extrapolated to a small pressing depth of the current test section ( $b = 1$  mm) and they were able to estimate the correct trend of the experimental data but varying accuracy, indicating the proper functioning of the test facility. A discrete agreement between the experimental data and the predicted values was reached adopting the correlations provided by Martin (1996a), Focke et al. (1985) and Hayes et al. (2012a).

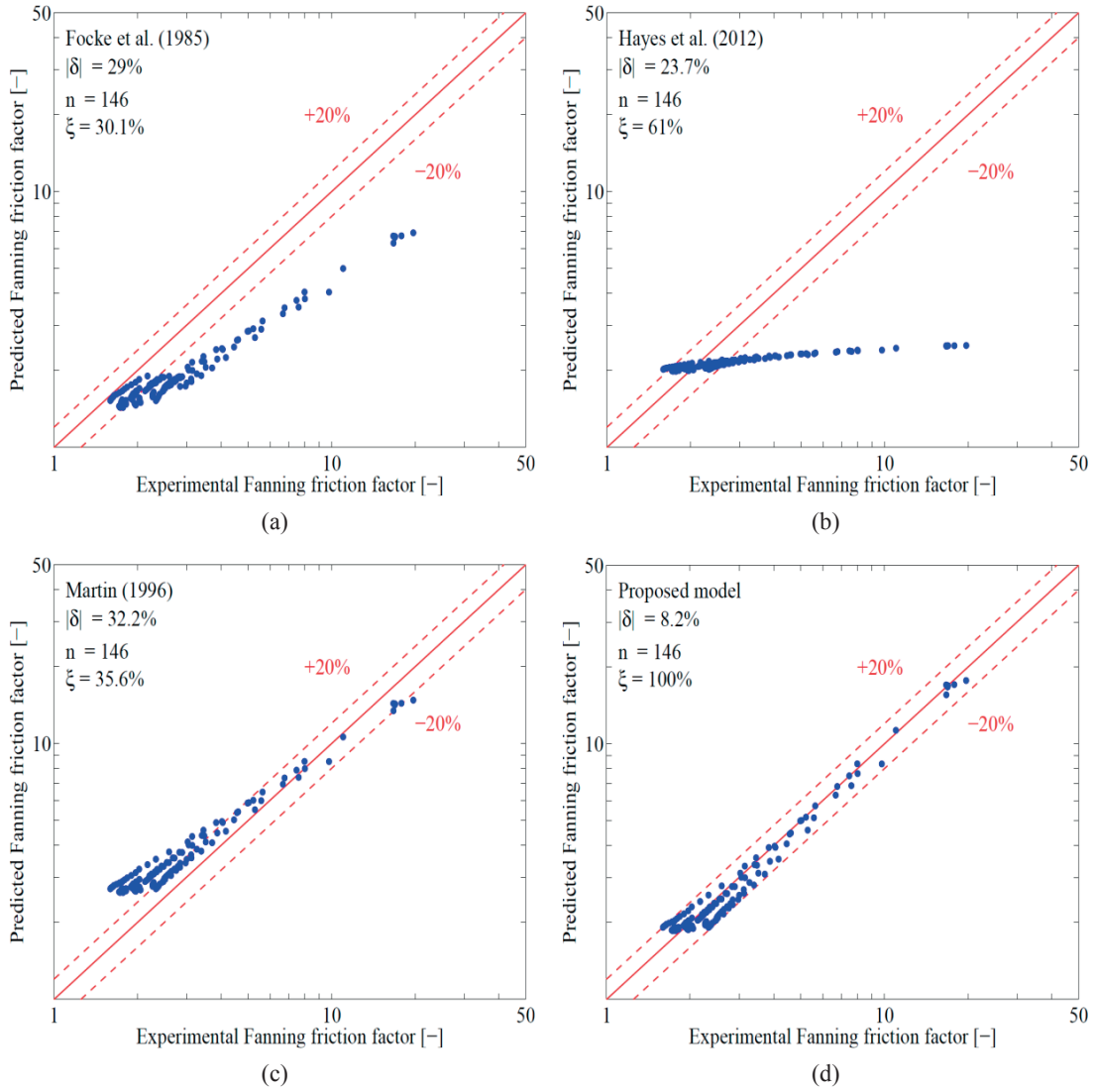


Figure 5.1: Single-phase experimental Fanning friction factor predicted by different prediction methods: (a) Focke et al. (1985), (b) Hayes et al. (2012a), (c) Martin (1996a), (d) proposed model.

The results are respectively displayed in Figure 5.1a, Figure 5.1b and Figure 5.1c. In Figure 5.1d, a new correlation was proposed, based on the nonlinear multi regression



technique to the main dimensionless parameters which was able to predict the entire single-phase pressure drop database (146 experimental data points) with a mean absolute error of 8.2% and mean error of -2.6% within a bandwidth of 20%:

$$f = 1285 \cdot \text{Re}^{-1.25} + 1.73 \quad (5.2)$$

The Fanning friction factor was only dependent on the Reynolds number, while was not function of the Prandtl number and the imposed heat flux. The present correlation is not in the format of a general use correlation, as it will only be used later here in the two-phase heat transfer calculation to predict the local frictional pressure drop of the refrigerants in the subcooled liquid region in the two-phase tests with inlet subcooling.

### 5.3 Mean heat transfer coefficient

The mean heat transfer database, that included 85 experimental data points, has been assessed against 37 literature methods and only few correlations were able to predict the current set of data. In Table 5.2 the comparison between experimental and predicted heat transfer data for both refrigerants is reported.

Table 5.2: Predicted single-phase Nusselt number against the heat transfer database.

Prediction method (n = 85)	$ \delta %$	$\delta\%$	$\xi\%$	$\Upsilon\%$
Han et al. (2003b)	63.6	63.6	24.7	36.5
Jokar et al. (2006b)	39	35.6	41.2	48.2
Kovalenko and Maslov (1970)	29.3	10.7	51.8	67.1
Martin (1996a)	72.5	72.5	20	32.9
Muley et al. (1999b)	33.3	13.9	36.5	61.2
Rene et al. (1991b)	70	70	12.9	30.6
Proposed model	11.3	-1.8	89.4	97.6

As can be seen from Figure 5.2, most of the prediction methods overestimated the current database for this test section with a small pressing depth and the best predictions were achieved using the correlation proposed by Jokar et al. (2006b), Kovalenko and Maslov (1970) and Muley et al. (1999b). Following the same procedure as mentioned in the pressure drop analysis, in the case of the heat transfer data, a new prediction method was also provided for no swirl flow and steady swirl up to fully turbulent flow regimes respectively, taking into consideration a transition at Reynolds number equal to about 700:

$$Nu_m = (0.0295 \cdot Pr - 0.115) \cdot Re^{0.954} \quad \text{for } Re < 700 \quad (5.3)$$

$$Nu_m = (1.760 \cdot Pr - 5.391) \cdot Re^{0.262} \quad \text{for } Re > 700 \quad (5.4)$$

According to the results provided in chapter 4, the Nusselt number was only dependent on the Reynolds and Prandtl numbers, while was regardless of the imposed heat flux. The new model predicted the data with a mean absolute error of 11.3% and mean error of -1.8, while 89.4% and 97.6% of the current database fit in a bandwidth of 20% and 30% respectively.

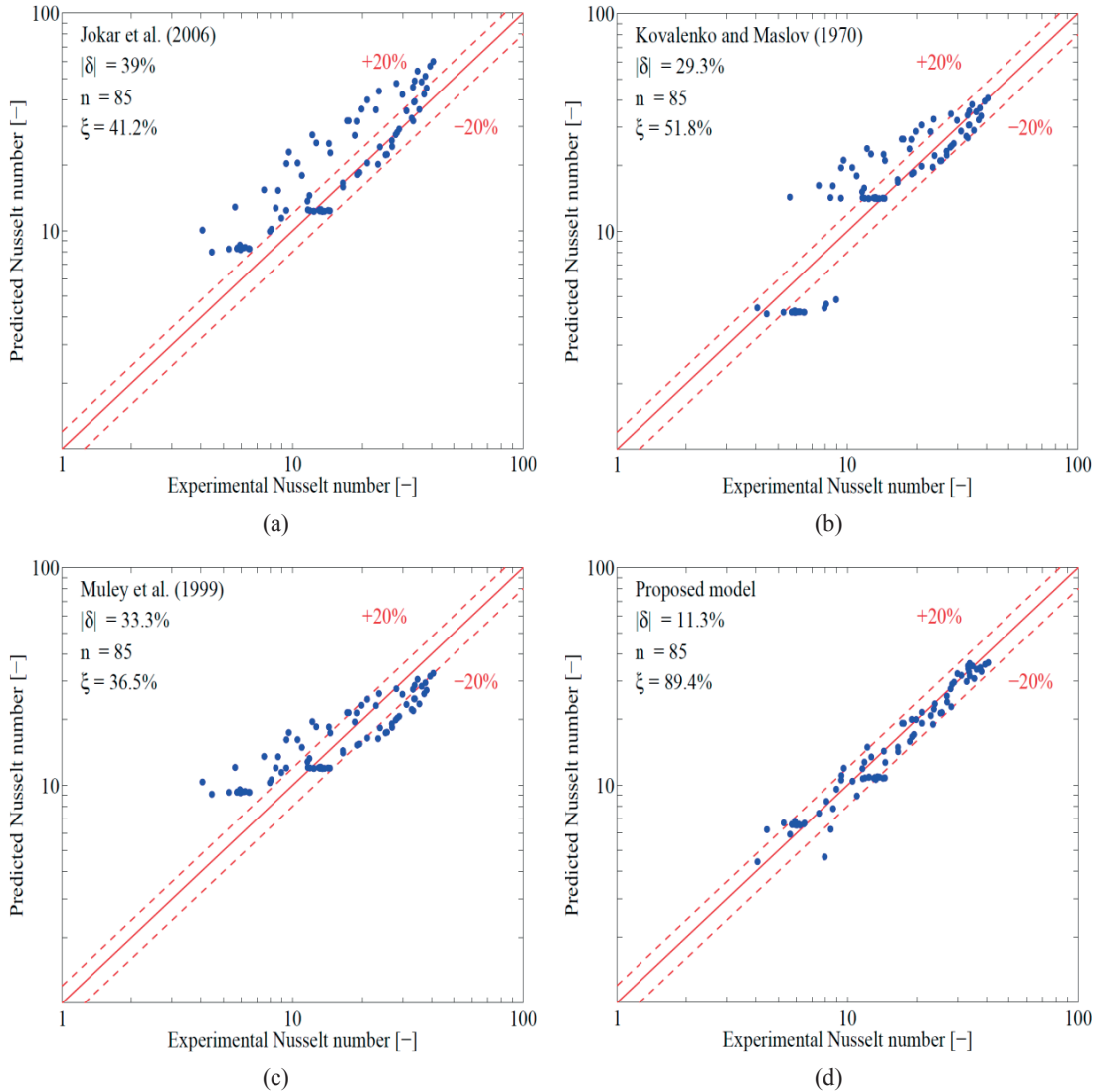


Figure 5.2: Single-phase experimental Nusselt number predicted by several prediction methods: (a) Jokar et al. (2006b), (b) Kovalenko-Maslov (1970), (c) Muley et al. (1999b), (d) proposed model.

## 5.4 Local heat transfer coefficient

In Table 5.3 the experimental quasi-local Nusselt number, described in chapter 4, has been compared against several prediction methods available in the open literature. The model proposed by Clark (1974), Kakac et al. (1987), Muley et al. (1999b) and Troupe et al. (1960b) have been locally extrapolated, in which the port to port length was replaced with the local length of the plate heat exchanger.

Table 5.3: Predicted quasi-local single-phase Nusselt number against the heat transfer database.

Prediction method (n = 510)	$ \delta %$	$\delta%$	$\xi%$	$\Upsilon%$
Clark (1974)	40.3	-39.4	14.8	30.7
Kakac et al. (1987)	50.9	-34.2	13.2	21.4
Muley et al. (1999b)	114.9	114.5	21.1	24.8
Troupe et al. (1960b)	255.2	255.2	0	0
Proposed model	14.8	0.7	88.2	93.6

As can be observed in Figure 5.3, these correlations poorly predicted the current quasi-local database (containing 510 data points), since they were developed adopting different plate geometries, experimental test conditions and mean heat transfer measurements rather than local data. Muley et al. (1999b) model was able to predict some of the data at higher mass fluxes, but globally also this model strongly overestimated the databank, since it was developed for a turbulent flow regime. The proposed quasi-local heat transfer prediction methods was developed applying the nonlinear multi-regression technique to the non-dimensional groups, which are listed below:

$$\text{Re} = \frac{G \cdot d_h}{\mu} \quad \text{Pr} = \frac{\mu \cdot c_p}{k} \quad z^* = \frac{z/d_h}{\text{Re} \cdot \text{Pr}} = \frac{L^*}{\text{Re} \cdot \text{Pr}} \quad (5.5)$$

Mainly, in order to gain in accuracy and take into consideration the inlet and outlet effects on the thermal performance, the plate length was divided into three parts according to the definition of  $L^*$  and in each of them the quasi-local Nusselt number was correlated. The equations are presented below:

$$Nu_{loc} = (2.301 \cdot z^{*-2.748} - 3802.9) \cdot \text{Re}^{-1.929} \quad \text{for } L^* \leq 21 \quad (5.6)$$

$$Nu_{loc} = 3.757 \cdot z^{*-0.459} - 6.517 \quad \text{for } L^* \geq 108 \quad (5.7)$$

$$Nu_{loc} = (0.0842 \cdot Pr - 0.319) \cdot z^{*0.155} Re^{0.823} \quad \text{for } 108 < L^* < 21 \quad (5.8)$$

Figure 5.3d shows the predicted capability of the novel local heat transfer prediction method, which captured with a mean absolute error of 14.7% and a mean error of -1.3, 85.8% and 93.9% of the quasi-local data within a bandwidth of 20% and 30% respectively.

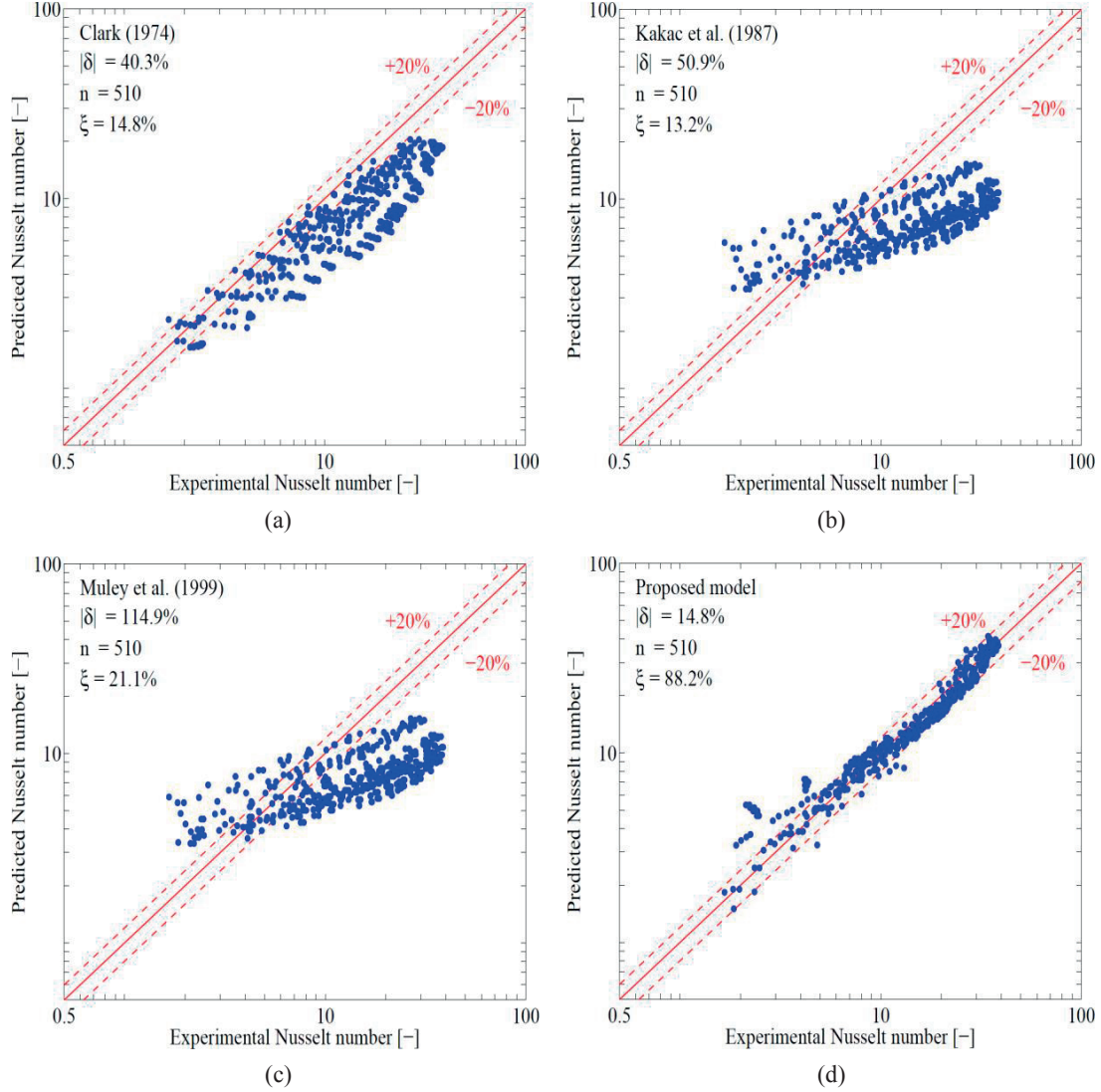


Figure 5.3: Local single-phase experimental Nusselt number predicted by different prediction methods: (a) Clark (1974), (b) Kakac et al. (1987), (c) Muley et al. (1999b), (d) proposed model.

## 5.5 Conclusions

For the present plate heat exchanger evaporator the experimental single-phase frictional pressure drop database has been compared against 23 prediction methods available in the open literature. Most correlations poorly predicted the current pressure drop databank and for this reason, a correlation to evaluate the Fanning friction factor was introduced, that captured 146 data points with a mean absolute error of 8.2% and mean error of -2.6%, within a bandwidth of 20%. Otherwise, the mean heat transfer databank has been validated against 37 correlations from literature, which strongly underestimated or overestimated the experimental data. According to the present mean heat transfer database, which was composed of 85 experimental data points, a new correlation was provided, and it predicted 89.4% and 97.6% of the data were respectively within a bandwidth of 20% and 30%, offering a mean absolute error of 11.3% and a mean error of -1.8. Finally, the local thermal performance were also correlated to handle the inlet and outlet effects in the plate arrangement and a model to estimate the local heat transfer coefficient was proposed. The set of correlations was developed based on 510 local experimental data points and predicted 88.2% and 93.6% of the experimental data within a bandwidth of 20% and 30%, with a mean absolute error of 14.8% and mean error of 0.7%. All the present methods were proposed applying a nonlinear multi regression technique on the non-dimensional parameters and they proved to work better than any other prediction methods currently available in the open literature.

# CHAPTER 6 – Two phase results

## 6.1 Introduction

In this chapter, the main trends of two-phase frictional pressure drop and heat transfer coefficient are discussed. In particular, the effect of saturation temperature, imposed heat flux, vapor quality, mass flux and axial location on the thermal and hydraulic performance are investigated. Two phase adiabatic tests were done by bringing the fluid into the test section in a two phase state while diabatic tests had either saturated liquid at the inlet or a desired inlet vapor quality. Based on the infrared measurements, a novel technique to evaluate the local saturation temperature of the refrigerants is also presented.

## 6.2 Frictional pressure drop

In order to analyze the two-phase frictional pressure drops in the present plate heat exchanger, the boiling process was initiated in the preheater and adiabatic refrigerant flow was investigated in the test section.

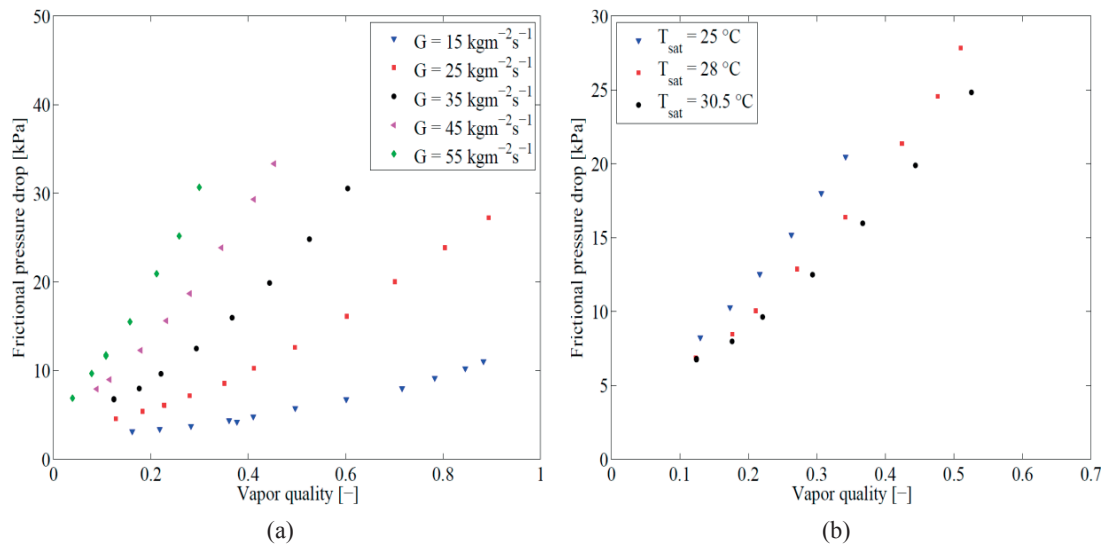


Figure 6.1: Adiabatic two-phase frictional pressure drop versus local vapor quality: (a) effect of mass flux at  $T_{\text{sat}} = 30.5$   $^{\circ}\text{C}$  and R245fa, (b) effect of saturation temperature at  $G = 35$   $\text{kg m}^{-2} \text{s}^{-1}$  and R245fa.

Due to the negligible heat losses to the ambient and small pressure drops, the variation of the vapor quality from the inlet to the outlet of the plate evaporator was negligible. Figure 6.1 shows the effect of refrigerant mass flux and saturation temperature during the evaporation process on the two-phase frictional pressure drop. The frictional pressure drop increased with vapor quality due to the greater shear stress between liquid and vapor phases and with mass flux since is proportional to the square of the mass velocity. When decreasing the saturation temperature, the frictional pressure drop rose because of the higher density ratio (liquid with respect to vapor) and due to the lower liquid dynamic viscosity. Additionally, the frictional pressure drop was not function of the imposed heat flux.

### 6.3 Evaluation of local saturation pressure

Figure 6.2a illustrates a temperature map measured by the infrared camera for all the pixels located inside the six “windows”, while the corresponding pixel-by-pixel pressure map is presented in Figure 6.2b.

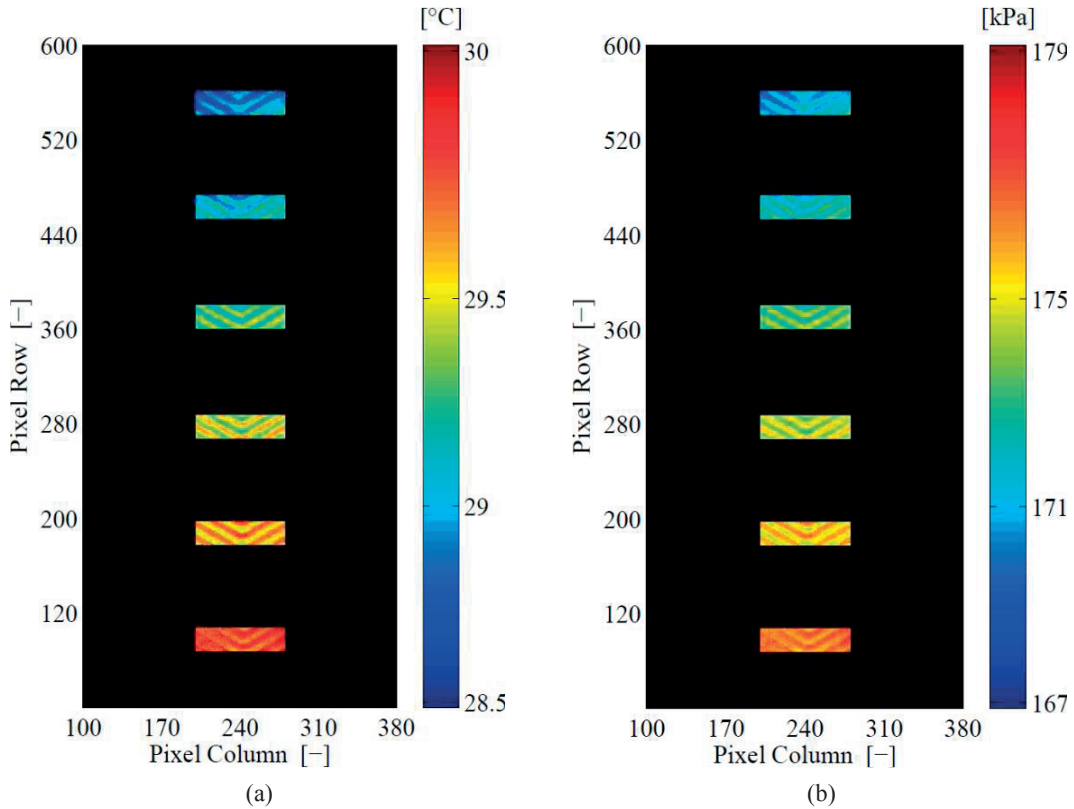


Figure 6.2: Adiabatic two-phase pressure drop results for  $G = 75 \text{ kg m}^{-2} \text{ s}^{-1}$ ,  $T_{\text{sat}} = 30.5 \text{ }^{\circ}\text{C}$ ,  $x = 0.12$  and R245fa: (a) temperature map measured by infrared camera, (b) corresponding absolute pressure map.

In this set of experiments, the boiling process was initiated in the preheater and adiabatic flow condition was kept in the test section. Due to the small temperature drop in the thickness of the plate and negligible heat loss to the ambient, the wall temperature was considered to be equal to the fluid temperature. The absolute pressure was then calculated through the refrigerant liquid-vapor pressure curve at the local saturated condition for all the pixels. The local temperature as well as the absolute pressure decreased along the plate heat exchanger due to the frictional and static pressure drops. The momentum pressure drop was negligible, since the vapor quality slightly changed from the inlet to outlet of the test section, only due to a small variation of the latent heat. The decreasing trends were also highlighted in the Figure 6.3a and Figure 6.3b, in which an average value of the temperatures and absolute pressures overall the pixels in each window are presented. The variation in the local temperature and absolute pressure within each window (shown by the colors in Figure 6.2) is apparently due to the local change of the flow velocity (and thus the local static pressure) due to the variation of the cross section along the corrugations.

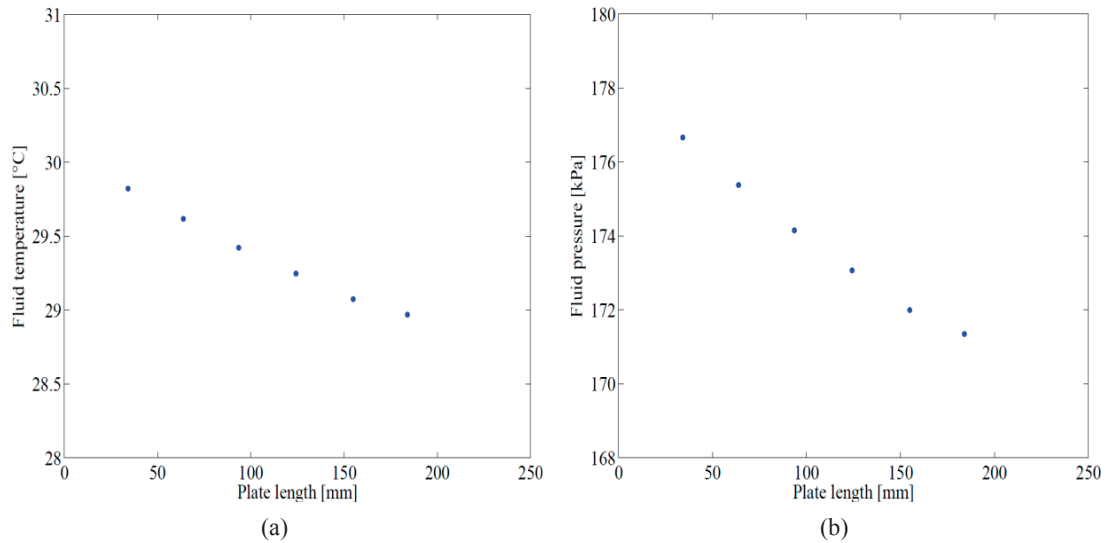


Figure 6.3: Adiabatic two-phase pressure drop results for  $G = 75 \text{ kg m}^{-2} \text{ s}^{-1}$ ,  $T_{\text{sat}} = 30.5 \text{ }^{\circ}\text{C}$ ,  $x = 0.12$  and R245fa: (a) quasi-local temperature versus plate length, (b) associated quasi-local absolute pressure versus plate length.

The two-phase frictional pressure drop was calculated based on the plate length of 150 mm (distance between the center line of the first and last window) in order to avoid the effect of inlet and outlet ports and then extrapolated to the overall the length of the test section. In Table 6.1, the predicted frictional pressure drop was compared to the measured experimental data and the results are displayed in Figure 6.4.



## CHAPTER 6 – Two phase results

Table 6.1: Predicted two-phase frictional pressure drop against the present measured pressure drop database.

Prediction method (n = 122)	$ \delta $ %	$\delta$ %	$\xi$ %	$\Upsilon$ %
Lee et al. (2014b)	24.4	-19.2	40.7	61.8
Nilpueng and Wongwises (2010c)	24.1	-20.4	49.6	69.9
Taboas et al. (2010d)	97.1	97	8.9	14.6
Proposed model	10	0.2	86.2	100

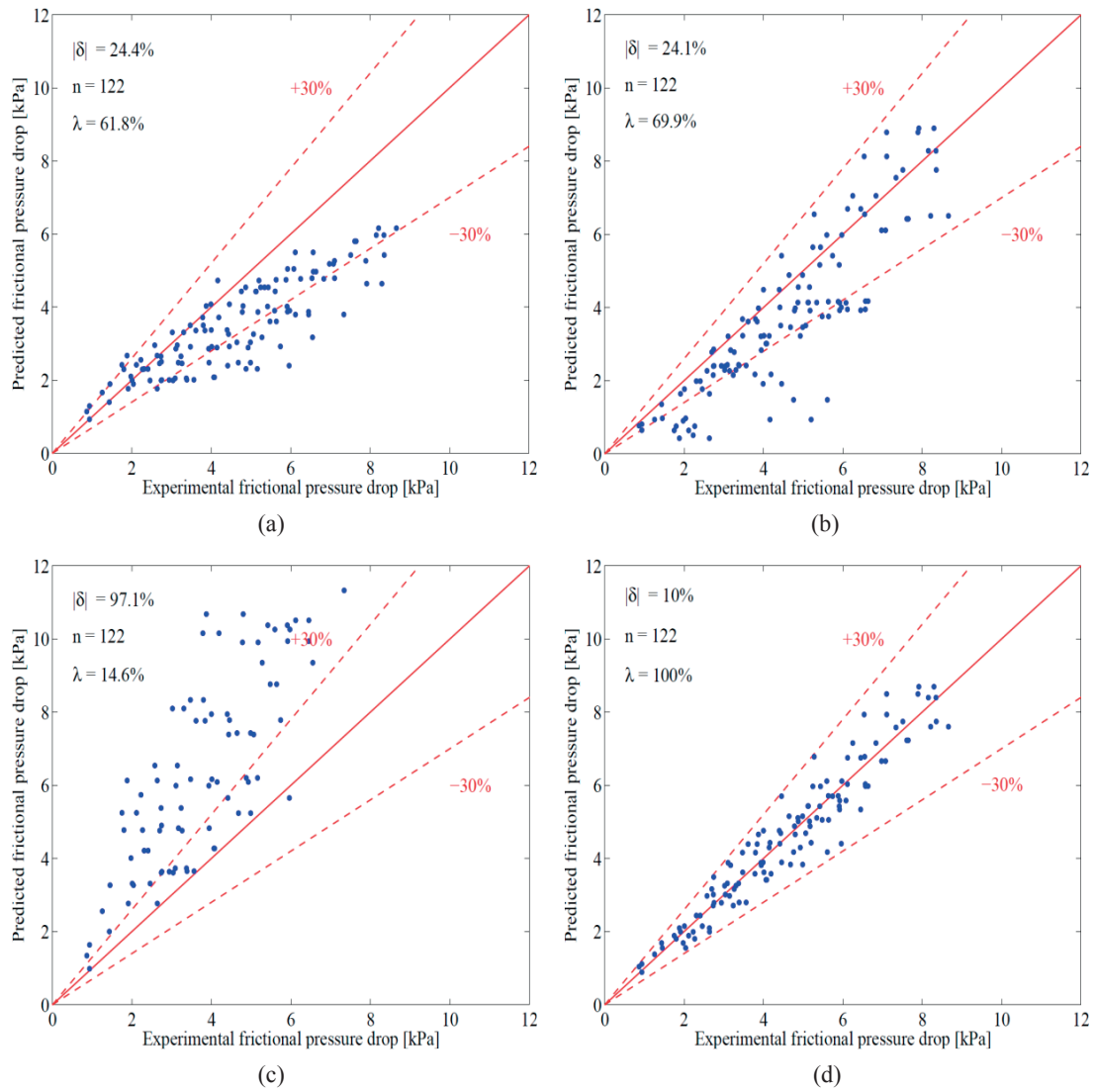


Figure 6.4: Two-phase experimental frictional pressure drop obtained by infrared measurements, predicted by four prediction methods: (a) Lee et al. (2014b), (b) Nilpueng and Wongwises (2010c), (c) Taboas et al. (2010d), (d) proposed model.

As can be seen from the above results, most of the correlations strongly overestimated the present databank, due to the different range of test conditions (much smaller pressing

depth of the new plate design) as well as an incorrect evaluation of the inlet and outlet pressure drops. The best agreement between the predicted and measured values was reached using the correlations provided by Lee et al. (2014b). The authors implemented local measurements to analyze flow boiling of water at low mass fluxes under uniform heat flux. A discrete matching was also discovered applying the model suggested by Nilpueng and Wongwises (2010c) and Taboas et al. (2010d), which investigated respectively flow boiling of ammonia/water mixture at low vapor qualities and adiabatic two-phase pressure drops of air and water. A prediction method to estimate the local frictional pressure drop was proposed and two-phase Fanning friction factor was correlated with vapor Reynolds number as follow:

$$f_{IR} = 15.080 \cdot \text{Re}_v^{-0.467} \quad (6.1)$$

The vapor Reynolds number quantified the shear stress between liquid and vapor phases, which is normally greater than the flow shear stress against the wall. Additionally, the ratio between the superficial vapor velocity and the liquid vapor velocity is function of the vapor quality and density ratio (liquid over vapor). Since the density of the liquid is three orders of magnitude larger than the density of the vapor, even at low vapor qualities, the vapor flows with a higher superficial velocity compared to the liquid phase. The proposed model was able to estimate 86.2% of the data in a narrow range of  $\pm 20\%$  and the entire databank, composed of 122 experimental points, within a bandwidth of 30%, providing a mean absolute error of 10% and mean error of 0.2%.

Figure 6.5 reports an example of the local pressure drop calculation during a heat transfer test, in which the static, momentum and frictional pressure losses were locally normalized to the total pressure drop in the cell.

The acceleration pressure drop was equal to zero in the subcooled length because no variation of vapor quality occurred. When the boiling process was initiated, the momentum pressure drop increased proportionally to the square of the mass flux as well as by the local variation of vapor quality and it remained almost constant along the plate length. Such a trend was due to the condition of uniform heat flux coupled to the small pressure drop overall in the test section, which provided a small variation of the fluid properties (vapor quality, liquid and vapor densities). Furthermore, the effect of the momentum pressure drop on the total loss was less than 2%; thus, it was negligible compared to the gravitational and frictional contributions.

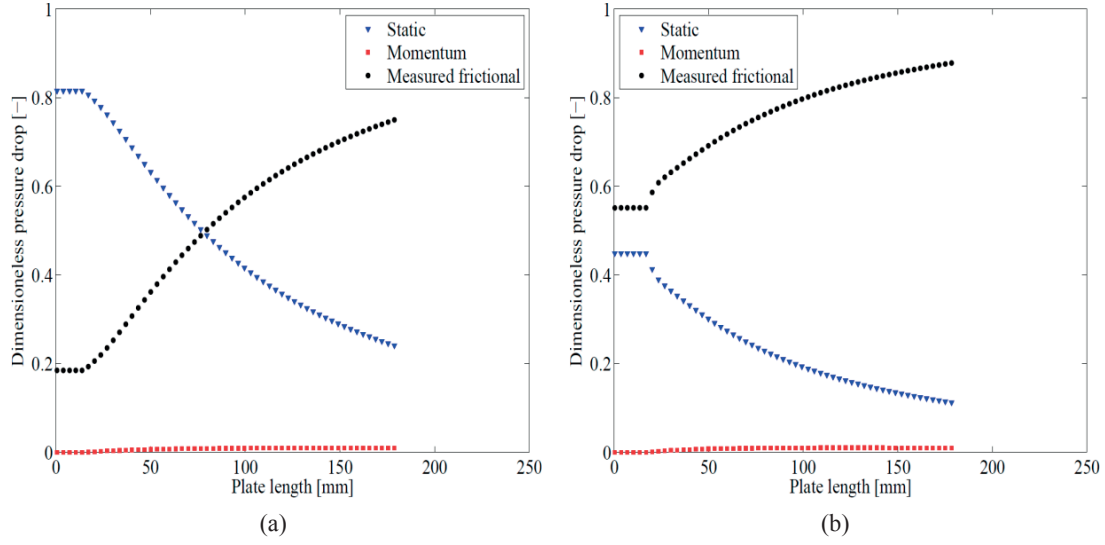


Figure 6.5: Dimensionless local static, momentum and frictional pressure drop in which: (a)  $G = 25 \text{ kg m}^{-2} \text{ s}^{-1}$ ,  $T_{\text{sat}} = 30.5 \text{ }^{\circ}\text{C}$ ,  $q = 4000 \text{ W m}^{-2}$ ,  $x_{\text{out}} = 0.33$  and R245fa, (b)  $G = 85 \text{ kg m}^{-2} \text{ s}^{-1}$ ,  $T_{\text{sat}} = 30.5 \text{ }^{\circ}\text{C}$ ,  $q = 4100 \text{ W m}^{-2}$ ,  $x_{\text{out}} = 0.10$  and R245fa.

The static pressure drop reached the maximum value at the beginning of the test section, where the refrigerant was completely subcooled and it was regardless of the position because of the slightly changing of the liquid density. Once the boiling process started, the gravitational pressure drop decreased with plate length due to an increasing of vapor fraction. The same trend was observed in the subcooled region for the frictional pressure drop and when the boiling process occurred, the contribution of the frictional pressure drop rose with the plate length because of the increasing of vapor quality, that provided a decreasing of the local two-phase homogeneous density. Figure 6.5a shows the results at low mass flux in which the dominant contributions was due to the static pressure drop from the inlet until a plate length of 75 mm. After that, the frictional pressure drop became greater than the gravitational one till the outlet of the evaporator. In Figure 6.5b, at relatively higher mass flux, the frictional pressure drop was the largest contributor overall the length of the plate heat exchanger.

In Figure 6.6 examples of local pressure profile and the associated fluid temperature are reported in two heat transfer experiments. Figure 6.6a shows the local absolute pressure of the refrigerant along the test section, evaluated with several schemes: linear pressure drop, prorated Khan et al. (2014a), prorated Huang et al. (2012b) and proposed model. It has to be pointed out that, the prorated pressures have been calculated according to the outlet pressure measured by the pressure transducer and the taking into consideration the outlet port pressure

drop by using the model proposed by Shah and Focke (1988). The absolute pressure decreased with two different slopes, due to the fact that, for the first 14 mm, the refrigerant was still subcooled, thus the single phase pressure drop model was applied (eq. 5.2), while in the flow boiling region, the novel prediction methods was adopted.

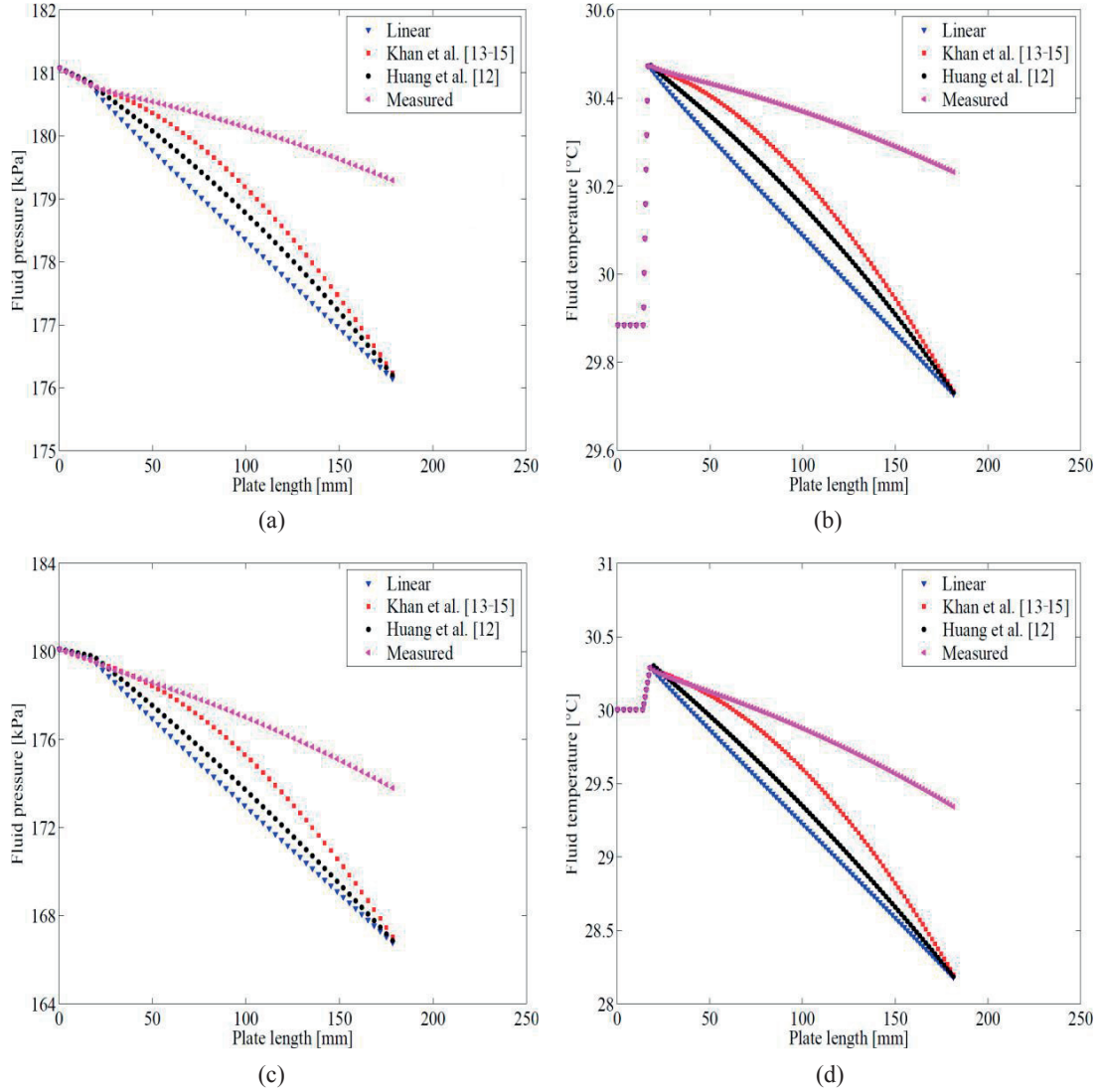


Figure 6.6: Local fluid pressure and temperature predicted adopting linear scheme, Khan et al. (2014a, 2012c, 2012d) (prorated), Huang et al. (2012b) (prorated) and proposed model: (a) pressure profile, (b) temperature profile both for  $G = 25 \text{ kgm}^{-2}\text{s}^{-1}$ ,  $T_{\text{sat}} = 30.5 \text{ }^{\circ}\text{C}$ ,  $q = 4000 \text{ Wm}^{-2}$ ,  $x_{\text{out}} = 0.33$  and R245fa, (c) pressure profile and (d) temperature profile both for  $G = 85 \text{ kgm}^{-2}\text{s}^{-1}$ ,  $T_{\text{sat}} = 30.5 \text{ }^{\circ}\text{C}$ ,  $q = 4060 \text{ Wm}^{-2}$ ,  $x_{\text{out}} = 0.10$  and R245fa.

In Figure 6.6b, the temperature profile was plotted against the plate length. After an adiabatic length of 14 mm, the fluid temperature increased linearly according to single phase heat transfer theory and on the contrary, the temperature decreased due to the pressure drop in

the two-phase flow region. Figure 6.6c and Figure 6.6d depict the refrigerant pressure profile and the associated local temperature, for a larger value of mass flux. In this scenario, a longer subcooled length has been observed, with greater pressure drops, which yielded a lower saturation temperature. Comparing the different schemes, the lowest frictional pressure drop was reached applying the proposed model, which properly took into account the pressure drop across the outlet port; thus, a higher saturation temperature was achieved. On the contrary, the other models provided higher frictional pressure drops, since they strongly underestimated the pressure drop through the outlet port.

## 6.4 Evaluation of outlet restriction pressure drop

The outlet singularity pressure drop was determined, according to the pressure measurements located respectively before and after the outlet port. Notably, the inlet singularity pressure drop was not quantified, since the measured values were below the accuracy of the instrumentation. Finally, in the present work, the correlation proposed by Shah and Focke (1988) was implemented to estimate the inlet singularity pressure loss, since most of the heat transfer experiments were carried out with subcooled liquid refrigerant at the inlet of the test section.

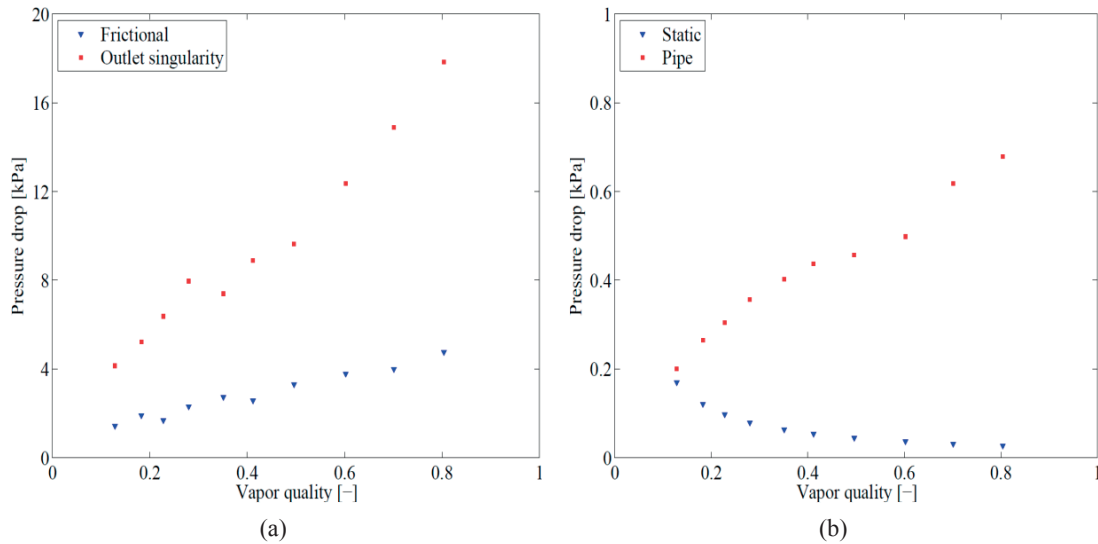


Figure 6.7: Different pressure drop contributors against local vapor quality for  $G = 25 \text{ kgm}^{-2}\text{s}^{-1}$ ,  $T_{\text{sat}} = 30.5 \text{ }^{\circ}\text{C}$ ,  $x = 0.33$  and R245fa: (a) frictional and outlet singularity pressure drops measured by infrared camera, (b) static and pipe pressure drops.

## 6.4 Evaluation of outlet restriction pressure drop

Figure 6.7a shows that the frictional and outlet singularity pressure losses increased with local vapor quality, due to the higher flow velocity as well as greater shear stress between the two phases. The frictional pressure drop rose with mass flux and also with decreasing of system pressure, as was mentioned earlier. Figure 6.7b illustrates the trends of the pipe and static pressure drops. The total pipe pressure loss grew with the local vapor quality, due to the larger friction inside the piping and as a consequence more energy has to be supply to promote the same mass flux. The static pressure drop diminished with the local vapor fraction, because more vapor was been generated from the vaporization of the liquid, during the flow boiling process. For the entire experimental databank, the outlet singularity pressure loss was the largest contributor, almost 70% of the total pressure drop. The frictional pressure drop was only 25%, while the piping and static pressure drops were classified as minor pressure drops, since they represented only 3% and 2% of the overall measured pressure drop.

Figure 6.8 depicts the effect of mass flux on the outlet pressure drop at a given saturation temperature. The outlet singularity pressure loss increased with mass flux, while it was moderately dependent on the saturation temperature (corresponding to the system pressure).

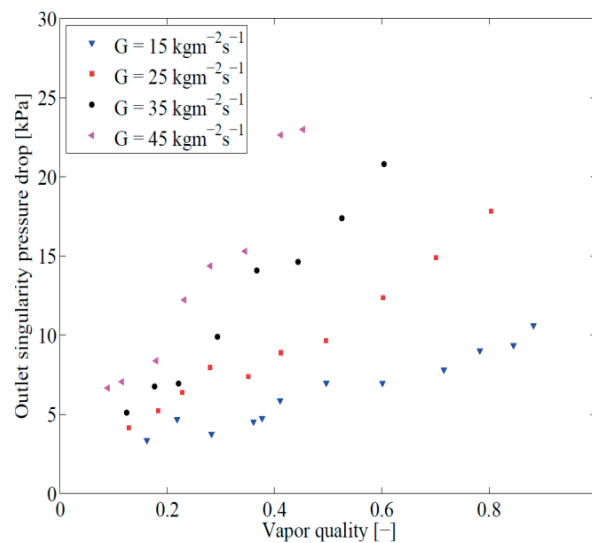


Figure 6.8: Effect of mass flux on the outlet singularity pressure drop in which  $T_{\text{sat}} = 30.5\text{ }^{\circ}\text{C}$  and R245fa.

According to the present adiabatic pressure drop databank, that involved 122 experimental data points, a correlation for predicting outlet singularity pressure drop function of equivalent mass flux and liquid density was suggested as follows:

$$\Delta p_{sing,out} = 1.7 \cdot 10^5 \cdot \left( \frac{G_{eq}}{\rho_l} \right)^{1.259}, \quad G_{eq} = G \left[ (1-x) + x \left( \frac{\rho_l}{\rho_v} \right)^{0.5} \right] \quad (6.2)$$

Figure 6.9 presents the predicted capability of the proposed model for evaluating the outlet singularity pressure drop. The new method captured 93.4% and 96.7% of the experimental data within a bandwidth of  $\pm 20\%$  and  $\pm 30\%$ , providing a mean absolute error of 11% and mean error of -0.3%. It has to be pointed out that, the model proposed by Shah and Focke (1988) strongly underestimated the current database, since it was developed for single phase flow data within plate heat exchangers. Consequently, no experimental data were predicted in the range of  $\pm 30\%$ , resulting a mean absolute error of 99.5% and mean error of -99.5%.

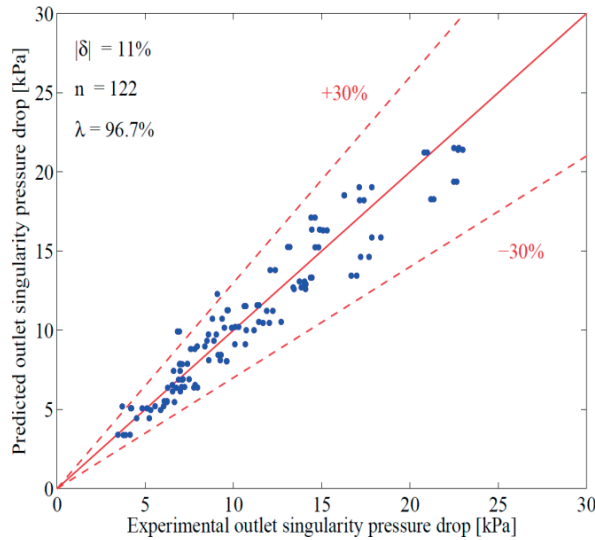


Figure 6.9: Predicted versus experimental outlet singularity pressure drop adopting the proposed prediction method.

## 6.5 Heat transfer coefficient

A set of flow boiling tests was performed in order to investigate the local thermal performance of the present plate heat exchanger prototype. During the experiments, the refrigerant was subcooled ( $\Delta T_{in,sub} < 1^\circ\text{C}$ ) or two-phase flow ( $x_{in} = 0.10 - 0.25$ ) at the inlet of the test section and the evaporation process was promoted by direct electrical heating into the plate heat exchanger.

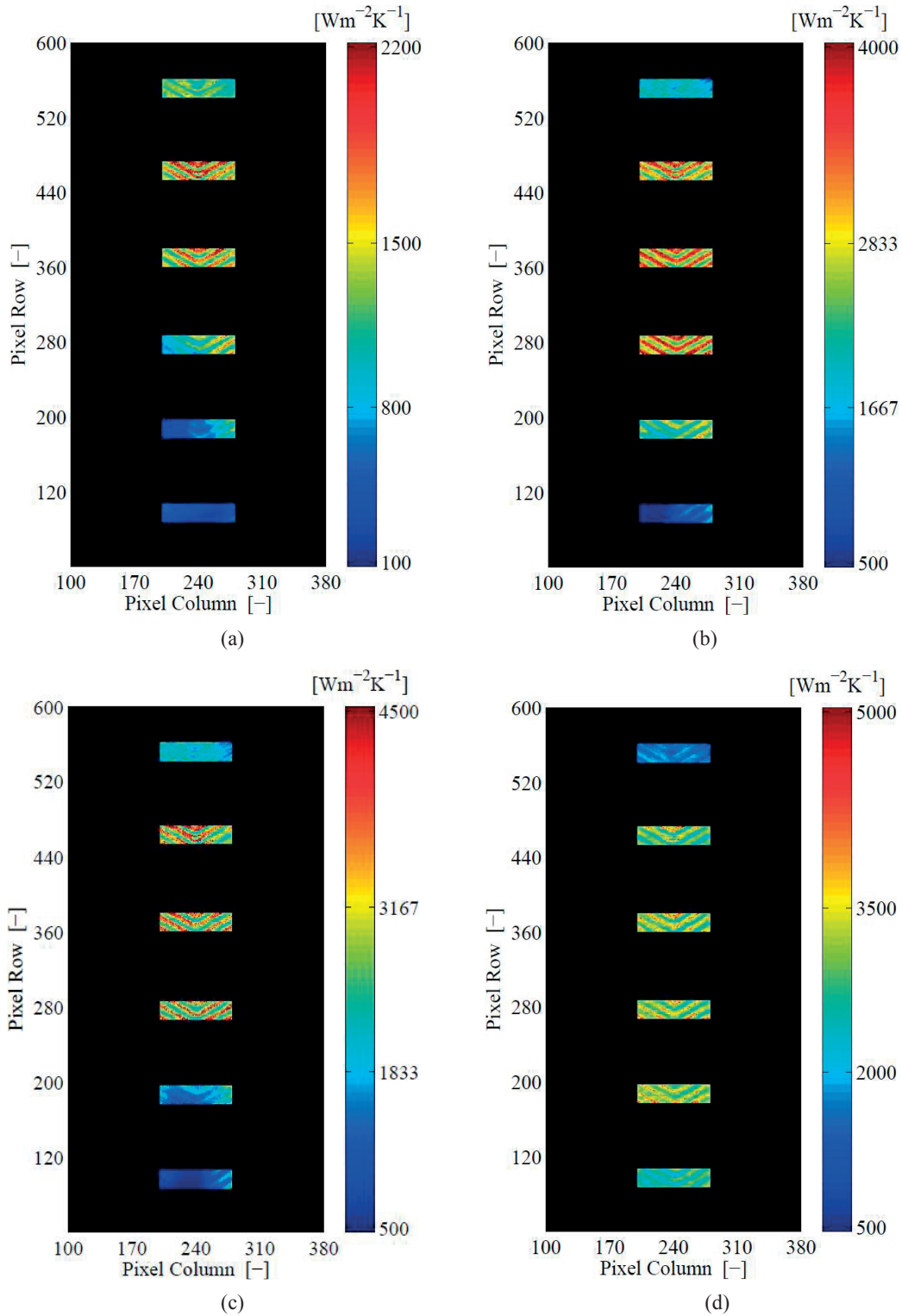


Figure 6.10: Local flow boiling heat transfer results for: (a)  $\Delta T_{\text{in,sub}} < 1^\circ\text{C}$ ,  $G = 25 \text{ kg m}^{-2}\text{s}^{-1}$ ,  $T_{\text{sat}} = 30.5^\circ\text{C}$ ,  $q = 1000 \text{ W m}^{-2}$ ,  $x_{\text{out}} = 0.05$ , (b)  $\Delta T_{\text{in,sub}} < 1^\circ\text{C}$ ,  $G = 25 \text{ kg m}^{-2}\text{s}^{-1}$ ,  $T_{\text{sat}} = 30.5^\circ\text{C}$ ,  $q = 1750 \text{ W m}^{-2}$ ,  $x_{\text{out}} = 0.33$ , (c)  $\Delta T_{\text{in,sub}} < 1^\circ\text{C}$ ,  $G = 45 \text{ kg m}^{-2}\text{s}^{-1}$ ,  $T_{\text{sat}} = 30.5^\circ\text{C}$ ,  $q = 1750 \text{ W m}^{-2}$ ,  $x_{\text{out}} = 0.08$ , (d)  $x_{\text{in}} = 0.25$ ,  $G = 25 \text{ kg m}^{-2}\text{s}^{-1}$ ,  $T_{\text{sat}} = 30.5^\circ\text{C}$ ,  $q = 1750 \text{ W m}^{-2}$ ,  $x_{\text{out}} = 0.45$ .



Figure 6.10a, Figure 6.10b and Figure 6.10c, show the local pixel-by-pixel heat transfer coefficient for all the pixels located in the six “windows” in the case of subcooled refrigerant flow at the inlet of the test section. As can be observed, the local heat transfer coefficient was lower in the subcooled liquid region and when the boiling process was initiated, higher thermal performance was achieved. According to the local energy balance, the subcooled liquid length increased with mass flux and decreased with the imposed heat flux as expected. Figure 6.10d illustrates the heat transfer coefficient map in the case of two-phase flow at the inlet of the test section, which allowed higher and more uniform heat transfer distribution. Overall, the lowest local heat transfer coefficients occurred downstream of the contact points, while the highest local thermal performances were found upstream along the corrugations.

Furthermore, for the local and quasi-local results presented below, the heat transfer coefficient increased with plate length because of the enhancing of the flow boiling process, while it suddenly dropped close to the outlet port due to the local flow maldistribution. In particular, in this area the refrigerant flow was apparently unable to wet all of the plate surface, provoking a partial dry-out and as consequence higher temperature differences between the wall and fluid were discovered. The effect of the dry-out phenomena next to the outlet port decreased with an increasing of the refrigerant mass flux, providing more uniform thermal performances. Similar results were discovered analyzing the local single-phase thermal performance of the present plate heat exchanger prototype.

In the following results, a quasi-local heat transfer coefficient was defined as the average over all the pixels inside each “window” and the effect of vapor quality, mass flux, imposed heat flux and saturation temperature on thermal performance have been investigated in detail.

Figure 6.11a illustrates the effect of mass flux on the quasi-local heat transfer coefficient, which rose slightly with mass velocity, indicating that convective flow boiling regime was influential on the heat transfer. Increasing the refrigerant mass flux, high turbulence and shear stress at the interface of the two phases were promoted, resulting in thinner liquid film thickness. Consequently, this flow regime provided less thermal resistance from the wall to the fluid; thus, this gave higher heat transfer coefficients.

In Figure 6.11b the effect of heat flux and on the quasi-local heat transfer coefficient is presented. The heat transfer strongly increased with the imposed heat flux at low vapor fractions, where the nucleate boiling regime was dominant. On the contrary, increasing vapor quality, the heat flux did not play a significant role, apparently because the nucleation sites were largely suppressed.

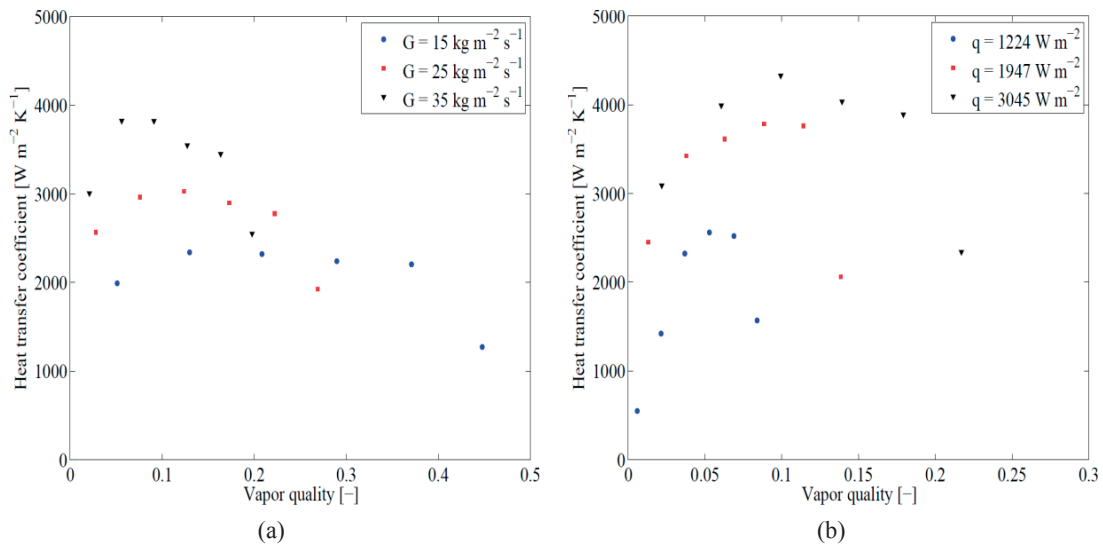


Figure 6.11: Quasi-local flow boiling heat transfer coefficient versus local vapor quality: (a) effect of mass flux at  $T_{\text{sat}} = 30^\circ\text{C}$ ,  $q = 3900 \text{ W m}^{-2}$  and R245fa, (b) effect of imposed heat flux at  $T_{\text{sat}} = 30^\circ\text{C}$ ,  $G = 25 \text{ kg m}^{-2} \text{s}^{-1}$  and R245fa.

The quasi-local heat transfer coefficients increased with the saturation temperature and the results are shown in Figure 6.12. In this case, the latent heat of vaporization decreases with increasing saturation temperature, so that, the liquid film has to evaporate more refrigerant to dissipate the heat flux, and the resulting thinner liquid film offers higher heat transfer coefficients. Moreover, the decreasing of the refrigerant thermal conductivity with a rise in system pressure was found to be negligible on the liquid film thermal resistance.

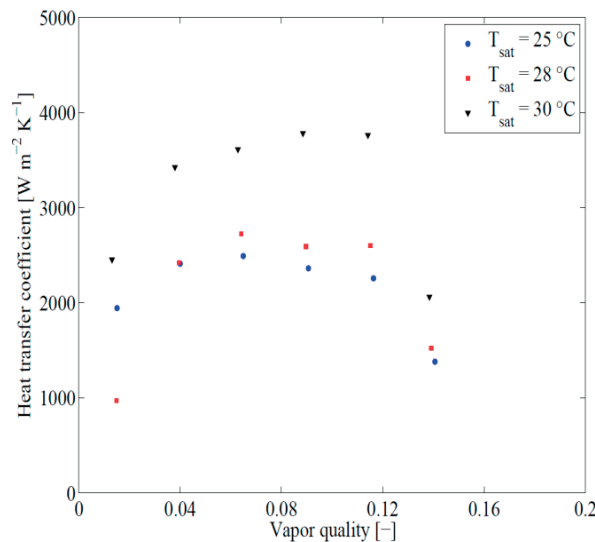


Figure 6.12: Quasi-local flow boiling heat transfer coefficient versus local vapor quality: effect of saturation temperature at  $G = 25 \text{ kg m}^{-2} \text{s}^{-1}$ ,  $q = 3900 \text{ W m}^{-2}$  and R245fa.

## **6.6 Conclusions**

High spatial and temporal resolution infrared measurements of two-phase flow in a novel compact chevron plate heat exchanger were carried out over a wide range of operating conditions. The frictional pressure drop increased with mass flux, vapor quality and decreased with saturation temperature (corresponding to the system pressure). The effect of the imposed heat flux on the two-phase hydraulic performance was seen to be negligible. The local heat transfer coefficient enhanced with mass flux, vapor quality, heat flux and saturation temperature. Compared to the subcooled liquid flow at inlet of the test section, higher and more uniform thermal performance have been achieved when the boiling process was initiated inside the preheater. The lowest local heat transfer coefficients were observed downstream of the contact points, while the highest local thermal performances were found upstream along the corrugations. The pressure loss at the inlet of the heat exchanger was found to be negligible, while the pressure drop and the associated flow instability close to the outlet port strongly influenced the heat transfer coefficient, especially at low values of mass flux.

# CHAPTER 7 – Two phase prediction methods

## 7.1 Introduction

In the present chapter a consolidated multi-lab database of flow boiling heat transfer coefficients and frictional pressure gradients for plate heat exchangers was culled, that included 3601 data points collected from thirteen research studies available in the open literature. Extensive comparisons of the most quoted two-phase pressure drop and flow boiling heat transfer prediction methods from literature were also performed versus this large diversified database. The experimental databank was then utilized to develop new general prediction methods here to evaluate local heat transfer coefficients and pressure drops within plate heat exchangers and they proved to work significantly better over a very wide range of operating conditions, plate designs and fluids (including ammonia) than all previous methods. The prediction for flow boiling heat transfer coefficients was broken down into separate macro- and micro-scale methods.

## 7.2 Collection of experimental database

As explained in Amalfi et al. (2015b, 2015c), the correlations available in the open literature have been proposed on rather limited data sets (usually only their own database) and for one specific geometry, one test fluid and over a limited experimental range.

In order to create a generalized approach in the present study, a wide diversified multi-lab experimental databank for plate heat exchangers was collected here, including flow boiling heat transfer and frictional pressure drop data published by thirteen research groups in the literature. In the present study, 3601 data points have been collected and they were gathered for evaporation heat transfer (1903 data) and frictional pressure drop (1698 data) studies in plate heat exchangers, including:

- Saturated, adiabatic and subcooled flow boiling.
- Several types of plate heat exchangers (gasketed, brazed, welded and shell and plate).
- Parallel and counter flow arrangements.

- Upward and downward flow as flow directions.
- Nine pure fluids (R134a, ammonia, R245fa, R236fa, R600a, R290, R1270, R1234yf).
- Four mixtures (R410A, R507A, ammonia/water, air/water).
- Hydraulic diameters ranging from 1.7 mm to 8.0 mm.
- Chevron angles from 27 ° to 70 °.
- Saturation temperatures from -25 °C to 39 °C.
- Mass fluxes from 5.5 kgm<sup>-2</sup>s<sup>-1</sup> to 610 kgm<sup>-2</sup>s<sup>-1</sup>.
- Heat fluxes from 0.1 kWm<sup>-2</sup> to 50.0 kWm<sup>-2</sup>.
- Vapor qualities from 0 to 0.95.

In Figure 7.1, a bar chart distribution of the database is presented to describe its components. The experimental heat transfer and pressure drop data have been segregated into different categories, according to chevron angle, wavelength of surface corrugation, hydraulic diameter, working fluid, saturation temperature and mass flux, for the entire range of heat flux and vapor quality. It has to be pointed out that Figure 7.1b involves only 3375 points, since the data provided by Ouazia (2001a), Nilpueng and Wongwises (2010c) and Müller and Steinhagen (2001b) were not included because the wavelength of the surface corrugation was not mentioned in their papers. Furthermore, due to the higher value of mass flux coupled with adiabatic flow condition, the experimental data obtained by Nilpueng and Wongwises (2010c) and Müller and Steinhagen (2001b) were also omitted in the Figure 7.1f, that included 3416 points.

The following statistical comparisons in terms of heat transfer and pressure drop of the experimental data points for the evaporation processes have been performed against the most quoted literature prediction methods. This statistical analysis has been based on several pertinent statistical parameters: mean error, mean absolute error, and percentage of the data points predicted within  $\pm 30\%$  and within  $\pm 50\%$ .

## 7.2 Collection of experimental database

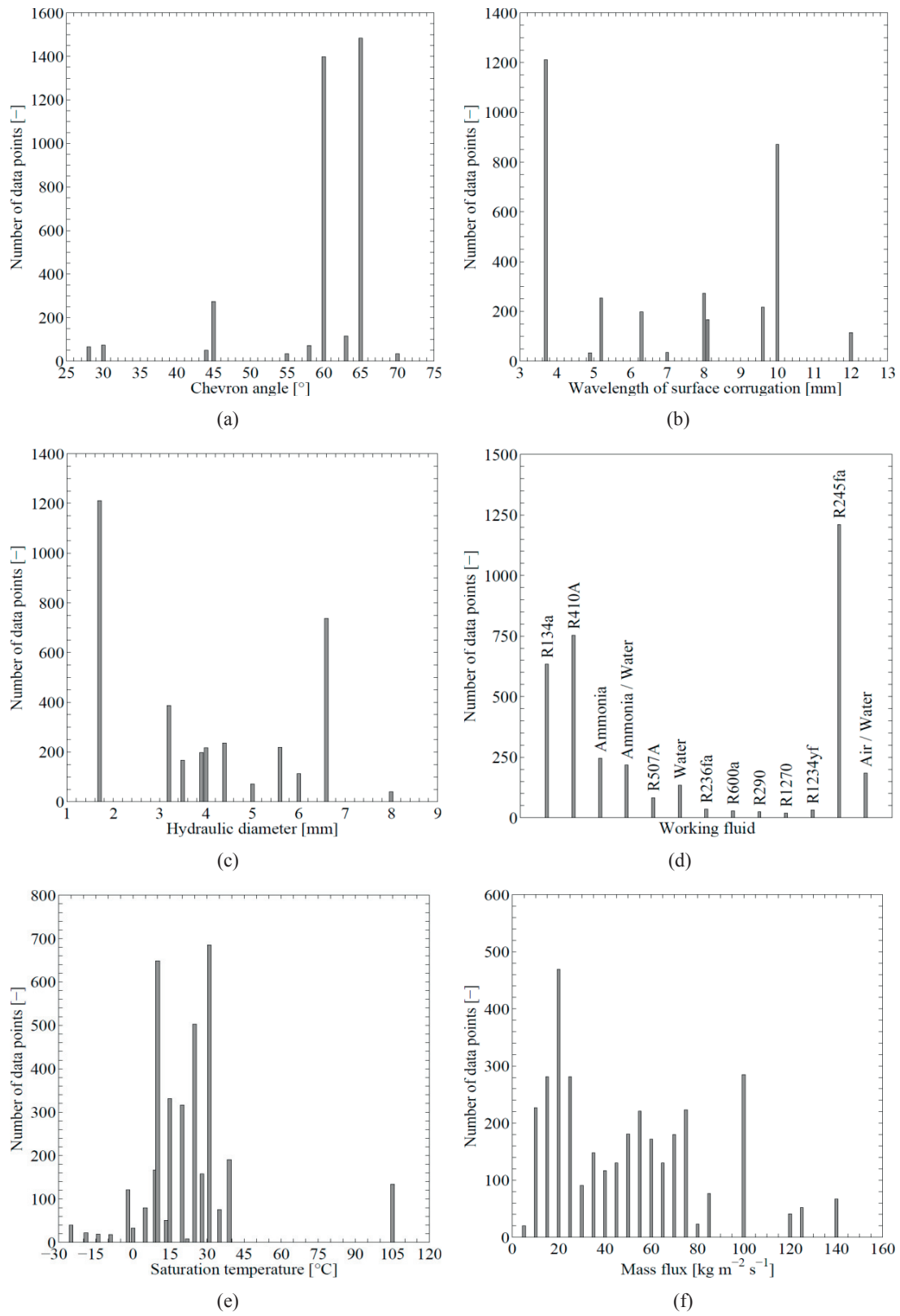


Figure 7.1: Distribution of data points related to: (a) chevron angle, (b) wavelength of surface corrugation, (c) hydraulic diameter, (d) working fluid, (e) saturation temperature, (f) mass flux.

In order to evaluate the prediction methods at any individual operating condition, the following assumptions have been made for which the experimental data points were obtained:

- In the case that the surface enlargement factor was not specified, the hydraulic diameter was evaluated as the equivalent diameter, thus two times the mean spacing between the plates.
- Since in several articles some relevant parameters are missing (e.g., inlet/exit vapor quality, or heat flux, or wall temperature), in these cases the data were reprocessed to determine the missing parameters based on the available information presented in the corresponding article.
- Some prediction methods require the temperature difference between plate wall and refrigerant. The value has been quantified as the ratio of the average imposed heat flux to the corresponding experimental heat transfer coefficient, i.e. by applying Newton's law of cooling.
- In the definition of the modified Jacob number, Hsieh et al. (2002a) took into account the cross-channel superheat, characterized as the temperature difference between the water and refrigerant streams. First, it has to be noted that this is different compared to the classical definition of the Jacob number in which the wall to refrigerant temperature difference is used. Since the publication did not provide sufficient information about the secondary fluid, in the present analysis the corresponding temperature difference was assumed as two times the wall to refrigerant temperature difference (i.e. the thermal resistances were assumed to be approximately equivalent in both streams).
- Several prediction methods were developed based on the mean value of complete evaporation of the fluid (mean value for the entire plate). In this case, the mean refrigerant vapor quality of  $x_m = 0.5$  was used in order to evaluate the correlations. These prediction models are not of course able to predict the local trend of heat transfer coefficient with vapor quality.
- As mentioned in the previous section, the Khan et al. (2012c) correlation to predict Fanning friction factor in the plate of 30° chevron angle has been disqualified, as it is not able to reproduce the experimental data presented in their own article. Hence, to perform the comparison, the Khan et al. (2014a) correlation for the mixed arrangement of 45° chevron angle was also applied to the test condition for which the chevron angle was below 45°.

- The thermal performance estimated by the Huang et al. (2012b) model was scaled up to be compared in terms of hydraulic diameter, since the authors considered the bubble departure diameter as the characteristic length in their expression of the Nusselt number.
- The pressure drops across the inlet and outlet headers were quantified by applying the scheme suggested by Shah and Focke (1988), in which the mass flux was calculated based on the cross section of the ports, while the fluid density was estimated according to the state of the refrigerant at the inlet and outlet, respectively. This correlation was developed only for single phase experimental data and the use of the model for two-phase flow, simply replacing the liquid with homogeneous two-phase density, represents an extrapolation. Consequently, the heat transfer coefficient and the associated frictional pressure drop could be underestimated.

The database provided by Müller and Steinhagen (2001b, 2001c) and Nilpueng and Wongwises (2010c) were not included for developing the general prediction methods, since the authors experimentally investigated adiabatic two-phase pressure drops of air/water within plate heat exchangers.

The best agreements between the predicted and the experimental evaporation heat transfer were achieved by the following six methods: Danilova et al. (1981), Han et al. (2003b), Huang et al. (2012b), Donowski and Kandlikar (2000b) and two by Hsieh and Lin (2003c, 2002b). In Figure 7.2 these methods are graphically compared against the current databank and, inside the graph, information on their mean absolute error, number of data points and percentage of the data points within  $\pm 50\%$  are shown.

In the same way, Figure 7.3 depicts the evaporation frictional pressure drop databank compared to the corresponding values predicted by six selected prediction methods.



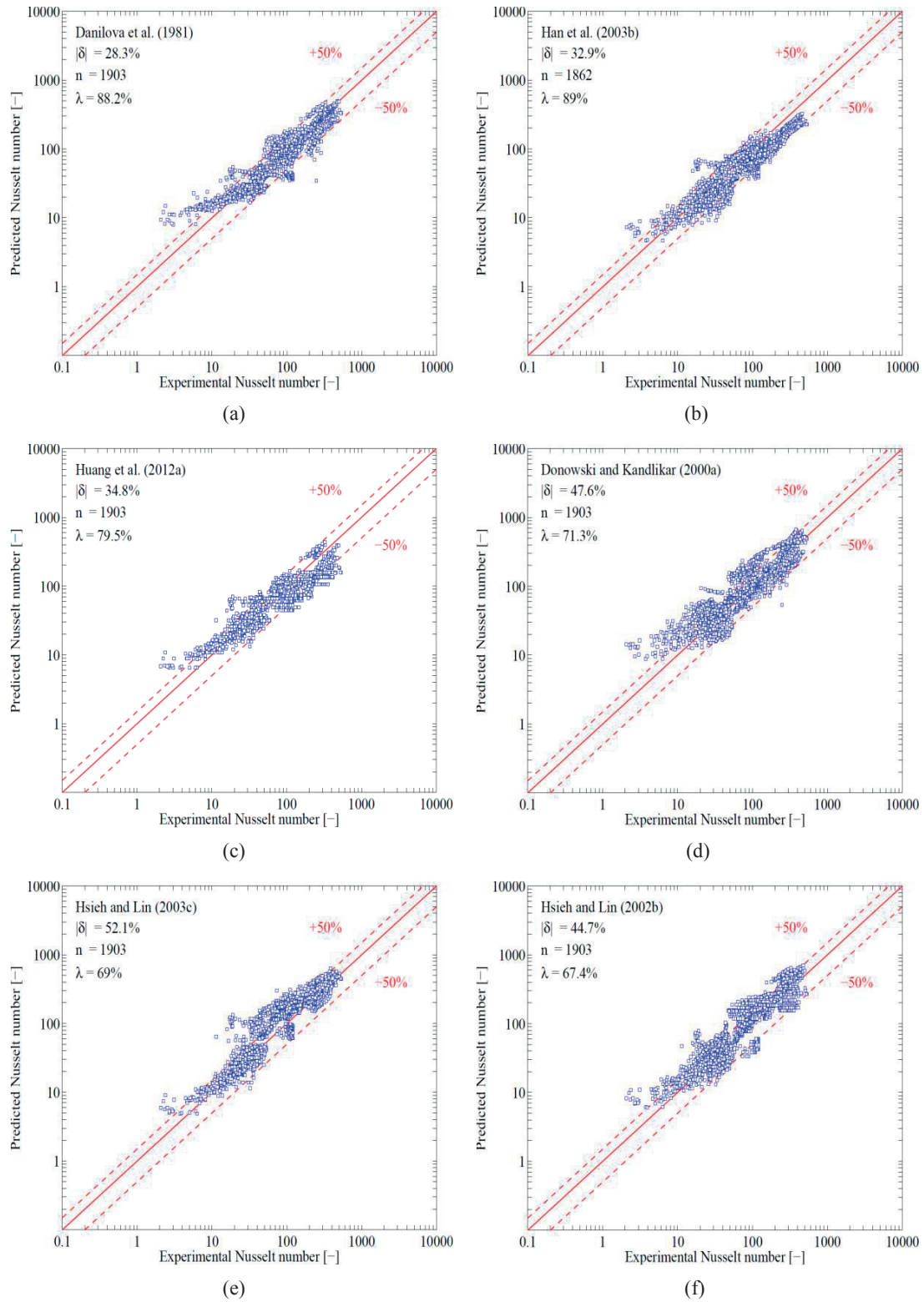


Figure 7.2: Flow boiling predicted Nusselt number against experimental Nusselt number using the correlations proposed by: (a) Danilova et al. (1981), (b) Han et al. (2003b), (c) Huang et al. (2012b), (d) Donowski and Kandlikar (2000b), (e) and (f) Hsieh and Lin (2003c, 2002b).

## 7.2 Collection of experimental database

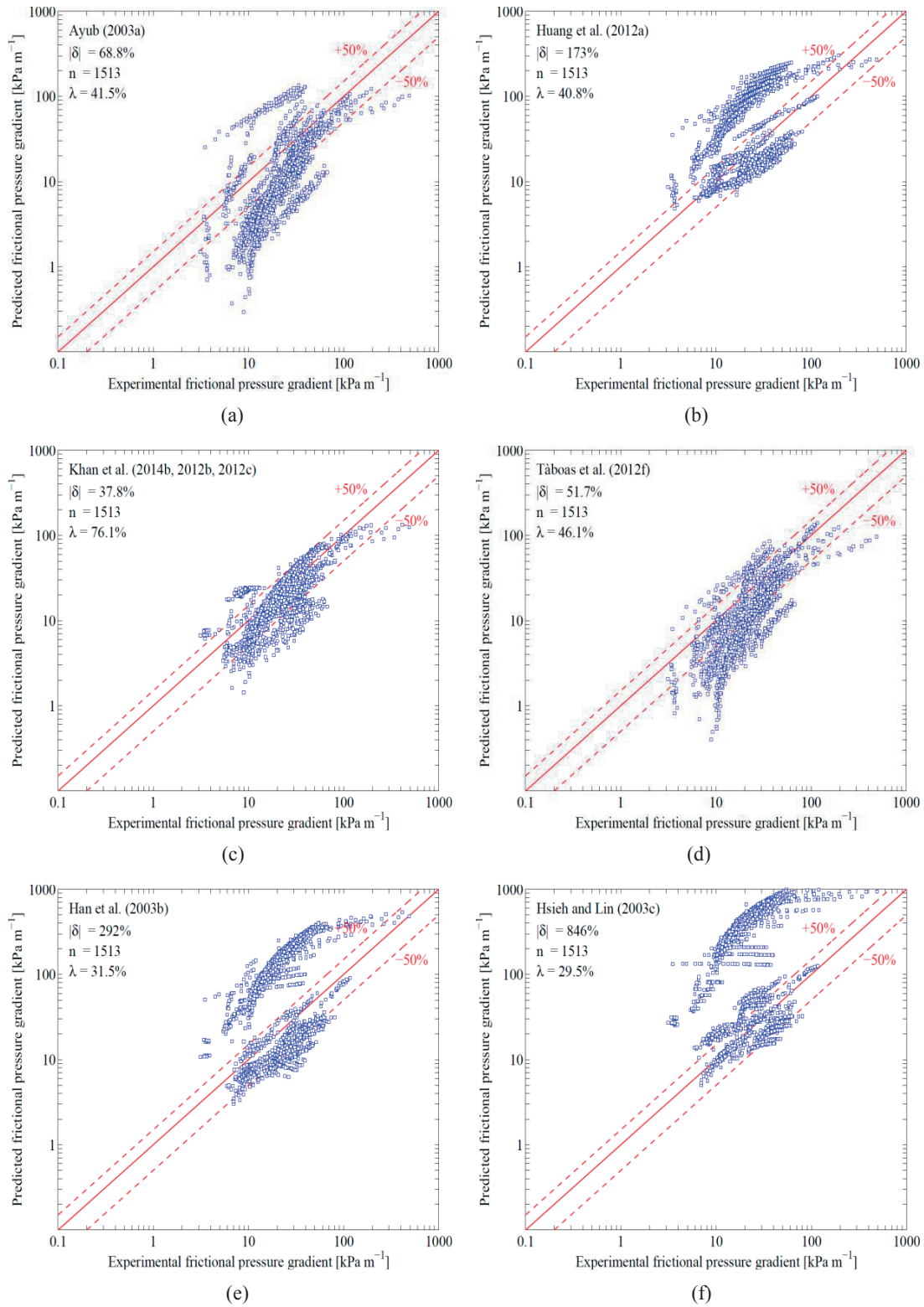


Figure 7.3: Flow boiling predicted frictional pressure gradient against experimental pressure gradient using the correlations proposed by: (a) Ayub (2003a), (b) Huang et al. (2012b), (c) Khan et al. (2014a, 2012c, 2012d), (d) Taboas et al. (2012g), (a) Han et al. (2003b), (b) Hsieh and Lin (2003c).

### 7.3 Dimensional analysis and new general pressure drop model

In what follows, a new flow boiling approach is taken to predict frictional pressure gradients within plate heat exchangers. The theory adopted here has been previously used in some pool boiling and flow boiling studies; that is, it is based on dimensional analysis coupled with a multiple regression technique which identifies the most important parameters that can influence thermal and hydraulic performance.

In order to develop a prediction method for the local frictional pressure gradient, the wall shear stress was assumed to be dependent on the chevron angle  $\beta$ , hydraulic diameter  $d_h$ , densities of the liquid  $\rho_l$  and vapor phases  $\rho_v$ , homogeneous density  $\rho_m$ , superficial velocities of the liquid  $u_l$  and vapor phases  $u_v$ , homogeneous superficial velocity  $u_m$ , surface tension  $\sigma$ , dynamic viscosities of the liquid  $\mu_l$  and vapor phases  $\mu_v$  and the gravitational term  $(\rho_l - \rho_v)g$  to consider the buoyancy force. Consequently, the shear stress was expressed with the following independent variables:

$$\tau_{wall} = \tau_{wall}(\beta, d_h, \rho_l, \rho_v, \rho_m, u_l, u_v, u_m, \sigma, \mu_l, \mu_v, (\rho_l - \rho_v)g) \quad (7.1)$$

Next, the homogeneous density, velocity and hydraulic diameter were selected to take into account the primary dimensions involved:

$$[M] = \rho_m d_h^3, \quad [L] = d_h, \quad [t] = u_m^{-1} d_h \quad (7.2)$$

As a consequence, the number of dimensionless parameters to be included in this analysis was found to be equal to nine. The variables mentioned in eq. 2 were integrated with each variable introduced in eq. 1 to determine the non-dimensional parameters. Based on dimensional analysis, eq. 1 was expressed in dimensionless form as follows:

$$f_{ip} = f_{ip}(\Pi_1, \Pi_2, \dots, \Pi_9) \quad (7.3)$$

$$\begin{aligned} \Pi_1 &= \frac{\sigma}{\rho_m u_m^2 d_h}, \quad \Pi_2 = \frac{\mu_l}{\rho_m u_m d_h}, \quad \Pi_3 = \frac{\mu_v}{\rho_m u_m d_h}, \quad \Pi_4 = \frac{\rho_l}{\rho_m} \\ \Pi_5 &= \frac{\rho_v}{\rho_m}, \quad \Pi_6 = \beta, \quad \Pi_7 = \frac{u_l}{u_m}, \quad \Pi_8 = \frac{u_v}{u_m}, \quad \Pi_9 = \frac{(\rho_l - \rho_v)g d_h}{\rho_m u_m^2} \end{aligned} \quad (7.4)$$

The non-dimensional groups were then manipulated in order to simplify their interpretations and attempt to capture the physical mechanisms involved in the two-phase flow process:

### 7.3 Dimensional analysis and new general pressure drop model

$$\begin{aligned}
\Psi_1 = \Pi_1^{-1} &= \frac{\rho_m u_m^2 d_h}{\sigma} = \frac{G^2 d_h}{\rho_m \sigma} = We_m, \quad \Psi_2 = \Pi_2^{-1} = \frac{\rho_m u_m d_h}{\mu_l} = \frac{G d_h}{\mu_l} = Re_{lo} \\
\Psi_3 = \Pi_3^{-1} &= \frac{\rho_m u_m d_h}{\mu_v} = \frac{G d_h}{\mu_v} = Re_{vo}, \quad \Psi_4 = \Pi_4 \cdot \Pi_5^{-1} = \frac{\rho_l}{\rho_v} = \rho^* \\
\Psi_5 = \Pi_6 &= \frac{\beta}{\beta_{\max}} = \beta^*, \quad \Psi_6 = \Pi_7 \cdot \Pi_4 \cdot \Pi_2^{-1} = \frac{G(1-x)d_h}{\mu_l} = Re_l \\
\Psi_7 = \Pi_8 \cdot \Pi_5 \cdot \Pi_3^{-1} &= \frac{G x d_h}{\mu_v} = Re_v, \quad \Psi_8 = \Pi_9 \cdot \Pi_1^{-1} = \frac{(\rho_l - \rho_v) g d_h^2}{\sigma} = Bd
\end{aligned} \tag{7.5}$$

The experimental range in the database of each non-dimensional parameter presented above is summarized in the Table 7.1.

Table 7.1: Range of dimensionless numbers for flow boiling pressure drop database.

Parameter	Min value	Max value
Bond number, $Bd$	2.40	$4.91 \cdot 10^1$
Density ratio, $\rho^*$	$1.91 \cdot 10^1$	$1.35 \cdot 10^3$
Fanning friction factor, $f_{tp}$	$1.75 \cdot 10^{-1}$	$3.57 \cdot 10^1$
Homogeneous Weber number, $We_m$	$2.67 \cdot 10^{-2}$	$1.50 \cdot 10^2$
Liquid Reynolds number, $Re_l$	8.02	$4.72 \cdot 10^3$
Liquid only Reynolds number, $Re_{lo}$	$3.31 \cdot 10^1$	$4.74 \cdot 10^3$
Reduced chevron angle, $\beta^*$	$4.29 \cdot 10^{-1}$	$9.29 \cdot 10^{-1}$
Vapor Reynolds number, $Re_v$	$1.01 \cdot 10^1$	$3.46 \cdot 10^4$
Vapor only Reynolds number, $Re_{vo}$	$1.69 \cdot 10^3$	$5.98 \cdot 10^4$

From the above manipulations, some well-known dimensionless groups were obtained, which are commonly used to provide some physical insight of the two-phase flow mechanisms. The homogeneous Weber number  $We_m$  is the ratio between the inertia and tension forces and is adopted to characterize flow regime transitions in some flow pattern maps. The liquid only and vapor only Reynolds numbers,  $Re_{lo}$  and  $Re_{vo}$ , are ratios between inertial to viscous forces and they consider respectively that the flow streaming in the plate is totally liquid or totally vapor. The non-dimensional groups  $\Psi_4$  and  $\Psi_5$  were combined to obtain the ratio between the liquid and vapor densities  $\rho^*$ . This parameter is adopted here to take into account the fluid properties, which can significantly change from one fluid to another. The dimensionless group  $\Psi_6$  took into consideration the effect of the chevron angle  $\beta$ , which is one of the most important geometrical parameters in plate heat exchangers and it can strongly affect the performance as well as the flow distribution. In the present analysis  $\beta_{\max}$  was the largest chevron angle investigated in the current databank and it was thus set

equal to 70°. The liquid and vapor Reynolds numbers,  $Re_l$  and  $Re_v$ , are commonly used in the separated flow model approach, in which it is important to distinguish between liquid and vapor phase contributions on the flow boiling mechanism. The Bond number  $Bd$  represents the ratio between the buoyancy and the surface tension forces and it has been used in recent years to characterize the transition between macro-to-microscale two-phase flows as the plate's corrugation height is decreased.

The two-phase Fanning friction factor was correlated adopting the power law representation as shown below:

$$f_{tp} = f_{tp}(\Psi_i) = C \cdot \Psi_i^{a_i}, \quad i = 1, 2, \dots, 8 \quad (7.6)$$

For the present investigation, the power law scheme coupled with a multiple regression analysis was adopted to calculate the leading coefficient  $C$  and the exponents  $a_i$  which return the best fit of the entire experimental database. Precisely, for each dimensionless group the leading constant and exponents were evaluated by fitting the experimental databank using a least square method, where the smallest square error sum identifies the most influential groups. Finally, this procedure was applied until all the dimensionless numbers were grouped. Even though all dimensionless numbers could be kept for correlating the two-phase Fanning friction factor, it is common practice to define a ranking of importance, thus neglecting the non-dimensional numbers that provide little gain in accuracy and thus simplifying the resulting correlation. In addition, a prediction method which is easy to implement and able to predict the flow boiling performance over a wide range of test conditions is preferred.

According to the experimental database, the two-phase Fanning friction factor was best correlated based on the homogeneous Weber number, Bond number, density ratio (liquid/vapor) and chevron angle. Here, it is interesting to note that the annular flow model of Cioncolini et al. (2009) found the core Weber number to be the most dominant group in their similar analysis for tubular annular flows. The other non-dimensional numbers (liquid/liquid only and vapor/vapor only Reynolds numbers) were eliminated here because they did not provide any significant improvement for the prediction capability. Finally, the two-phase Fanning friction factor and thus the frictional pressure gradient within plate heat exchangers can be predicted as follows:

$$f_{tp} = C' \cdot 15.698 \cdot We_m^{-0.475} Bd^{0.255} \rho^{*-0.571} \quad (7.7)$$

where the  $C$  parameter takes into consideration the effect of the corrugation angle (expressed in degrees, not radians) on the pressure drop and it was correlated as:

$$C' = 2.125\beta^{*9.993} + 0.955 \quad (7.8)$$

In Figure 7.4, the comparisons between the predicted and experimental frictional pressure gradient are shown and a reasonable agreement with the experimental database was found. Precisely, the proposed method is able to predict 90.9% of the experimental frictional pressure drop database (which included 1513 data points) with a mean absolute error of 21.5% and a mean error of -6.8%, with 90.9% of the database within a bandwidth of  $\pm 50\%$  while 74.1% of the data fall within  $\pm 30\%$ . With respect to Figure 7.3, there is a visibly significant improvement.

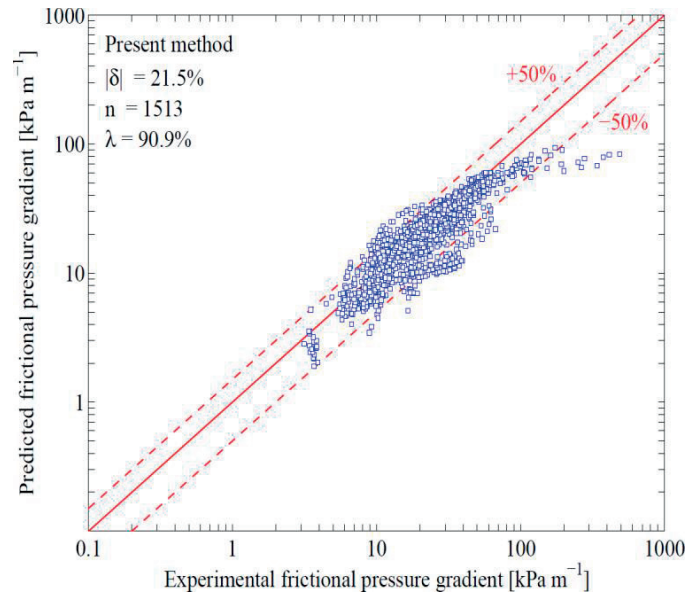


Figure 7.4: Prediction method for two-phase frictional pressure drops within plate heat exchangers: predicted against experimental frictional pressure gradient.

One can see that the friction factor increases with chevron angle because of the longer fluid path, but decreases with the Weber number. The reason may be explained by the fact that with an increasing vapor quality the liquid film thickness close to the wall becomes thinner and as a consequence lower shear stress can be observed. Furthermore, the friction factor rises when the Bond number grows because of the late transition from laminar to turbulent flow regime, which provides higher shear stress but on the other hand it decreases with an increase of the density ratio.

## 7.4 Dimensional analysis and new general heat transfer model

In order to develop a more general prediction method for flow boiling heat transfer within plate heat exchangers, the same procedure as above was followed. In the case of the heat transfer coefficient, three more independent variables were added: the latent heat of vaporization  $i_{lv}$ , the heat flux  $q$ , and the thermal conductivity of the liquid phase  $k_l$ . The final relationship is as follows:

$$h_{tp} = h_{tp}(\beta, d_h, \rho_l, \rho_v, \rho_m, u_l, u_v, u_m, \sigma, \mu_l, \mu_v, (\rho_l - \rho_v)g, i_{lv}, q, k_l) \quad (7.9)$$

In addition to the homogeneous density, velocity and hydraulic diameter, the liquid thermal conductivity was also selected in order to include the effect of temperature as a primary dimension, which was not included in the pressure drop analysis, and thus:

$$[M] = \rho_m d_h^3, \quad [L] = d_h, \quad [t] = u_m^{-1} d_h, \quad [T] = \rho_m d_h u_m^{-3} k_l \quad (7.10)$$

As a consequence, the number of dimensionless groups is eleven. Using the parameters selected in the previous equation, according to the dimensional analysis, eq. 9 was expressed in dimensionless form as follows:

$$Nu_{tp} = Nu_{tp}(\Pi_1, \Pi_2, \dots, \Pi_{11}) \quad (7.11)$$

and two extra dimensionless numbers appeared:

$$\Pi_{10} = \frac{i_{lv}}{u_m^2}, \quad \Pi_{11} = \frac{q}{\rho_m u_m^3} \quad (7.12)$$

Next, the above two parameters were combined to obtain the well-known Boiling number, which took into account the effect of heat flux, mass flux and latent heat on the heat transfer rate:

$$\Psi_9 \rightarrow \Pi_{10}^{-1} \cdot \Pi_{11} = \frac{q}{Gi_{lv}} = Bo \quad (7.13)$$

Following to the procedure applied in the case of the pressure drop analysis, the power law notation combined with multiple regression analysis was used to correlate the two-phase Nusselt number and the unknown empirical coefficients were obtained by fitting the experimental data points based on the least square method. Again, any non-dimensional



group which did not provide an significant improvement in accuracy (2% threshold) in the prediction method was eliminated. As suggested by Kew and Cornwell (1997), the transition from macro-to-microscale for tubular geometries occurs at a Bond number  $Bd = 4$ , being microscale when  $Bd < 4$ . Consequently, the prediction of the two-phase Nusselt number should be performed according to the value of the Bond number. When the experimental Bond number was less than 4 (microscale), the two-phase Nusselt number was found to be associated to the homogeneous Weber number, Bond number, Boiling number, density ratio (liquid over vapor) and chevron angle as follows:

$$Nu_{tp} = 982 \cdot \beta^{*1.101} We_m^{0.315} Bo^{0.320} \rho^{*-0.224} \quad (7.14)$$

Otherwise, for values of the Bond number greater than or equal to 4 (macroscale), the homogeneous Weber number was replaced by the regression technique by vapor Reynolds and liquid only Reynolds numbers. In this scenario, the two-phase Nusselt number was correlated as:

$$Nu_{tp} = 18.495 \cdot \beta^{*0.248} Re_v^{0.135} Re_{lo}^{0.351} Bd^{0.235} Bo^{0.198} \rho^{*-0.223} \quad (7.15)$$

According to these two expressions, the heat transfer in plate heat exchangers is enhanced by increasing the chevron angle (much more so when  $Bd < 4$ ). According to the two-phase flow theory in the channels, the heat transfer coefficient passing from macro-to-microscale should be enhanced because of the confinement effect, which provides a gradual expansion of the annular flow regime and the gradual suppression of the isolated bubble regime, and thus the transition appears earlier. This also promotes stronger turbulence in the flow coupled to the complex flow passage. The forced convection mechanism was found to be the dominant mechanism, even at low vapor quality. The Nusselt number rose with an increase of Boiling number due to the effect of the heat flux, which was important especially at the beginning of the plate when the flow initiates the evaporation process. Notably, the exponents on  $q$  in the two expressions are much less than 0.7, the value that is common to nucleate pool boiling correlations improvised to match some test data as noted earlier. Moreover, the heat transfer rate increased with the Bond number and on the contrary, it decreased with the density ratio. Based on the proposed correlation, the behavior seemed to be the opposite and the reason may be due to the fact that the flow is primarily a complex film flow with little nucleate boiling over this entire range of corrugations. Finally, these two expressions can be considered as macro- and micro-scale plate heat exchanger flow boiling correlations.



## CHAPTER 7 – Two phase prediction methods

A complete overview of the non-dimensions groups covered in the case of heat transfer is shown in Table 7.2 and Table 7.3, where the experimental range of each is reported for macro- and micro-scale accordingly. Of the present database, 56% of the data fell within the macro-scale range and 44% fell within the micro-scale range.

Table 7.2: Range of dimensionless numbers for macroscale flow boiling heat transfer database.

Parameter	Min value	Max value
Boiling number, Bo	$1.15 \cdot 10^{-4}$	$3.75 \cdot 10^{-3}$
Bond number, Bd	4.33	$7.89 \cdot 10^1$
Density ratio, $\rho^*$	$1.91 \cdot 10^1$	$1.28 \cdot 10^2$
Homogeneous Weber number, $We_m$	$2.41 \cdot 10^{-1}$	$1.62 \cdot 10^2$
Liquid Reynolds number, $Re_l$	$3.48 \cdot 10^1$	$5.32 \cdot 10^3$
Liquid only Reynolds number, $Re_{lo}$	$8.38 \cdot 10^1$	$5.36 \cdot 10^3$
Nusselt number, Nu	$3.92 \cdot 10^1$	$5.29 \cdot 10^2$
Reduced chevron angle, $\beta^*$	$4.00 \cdot 10^{-1}$	1.00
Vapor Reynolds number, $Re_v$	7.94	$3.45 \cdot 10^4$
Vapor only Reynolds number, $Re_{vo}$	$1.85 \cdot 10^3$	$8.58 \cdot 10^4$

Table 7.3: Range of dimensionless numbers for microscale flow boiling heat transfer database.

Parameter	Min value	Max value
Boiling number, Bo	$2.97 \cdot 10^{-5}$	$4.05 \cdot 10^{-3}$
Bond number, Bd	1.89	3.76
Density ratio, $\rho^*$	$7.75 \cdot 10^1$	$1.35 \cdot 10^3$
Homogeneous Weber number, $We_m$	$2.67 \cdot 10^{-2}$	$4.15 \cdot 10^1$
Liquid Reynolds number, $Re_l$	$2.34 \cdot 10^1$	$2.58 \cdot 10^3$
Liquid only Reynolds number, $Re_{lo}$	$4.12 \cdot 10^1$	$2.72 \cdot 10^3$
Nusselt number, Nu	2.07	$1.21 \cdot 10^2$
Reduced chevron angle, $\beta^*$	$4.29 \cdot 10^{-1}$	$9.29 \cdot 10^{-1}$
Vapor Reynolds number, $Re_v$	8.58	$6.52 \cdot 10^3$
Vapor only Reynolds number, $Re_{vo}$	$1.58 \cdot 10^3$	$4.22 \cdot 10^4$

Note that for the frictional pressure drop and heat transfer calculations, the hydraulic diameter was only used as the characteristic dimension of the channels. The mass flux was that calculated using the actual cross-sectional area of axial flow along the plate, *not* that using the cross-sectional area that could be calculated using the hydraulic diameter.

Furthermore, the actual cross-sectional area was calculated as  $b \cdot W$  and the hydraulic diameter for the plate was calculated as  $2b/\phi$ .

In Figure 7.5 the newly proposed methods are shown compared to the entire database. It can be concluded that there is a good agreement between the predicted and experimental data, since the new methods predicted 92.3% of the entire flow boiling databank (which included 1903 data points) with a mean absolute error of 22.1%, with 92.3% within  $\pm 50\%$  while 76.1% could be captured within  $\pm 30\%$ . Compared to Figure 7.2, the improvement is visibly evident.

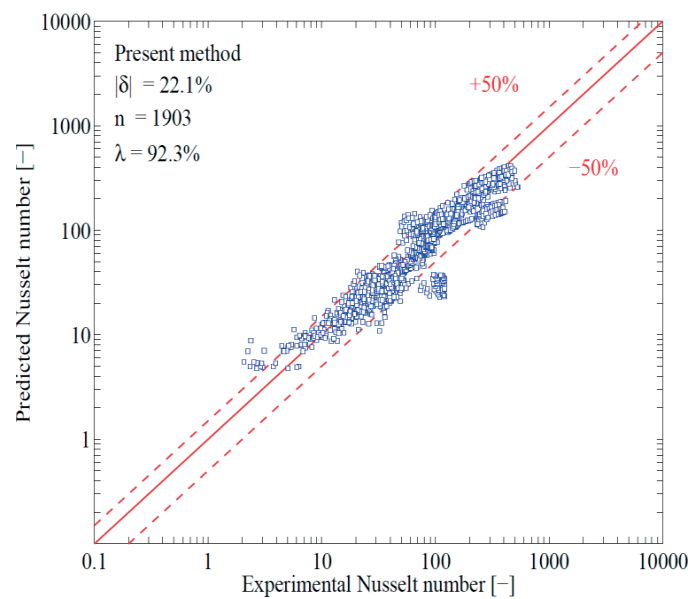


Figure 7.5: Flow boiling prediction methods for heat transfer within plate heat exchangers: predicted against experimental Nusselt number.

## 7.5 Comparison of general prediction methods to data

In order to highlight the predicted capabilities of the new frictional pressure drop method versus the next best methods, several more comparisons have been performed. One can see the new method followed the trends in the data and it worked for fluids as diverse as R507A and ammonia. As can be seen from the Figure 7.6, the new model closely predicted the four independent databases selected for this comparison. In the Figure 7.6b, the proposed model exhibited better capability to evaluate the hydraulic performance of a  $60^\circ$  chevron plate with ammonia compared to their own correlations, which slightly underestimated their experimental data. Furthermore, it has to be pointed out that only in the case of the Hsieh and Lin (2003c) data and Yan and Lin (1999c) data at relatively high mass flux, the new method

was not able to follow the entire trend. At low vapor quality the frictional pressure drop was underestimated as well as in the turbulent flow region, in which the Fanning friction factor approximated to an asymptote and the frictional pressure drop was strongly dependent to the mean vapor quality. In conclusion, the proposed model underestimated the pressure drop database provide by Lee et al. (2014b) since flow boiling of water at low mass fluxes exhibits different behavior compared to the traditional refrigerants.

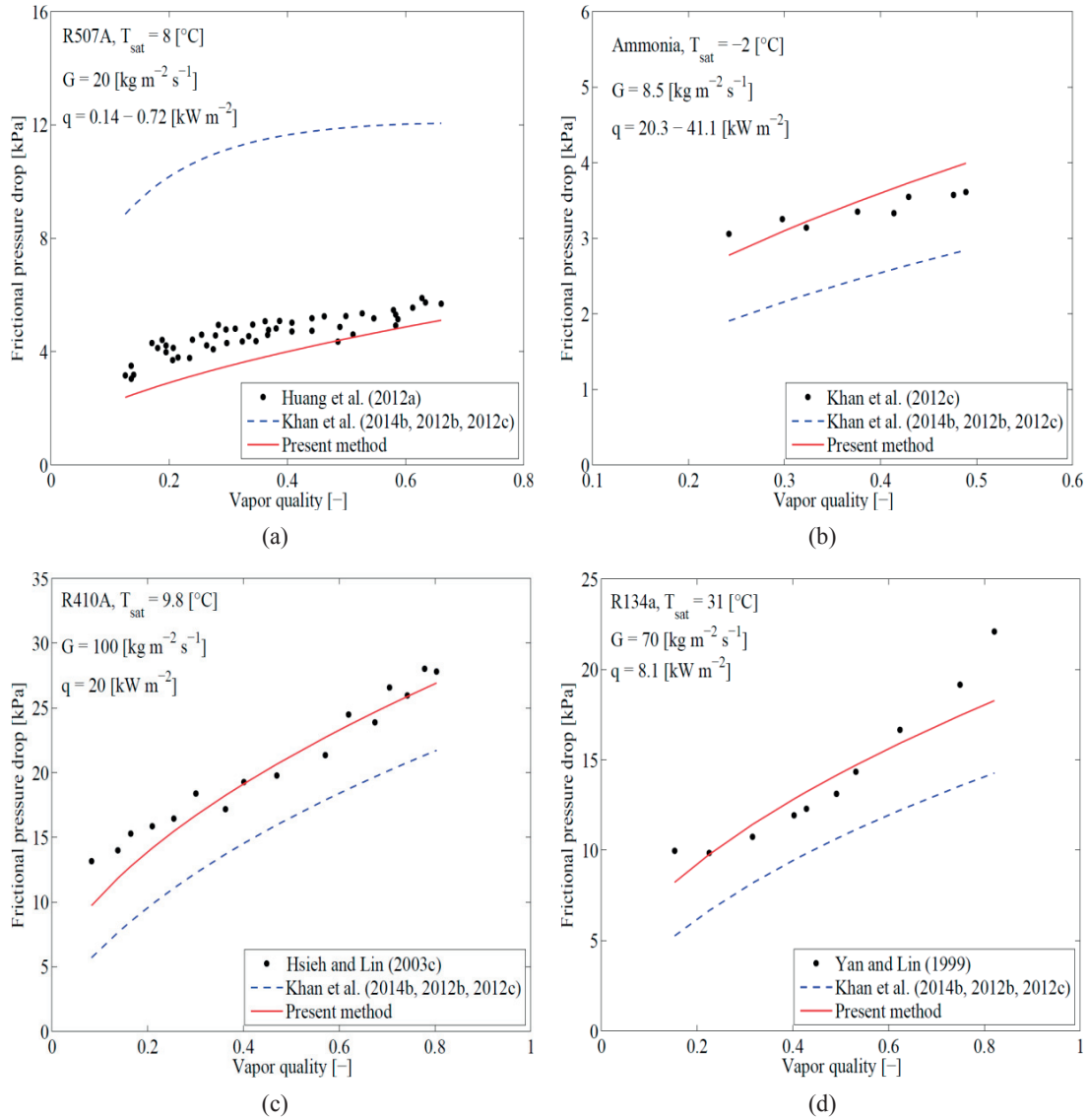


Figure 7.6: Experimental frictional pressure drops versus vapor quality predicted by Khan et al. (2014a, 2012c, 2012d) and new method in case of: (a) Huang et al. data (2012b), (b) Khan et al. data (2014a, 2012c, 2012d), (c) Hsieh and Lin (2003c), (d) Yan and Lin (1999c).

## 7.5 Comparison of general prediction methods to data

Figure 7.7 depicts a similar comparison, but now the heat transfer coefficient against the vapor quality was examined.

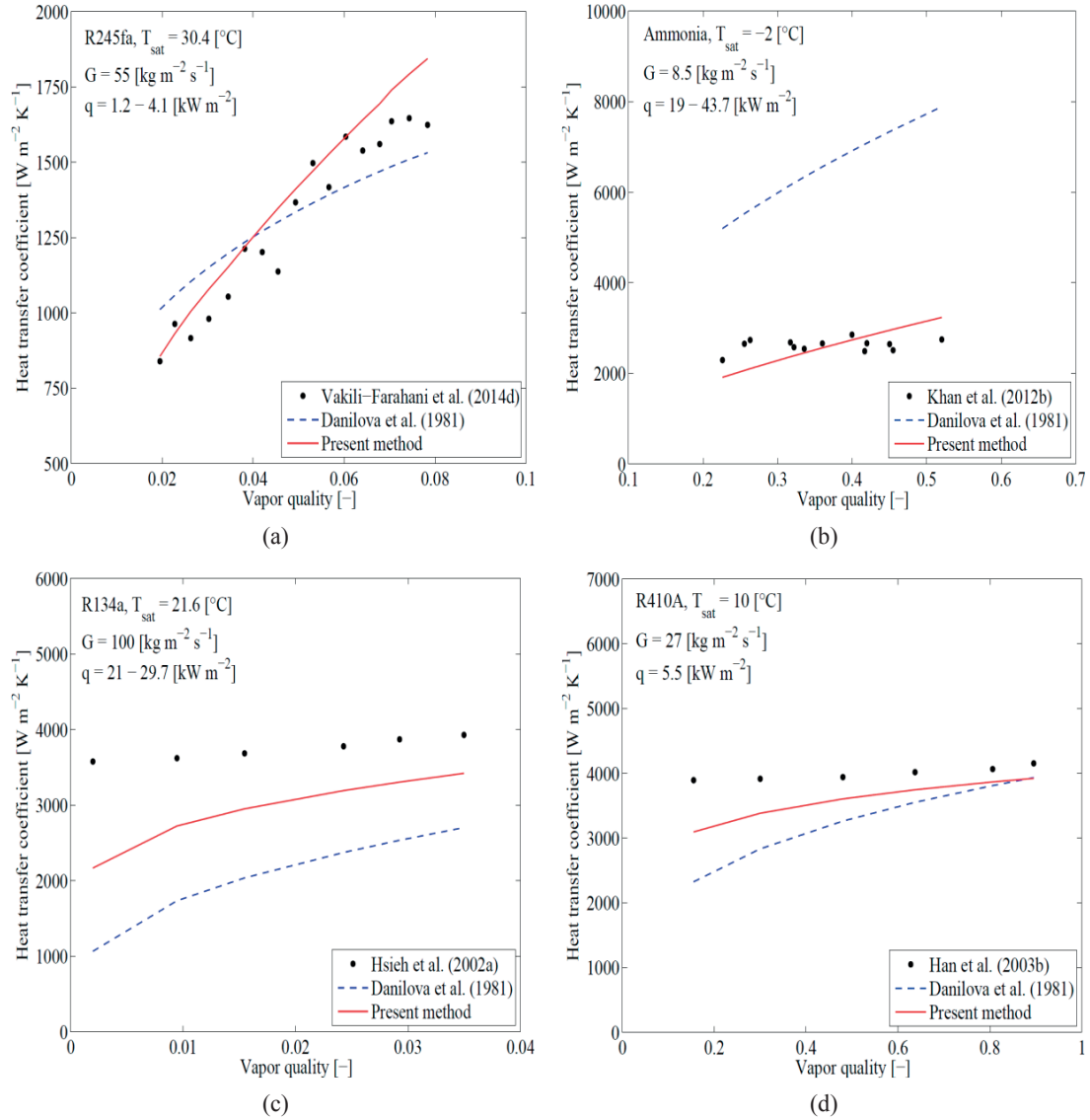


Figure 7.7: Experimental heat transfer coefficients versus vapor quality predicted by Danilova et al. (1981) and new method in case of: (a) Vakili-Farahani et al. data (2014c, 2014d), (b) Khan et al. data (2014a, 2012c, 2012d), (c) Hsieh et al. (2002a), (d) Han et al. data (2003b).

It can be observed that the new method predicted the heat transfer rate with a good agreement to the experimental data points for both microscale (Vakili-Farahani et al (2014c, 2014d) and Khan et al. data (2014a, 2012c, 2012d)) and macroscale Hsieh et al. (2002a) and Han et al. data (2003b)) conditions as well as different corrugation angles. In particular, in the case of ammonia, the prediction method provided by Danilova et al. (1981) strongly

overestimated the experimental values; thus, their extrapolation at low mass fluxes and 30° chevron angle plate with ammonia is not recommended. It has also to be highlighted that the present method could only predict qualitatively the subcooled flow boiling data of Hsieh et al. (2002a) due to the fact that no subcooling parameter was introduced into the present new prediction method. Moreover, the present prediction method underestimated the database collected by Lee et al. (2014b) because no parameter was involved to take into account the heat transfer within the dry-out region, thus a future study should look specifically at these conditions. It has also to be highlighted, that the new correlation underestimated the databank provided by Park and Kim (2004b) and the reason may be due to the fact that those authors investigated flow boiling of refrigerants inside an oblong shell and plate heat exchanger.

## **7.6 Conclusions**

Most research studies investigated the overall performance of plate heat exchangers for specific test conditions and only a few publications carried out local characterization of thermal-hydraulic performance. Attempts to propose a universal correlation predicting the evaporation heat transfer coefficients and frictional pressure drops are very rare due to the large number of parameters involved in the heat transfer process: plate arrangements and geometry, experimental test conditions, flow distribution and transition between different two-phase flow regimes. The leading published methods were compared statistically versus large multi-lab databases for flow boiling heat transfer coefficients and frictional pressure drops in plate heat exchangers (a huge effort was made to put this databank together). The flow boiling heat transfer coefficients were discretely predicted by the Danilova et al. (1981) and Han et al. (2003b) methods, while in the case of frictional pressure drops the best existing method was that of Khan et al. (2014a, 2012c, 2012d). Also, it was shown that most of the correlations should not be extrapolated out of their original range of test conditions. Based on a dimensional and multiple regression analysis, new prediction methods for flow boiling heat transfer coefficient and frictional pressure gradient within plate heat exchangers have been proposed. These methods were developed from 1903 heat transfer and 1513 frictional pressure drop data points, respectively, and were proved to work better than any other published method over a very wide range of operating conditions, plate designs and fluids (including ammonia).

# **CHAPTER 8 – Heat exchanger simulation code**

## **8.1 Introduction**

In the current chapter, a simulation code to analyze thermal and hydraulic performance, under steady-state condition, of commercial chevron plate heat exchangers is presented. A local one dimension effectiveness-NTU approach coupled with suitable prediction methods for local heat transfer coefficient and local frictional pressure drop have been implemented in MATLAB and the predicted performances validated against independent databases from literature. A comprehensive overview of the modeling and the associated flow chart are first addressed in the present chapter. Then, some relevant simulation cases of parallel- and counter-flow arrangements are analyzed in detail and a sensitivity analysis is performed to highlight the effect of the plate geometry (chevron angle and corrugation aspect ratio) on the thermal and hydraulic performance.

## **8.2 Overview of the simulation code**

The goal of the present simulation tool is to analyze the thermal and hydraulic performance of the refrigerant-to-water heat transfer and flow for single- and multi-passages commercial chevron plate heat exchangers. This simulation code is able to model evaporation, condensation and single-phase (liquid or vapor) flow of the refrigerant side, while the water side was assumed to flow only in single-phase liquid condition, i.e. so simulate water-chillers and water cooled condensers in refrigeration systems. In addition, this tool can handle several flow configurations (parallel- and counter-flow), different flow orientations (horizontal and vertical), many plate arrangements and geometries.

A set of appropriate correlations have been selected and implemented in order to predict the overall thermal and hydraulic performance, starting from the local heat transfer coefficients and frictional pressure drops along the plate heat exchanger, i.e. this is an incremental design approach in which the heat exchanger is simulated in numerous small steps from inlet to outlet that are then added together to get the total design. In particular, in the case of flow boiling, the local heat transfer coefficients and the local two-phase frictional

pressure drops have been evaluated according to Amalfi et al. models (2015b, 2015c), described in chapter 7 of this thesis, while for condensation heat transfer the method proposed by Yan et al (1999d) has been adopted. On the contrary, for complete single-phase liquid or vapor flow through the plate heat exchanger, the local thermal and hydraulic performance have been evaluated according to the correlations provided by Kumar (1984b). This simulation code took into consideration also the possibility to have some lubricant oils dissolved in the refrigerant flow. A small percentage of the mineral oils (between 2% and 5%) strongly influence the thermal and hydraulic performance of the heat exchangers, decreasing the overall heat transfer coefficient and increasing the total pressure drop as well as the energy consumption. The influence was accounted for through the increase of the liquid viscosity of the liquid refrigerant by the oil within the prediction methods for the refrigerant-side. Finally, the current tool can be easily managed by the users, thanks to a friendly and dynamic Graphic User Interface (GUI), which included description, comments of the code and error handling in case of user's mistakes or input values that are out of range.

### **8.3 Structure of the simulation code**

In Figure 8.1 the code structure and the associated flow chart for rating commercial parallel- or counter- flow plate heat exchangers by using the present tool are described. All the variables calculated at each step of the simulation process are reported in blue.

The first step was to define the simulation conditions in terms of mass flow rates, inlet temperatures and inlet pressures of the water and refrigerant streams. The type of refrigerant, the geometry specification of the plates and the flow arrangement and orientation were also defined. Next, the evaluation of additional geometrical parameters, e.g. flow cross sectional area, heat transfer area, surface enlargement factor and characteristic lengths, as well as the mass fluxes for both sides and the number of control volumes needed for the local calculation were defined.

The calculation of the above mentioned parameters has been performed according to the data reduction schemes, which was fully detailed in chapter 3 of the present thesis. In order to guarantee an efficient simulation, all the variables were initialized and the properties for both water and refrigerant streams were calculated adopting REFPROP 9.0.

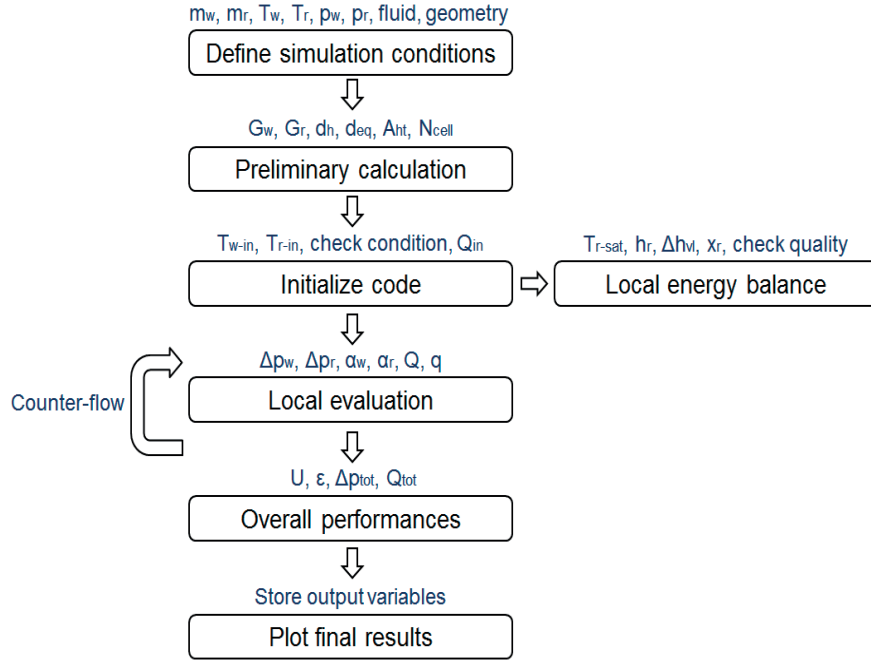


Figure 8.1: Schematic of the plate heat exchanger simulation code and the related flowchart in case of parallel- and counter-flow arrangement, in which the subscript  $w$  and  $r$  are referred to water and refrigerant streams.

According to the inputs defined by the users, the inlet fluid temperatures in case of parallel- flow were defined as follow:

$$\begin{aligned} T_{w,in} &= T_{w,input} \\ T_{r,in} &= T_{r,input} \end{aligned} \quad (8.1)$$

while for counter-flow arrangement:

$$\begin{aligned} T_{w,out} &= \frac{T_{w,input} + T_{r,input}}{2} \\ T_{r,in} &= T_{r,input} \end{aligned} \quad (8.2)$$

In order to define the state of the refrigerant at the inlet of the heat exchanger, its temperature was compared to the saturation temperature at the given input pressure and an energy balance on the first control volume were carried out in order to determine the refrigerant vapor quality. It has to be pointed out that, the water-side was always maintained in single-phase liquid flow through the plate heat exchanger.

For the parallel-flow configuration, the local calculation proceeded by evaluating the local pressure drop and the overall heat transfer coefficient until the end of the plate heat exchanger, since the outlet conditions of each control volume were assumed to be coincident



with the inlet conditions of the next one. On the other hand, for counter-flow arrangement, the local calculation was developed as a normal parallel-flow, considering the assumption of the outlet temperature of the water-side as shown in the eq. 2. For this reason, an iteration at the end of the simulation process was required in order to match the calculated outlet temperature of the water-side (corresponding to the inlet temperature for counter-flow) with the input value given by the users (defined as  $T_{input,w}$ ). The details of this step are listed in Figure 8.2 and discussed in the next paragraph. The overall performance of the plate heat exchanger was then defined based on the definitions of the total pressure drop in both sides, the overall heat transfer coefficient, the overall effectiveness and the total heat exchanged from one fluid to the other. The thermal and hydraulic performance were determined taking into account the pressure drops at the inlet and outlet ports, using the Shah and Focke (1988) model, as well as the pressure losses due to the inlet and outlet pipes (according to their internal diameters and lengths), adopting the homogeneous model with two-phase viscosity evaluated by Cicchitti et al. (1960a). These pressure losses were accounted for, in the local calculation, only in the first and last control volumes respectively. Finally, the main results of the simulation were transferred to the Graphical User Interface to be displayed in time and then saved in a output structure file.

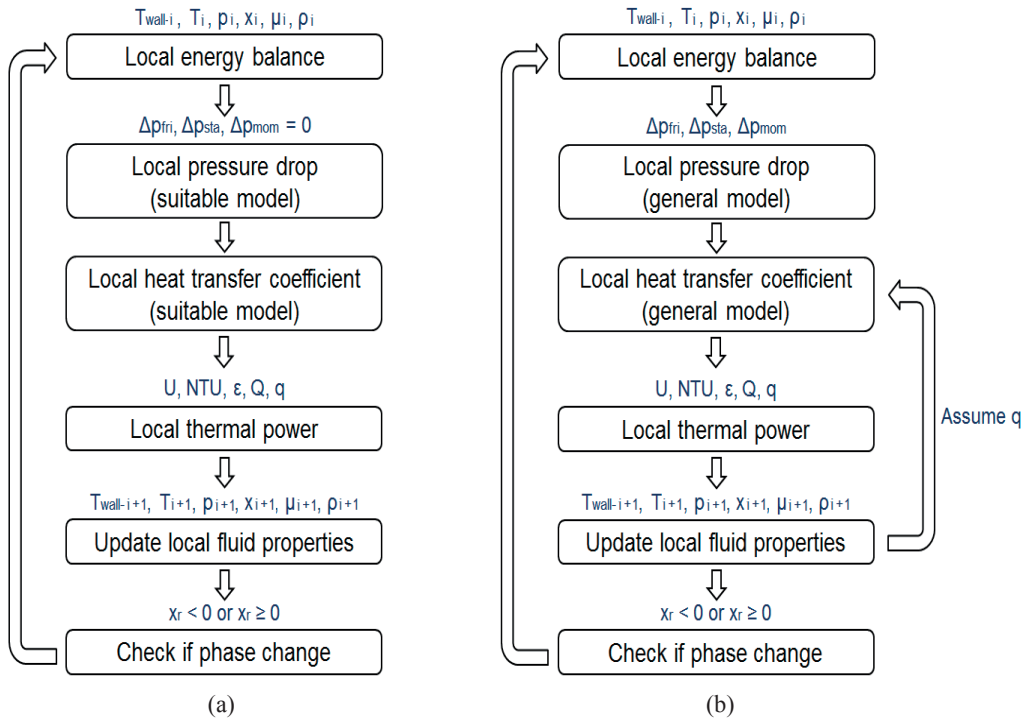


Figure 8.2: Local plate heat exchanger calculation and the associated flowchart for: (a) single-phase liquid or vapor flow of refrigerant side and single-phase liquid flow of water side, (b) evaporation or condensation of refrigerant side and single-phase liquid flow of water-side.

Figure 8.2 illustrates the details of the local heat transfer and pressure drop simulation, highlighting the main differences between single- and two-phase flow of the refrigerant-side. In case of single-phase liquid or vapor flow over all the plate heat exchanger, for each control volume, the local wall temperature has been calculated as an average value between the mean fluid temperatures of the two streams, while the thermodynamic fluid properties were evaluated according to the local temperature and pressure at both sides. The local vapor qualities for the water- and refrigerant-sides were also carried out performing a local energy balance on each stream, resulting in  $x < 0$  in case of single-phase liquid flow and  $x > 1$  for single-phase vapor flow. Locally, the total pressure drop was the sum of static and frictional pressure losses, while the acceleration pressure drop was equal to zero because there was no variation of the vapor quality for an all liquid or all vapor flow. In particular the equation implemented for the static pressure drop as well as for the frictional pressure drop are the following:

$$\Delta p_{sta} = \rho \cdot g \cdot L \quad (8.3)$$

$$f = \frac{a}{Re^b}, \quad \Delta p_{fri} = 2 \cdot f \cdot \frac{L}{d_h} \cdot \frac{G^2}{\rho} \quad (8.4)$$

The frictional pressure drop was obtained using the model proposed by Kumar (1984b), in which the Fanning friction factor was a function of the Reynolds number and the coefficients  $a$  and  $b$  were chosen according to the plate chevron angle and the flow regime.

On the other hand, the heat transfer coefficient was also computed adopting the prediction method developed by Kumar (1984b) and in the same way, the empirical constants  $a$  and  $b$  were linked to the chevron angle and the flow regime.

$$Nu = \frac{h \cdot d_h}{k} = a \cdot Re^b \cdot Pr^{0.33} \quad (8.5)$$

The overall heat transfer coefficient and the Number of Transfer Units,  $NTU$ , were computed as follow:

$$U = \left( \frac{1}{h_w} + \frac{t}{k_{wall}} + \frac{1}{h_r} \right)^{-1} \quad (8.6)$$

$$NTU = \frac{U \cdot A_{ht}}{C_{min}}, \quad C_{min} = \min(C_w, C_r) \quad (8.7)$$

The effectiveness was calculated based on the type of flow arrangement,  $NTU$  and  $C_r$  (ratio between the minimum and maximum heat capacity rates) values. In particular for the parallel flow configuration, the effectiveness was defined by the following expression:

$$\varepsilon = \frac{Q}{Q_{id}} = \frac{1 - \exp[-NTU \cdot (1 + C_r)]}{1 + C_r} \quad (8.8)$$

while for the counter flow arrangement, the evaluation of the effectiveness was performed according to the value of  $C_r$ :

$$\varepsilon = \frac{Q}{Q_{id}} = \frac{1 - \exp[-NTU \cdot (1 - C_r)]}{1 - C_r \cdot \exp[-NTU \cdot (1 - C_r)]}, \quad C_r < 1 \quad (8.9)$$

$$\varepsilon = \frac{Q}{Q_{id}} = \frac{NTU}{1 + NTU}, \quad C_r = 1 \quad (8.10)$$

Next, the thermal power exchanged between the two fluids and the associated effective heat flux were determined as follows:

$$Q = \varepsilon \cdot Q_{id} = \varepsilon \cdot C_{\min} \cdot \Delta T_{\max} \quad (8.11)$$

$$q = \frac{Q}{A_{ht}} \quad (8.12)$$

The updated local temperatures for the refrigerant- and water-sides were calculated by performing an energy balance, while the associated absolute pressures were dependent on the static and frictional pressure drops. After that, all the fluid properties were again evaluated, the vapor qualities were updated and a check was done for possible phase change. Finally, the same loop was locally repeated until the exit of the plate heat exchanger.

A performance index, defined as the ratio between the heat exchanged and the total pressure drop (sum of the refrigerant and water sides), was additionally calculated:

$$\chi = \frac{Q}{\Delta p_{tot}} = \frac{(m \cdot c_p \cdot \Delta T)_w}{\Delta p_r + \Delta p_w} \quad (8.13)$$

Figure 8.2b presents the flowchart in case of a two-phase flow of refrigerant within the plate heat exchanger and the main differences compared to the single-phase flow scenario are summarized below:

- During the boiling process the vapor quality increased with the plate length and for this reason the momentum pressure drop has been involved in the local pressure drop calculation. The homogeneous model has been adopted to characterize this contribution:

$$\Delta p_{mom} = G^2 \cdot \left[ x_{out} \left( \frac{1}{\rho_{v,out}} - \frac{1}{\rho_{l,out}} \right) - x_{in} \left( \frac{1}{\rho_{v,in}} - \frac{1}{\rho_{l,in}} \right) \right] \quad (8.14)$$

- In the evaluation of the static pressure drop using eq. 8.3, the liquid or vapor densities have been replaced by the two-phase homogeneous density:

$$\rho_m = \left[ \frac{x}{\rho_v} + \frac{1-x}{\rho_l} \right]^{-1} \quad (8.15)$$

- The local frictional pressure drops and the local heat transfer coefficients have been determined based on the definitions of the two-phase Fanning friction factor and two-phase Nusselt number. They were defined according to the general flow boiling models proposed by Amalfi et al. (2015b, 2015c) and explained in detail in chapter 7 of the present thesis:

$$f_{tp} = C' \cdot 15.698 \cdot We_m^{-0.475} \cdot Bd^{0.255} \cdot \rho^{*-0.571}, \quad C' = 2.125 \cdot \beta^{*9.993} + 0.955 \quad (8.16)$$

$$Nu_{tp} = 982 \cdot \beta^{*1.101} \cdot We_m^{0.315} \cdot Bo^{0.320} \cdot \rho^{*-0.224}, \quad Bd < 4 \quad (8.17)$$

$$Nu_{tp} = 18.495 \cdot \beta^{*0.248} \cdot Re_v^{0.135} \cdot Re_{lo}^{0.351} \cdot Bd^{0.235} \cdot Bo^{0.198} \cdot \rho^{*-0.223}, \quad Bd > 4 \quad (8.18)$$

- The local flow boiling heat transfer coefficient depends on the local thermal power (corresponding to the local heat flux) and as a consequence the calculation has to be iterative in each control volume. The thermal power, referred to the latent heat at the input pressure divided by the number of control volumes, has been used as an initial guess for the local thermal power transferred to one fluid to the other:

$$Q_{guess} = \frac{m_r \cdot i_{lv}}{N_{cell}} \quad (8.19)$$

- The relation between the effectiveness and the Number of Transfer Units for a fluid in phase change is regardless of the flow arrangement and for both parallel- and counter-flow configurations became:

$$\varepsilon = \frac{Q}{Q_{id}} = 1 - \exp(NTU) \quad C_r = 0 \quad (8.20)$$

The simulation results obtained with the present tool have been furnished under the following assumptions:

- The fluid properties for both water and refrigerant streams have been evaluated at the inlet of each control volume. The equations of mass, energy and momentum balance have been implemented according to the steady-state condition.
- The plate heat exchanger was supposed to be perfectly insulated, thus no heat losses due to natural convection and radiation to the ambient were involved in the simulation process.
- The local thermal conductivity of the material interface was estimated based on the local mean fluid temperature of the two streams and the coefficients of the polynomial expression were selected based on the type of material.
- Uniform flow distribution inside the plate inter-passages for both streams was assumed.

## 8.4 Validation of the simulation code

The simulation results were first validated against two independent databases, in terms of local heat transfer coefficient and local frictional pressure drop, obtained by Yan and Lin (1999c). The authors investigated upward flow boiling of refrigerant-to-water within a commercial plate heat exchanger in a counter-flow configuration, which was fabricated with a port-to-port length of 500 mm, width of 120 mm, pressing depth of 3.3 mm, wavelength of the surface corrugation of 10 mm and chevron angle equal to 60°. For the thermal validation, the experimental operating conditions were chosen as: saturation temperature of 25.5 °C, mass flux equal to 70 kgm<sup>-2</sup>s<sup>-1</sup>, heat flux of 8.6 kWm<sup>-2</sup>, vapor quality ranging from 0.1 to 0.5 and R134a as working fluid. In case of hydraulic validation, the test conditions were set as: saturation temperature of 9.7 °C, mass flux equal to 100 kgm<sup>-2</sup>s<sup>-1</sup>, heat flux of 20 kWm<sup>-2</sup>, and the vapor quality varied from 0.08 to 0.8 with R410A as the working fluid.

In the simulation code, the definition of the overall heat transfer coefficient involved the calculation of the thermal resistance on the water-side, that has been determined according to the model proposed by Yan and Lin (1999c). The authors performed a preliminary water-to-water experimental campaign and correlated the Nusselt number with Reynolds number, Prandtl number and viscosity ratio (fluid over wall) as follow:

$$Nu_w = 0.2121 \cdot Re^{0.78} \cdot Pr^{1/3} \left( \frac{\mu_w}{\mu_{wall}} \right)^{0.14} \quad (8.21)$$

Figure 8.3 shows the validation of the single-phase water-side heat transfer coefficient. In particular, the predicted and experimental Nusselt numbers were plotted as a function of the Reynolds number, resulting in fairly good agreement.

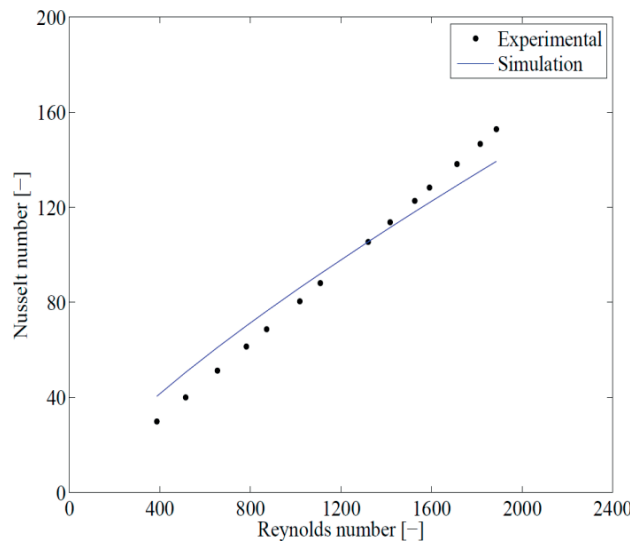


Figure 8.3: Validation of the single-phase water-to-water heat transfer coefficient prediction method: prediction and experimental data have been provided by Yan and Lin (1999c) and the Nusselt number were plotted against the Reynolds number.

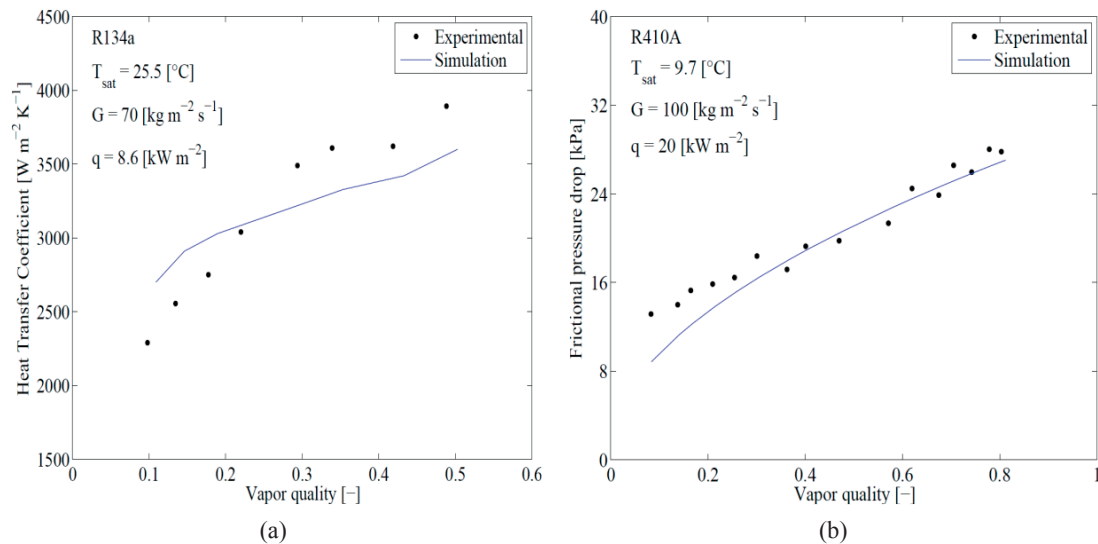


Figure 8.4: Validation of the present simulation code using the flow boiling databases provided by Yan and Lin (1999c): (a) local heat transfer coefficient versus local vapor quality, (b) local frictional pressure drop against local vapor quality.

Figure 8.4 illustrates the comparison of the experimental heat transfer and pressure drop data against the simulation results obtained by the present simulation code in the above mentioned operating conditions. For this analysis the local flow boiling heat transfer coefficients and local frictional pressure drops have been evaluated based on the models proposed by Amalfi et al. (2015b, 2015c), while the water side heat transfer coefficients were computed using the Yan and Lin (1999c) method (eq. 8.21) and water-side frictional pressure drops adopting the Kumar (1984b) correlation (eq. 8.4). An overall good agreement between experimental and simulation results has been observed and the small deviation may be due to the predicted capabilities of the prediction methods, that were proved within a reasonable bandwidths.

## 8.5 Simulation results

This paragraph presents a comparison between a parallel- and counter-flow water-to-refrigerant plate heat exchanger in terms of local thermal and local hydraulic performance. The simulation conditions are summarized in Table 8.1.

Table 8.1 - Simulation conditions for parallel- and counter-flow thermal and hydraulic analysis.

Parameter	Primary Fluid	Secondary Fluid
Fluid	R134a	Water
Mass flow rate ( $\text{kgs}^{-1}$ )	0.03	0.13
Inlet temperature ( $^{\circ}\text{C}$ )	8	22
Inlet pressure (kPa)	400	200
Flow direction in parallel-flow	Upward	Upward
Flow direction in counter-flow	Upward	Downward
Number of plates	3	
Length from port to port (mm)	1500	
Width (mm)	500	
Pressing depth (mm)	3.3	
Chevron angle ( $^{\circ}$ )	60	
Thickness (mm)	0.4	
Wavelength of surface corrugation (mm)	10	
Material	Stainless-steel	

In Figure 8.5, Figure 8.6 and Figure 8.7 the simulation results for parallel-flow arrangement are depicted. The refrigerant-side was slightly subcooled at the inlet and due to

the overall thermal power exchanged, was completely evaporated and superheated at the outlet of the plate heat exchanger. According to the parallel-flow arrangement, the temperature difference between the two fluids was larger at the beginning and then reduced along the plate length approaching zero asymptotically. It has to be pointed out that, the outlet temperature of the refrigerant-side never exceeded the outlet temperature of the water-side. Moreover, transferring heat from the water to the refrigerant in two-phase flow, the temperature gradient of the water-side was considerably greater than the one obtained when the refrigerant was fully vapor. The reason was due to the higher heat transfer coefficients provided by the boiling process, that allowed the fluid to locally exchange a large amount of heat. During the evaporation process, the refrigerant temperature decreased along the plate length due to the two-phase pressure drops.

The absolute pressure profiles for the two fluids are illustrated in Figure 8.5b. The local refrigerant pressure decreased along the plate length due to the local contribution of the frictional, static and momentum pressure drops. As expected, the pressure drop in the flow boiling region was found to be higher compared to the single-phase liquid and vapor regions due to the additional shear stress between liquid and vapor phases, which increased with the vapor quality. Presently, working with a high pressure refrigerant as well as lower mass flow rate, the total pressure drop in the refrigerant side was relatively small. The local absolute pressure of the water-side decreased linearly with the plate length since the frictional and static contributors were uniform over all the plate heat exchanger.

The local wall (interface) temperature and its thermal conductivity are shown in Figure 8.5c and Figure 8.5d respectively. The surface temperature followed the same trend of the water-side temperature and the thermal conductivity was linked to the wall temperature and the interface material.

In Figure 8.5e the local vapor quality for both fluid was plotted against the plate length. The vapor quality was calculated through the three (liquid, vapor and two-phase) regions in order to check the calculation at each control volume and also have a reference from the saturation condition. As can be seen from Figure 8.5e vapor quality of the water-side was negative going from inlet to the outlet of the plate heat exchanger, since the water flowed in single-phase liquid condition, while the vapor fraction for the refrigerant side increased with the axial coordinate going from -0.006 (slightly subcooled at the inlet ) to 1.014 (almost 3 °C vapor superheated at the outlet). The negative qualities for water are calculated dividing the subcooled enthalpy change by the latent heat, in order to plot on the same graph as the refrigerant.



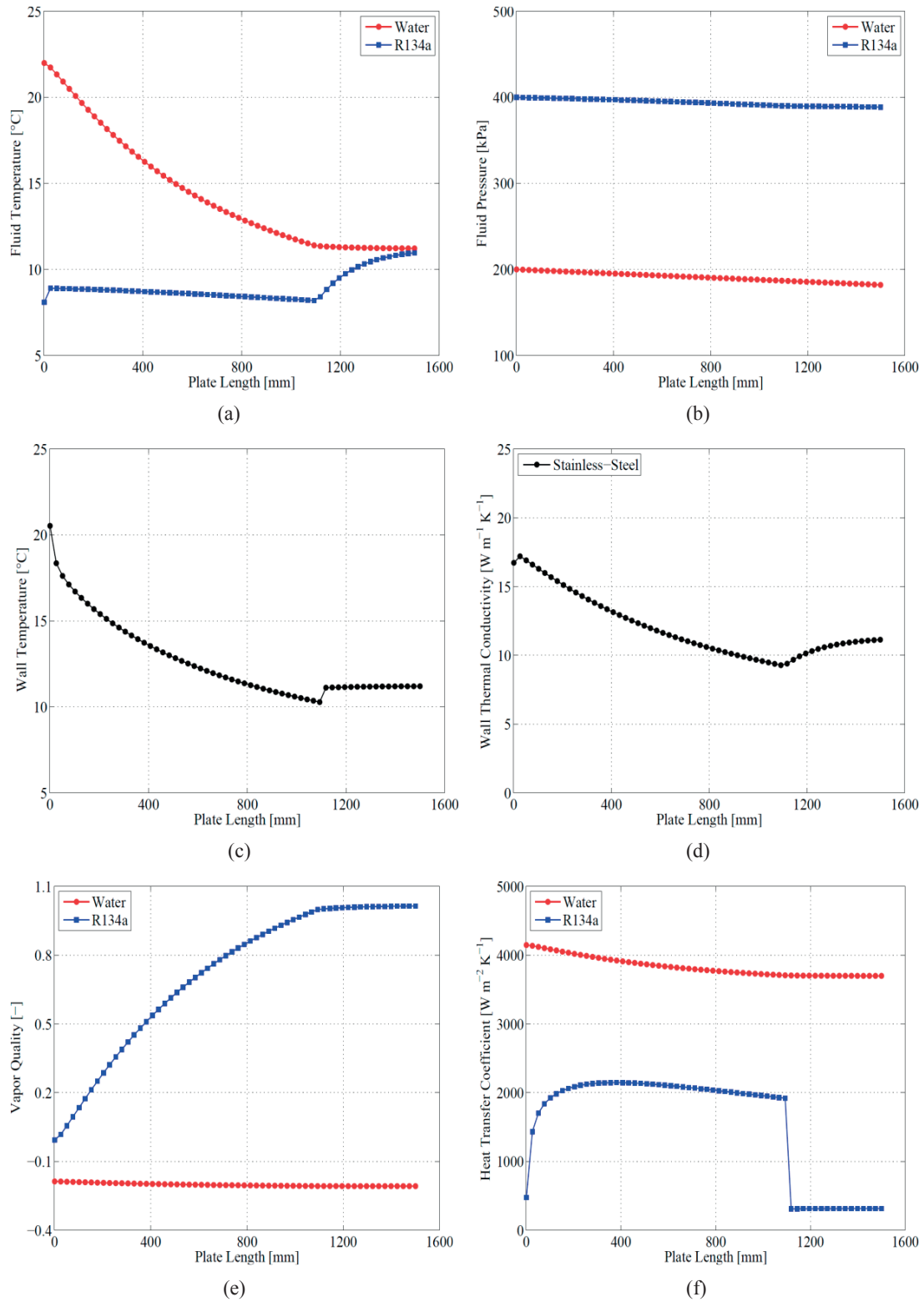


Figure 8.5: Numerical simulation of a parallel-flow plate heat exchanger and local results plotted against the plate heat exchanger length: (a) fluid temperatures, (b) fluid pressures, (c) interface (wall) temperature, (d) wall thermal conductivity, (e) vapor qualities, (f) heat transfer coefficients.

The local trends of the heat transfer coefficient for both fluids are shown in Figure 8.5f. The water-side heat transfer coefficient was much larger compared to the refrigerant one, due to the higher liquid thermal conductivity as well as the enhancement of the convective heat transfer mechanism promoted by a much larger value of the mass flow rate. Otherwise, the refrigerant-side heat transfer coefficient was higher in the flow boiling region due to the two-phase enhancement compared to the fully single-phase liquid or vapor regions.

In Figure 8.6a and Figure 8.6b the local thermal power and the associated local heat flux are displayed against the plate length. As can be observed, a larger amount of heat was transferred at the beginning of the plate heat exchanger, because of the larger temperature difference between the two streams and decreased along the axial coordinate becoming close to zero at the outlet where the temperatures of both fluids approached to each other. As expected, the local heat flux followed the same trends of the local thermal power, with an higher order of magnitude due to the small value of the local heat transfer area.

Inside the two-phase region the local heat transfer coefficient was a function of the local thermal power, which was iterated in each control volume until convergence and the results are presented in Figure 8.6c and Figure 8.6d respectively. They proved that, the iterated thermal power was very close to the effective value and the local systematic error was less than 0.1%. Furthermore, in the subcooled and fully vapor regions no iterations were performed because the local heat transfer coefficient was not function of the heat flux, as shown in Figure 8.6d, in which the systematic error was equal to zero.

Figure 8.6e shows the local overall heat transfer coefficient versus the axial coordinate of the plate heat exchanger. Due to the higher thermal resistance on the refrigerant-side, the overall heat transfer coefficient followed the same trend of the local heat transfer coefficient of the refrigerant-side. As expected higher heat transfer rates could be exchanged in the two-phase flow region, while poor values of the heat transfer coefficient were obtained in the single-phase liquid and vapor regions. Furthermore, the convective heat transfer was slightly larger for the liquid phase instead of the vapor phase because of the fluid thermal conductivity, which was 7 times higher.

The normalized local thermal resistances involved in the overall heat transfer process within the plate heat exchanger are depicted in Figure 8.6f. Each thermal resistance was normalized to the total thermal resistance, which represented the contributions of water-side convective heat transfer, refrigerant convective heat transfer and conduction through the stainless-steel interface. The smallest contributor was provided by the conduction term, mainly due to the thin stainless-steel interface.

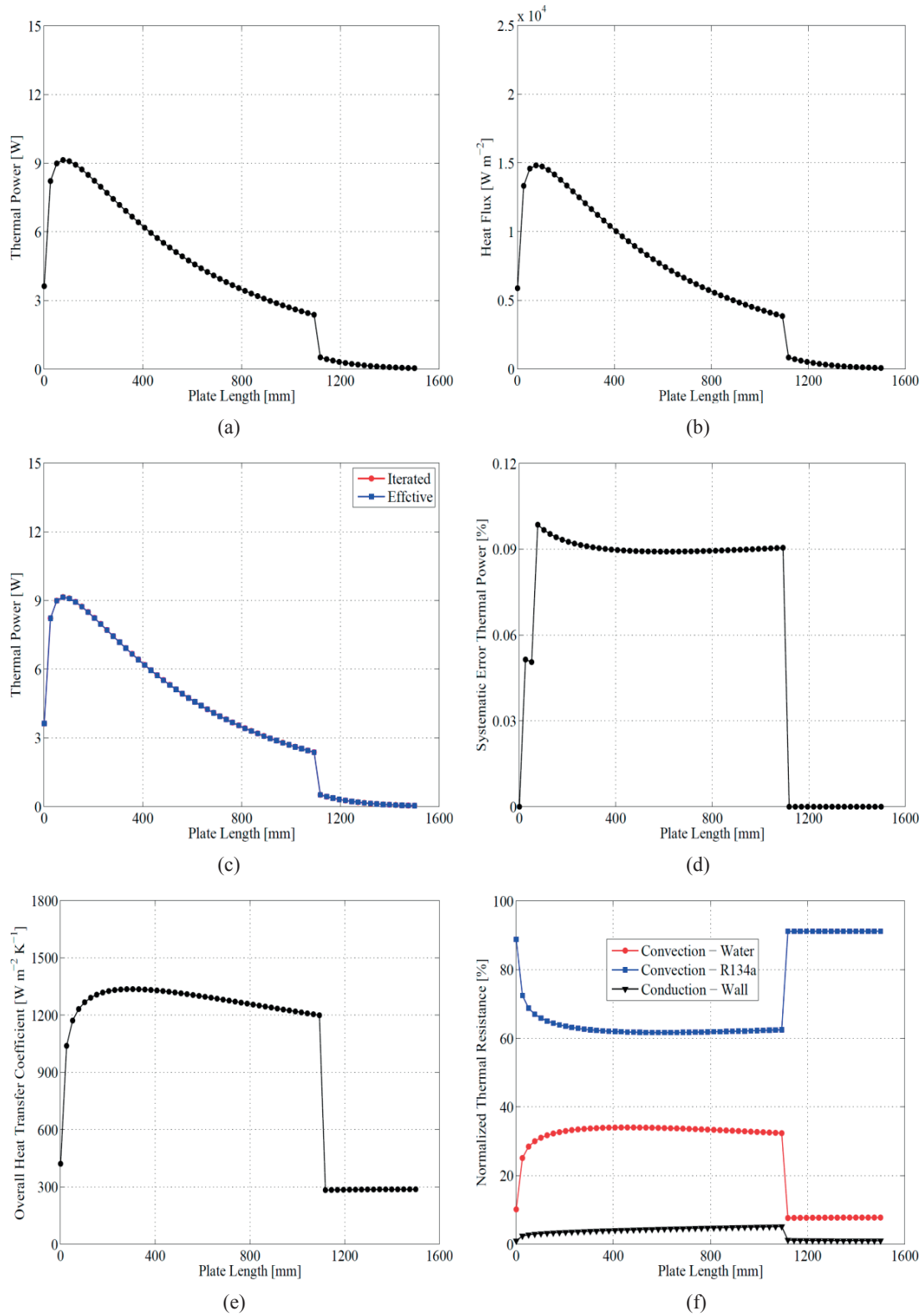


Figure 8.6: Numerical simulation of a parallel-flow plate heat exchanger and local results plotted against the plate heat exchanger length: (a) thermal power, (b) heat flux, (c) convergence of the thermal power, (d) systematic error of the thermal power, (e) overall heat transfer coefficient, (f) normalized thermal resistances.

Figure 8.7a depicts the trend of the Reynolds numbers for both fluids against the length of the heat exchanger. The water- and refrigerant-sides flowed in the turbulent flow regime and as shown in the previous chapters, due to the corrugated chevron pattern the transition for such kind of heat exchangers may occur at low Reynolds numbers around 200 (as discussed in Yan and Lin (1999c) research study). Furthermore, the Reynolds number for single-phase water was uniform along the plate heat exchanger, while in case of refrigerant, the equivalent Reynolds number increased with the vapor quality and then jumped to a higher value in the fully vapor region due to the lower dynamic viscosity.

In Figure 8.7b the local static pressure drops for water and refrigerant are displayed. Their values are negative because of the gravitational pressure drop for upward flow. The static pressure drop for the water-side was uniform over all the plate heat exchanger length because of the uniform value of the fluid density. On the contrary, the static pressure drop for the refrigerant side was maximum at the beginning, where the refrigerant was subcooled and then, decreased with the vapor quality reaching a value equal to zero in fully vapor region.

Figure 8.7c illustrates the local momentum pressure drop along the plate heat exchanger length. For the single-phase liquid flow of water, this contributor was equal to zero and similar behavior was observed in case of liquid and vapor flow of refrigerant. A different trend was encountered in the boiling region, in which the acceleration pressure drop reached a maximum at the beginning, where the temperature difference between the two fluids was large enough to promote more boiling, after that decreased, due to the decreasing of the local thermal power, which provided smaller evaporation rates.

In Figure 8.7d the local frictional pressure drops for both water and refrigerant streams were reported. This contributor was uniform for single-phase of water because of the uniform value of the fluid properties, while for the refrigerant-side increased with the axial coordinate, since the shear stress rose with the vapor quality. Moreover, less friction was observed in the subcooled liquid and vapor superheated regions, in which the frictional pressure drop only accounted for the shear stress between the flow and the wall.

Figure 8.7e reports the dimensionless pressure drops in case of water flow. In this scenario, 80% of the total pressure drop was addressed to the static component and only 20% was due to frictional pressure loss. The same graph for the refrigerant side was presented in Figure 8.7f, in which the static pressure drop played an important role only at the beginning of the plate heat exchanger while for the rest of the length the major contributor was the frictional pressure drop. The momentum pressure drop was the minor contributor among them over all the plate heat exchanger.

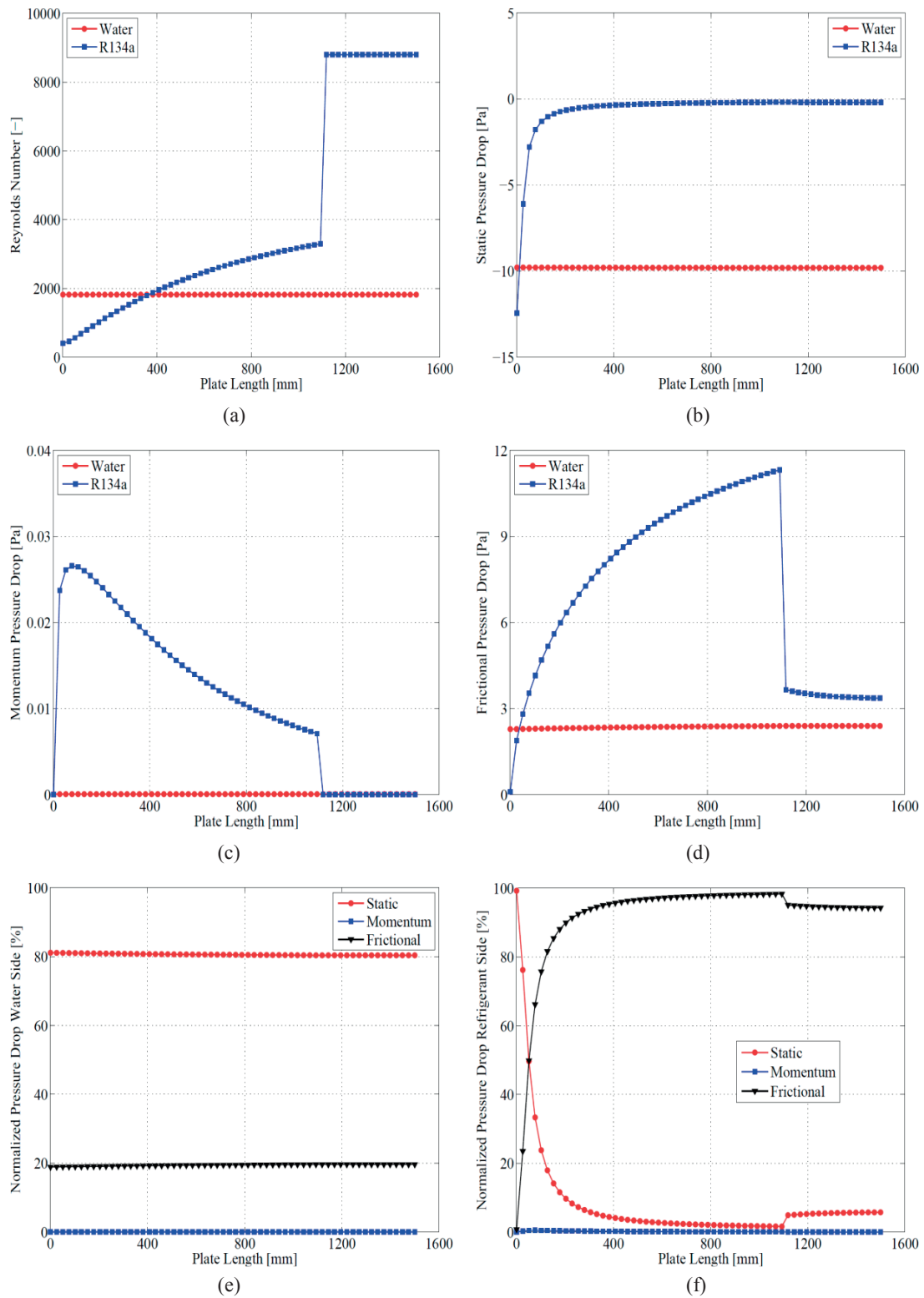


Figure 8.7: Numerical simulation of a parallel-flow plate heat exchanger and local results plotted against the plate heat exchanger length: (a) Reynolds numbers, (b) static pressure drops, (c) momentum pressure drops, (d) frictional pressure drops, (e) normalized pressure drops for water side, (f) normalized pressure drops for refrigerant side.

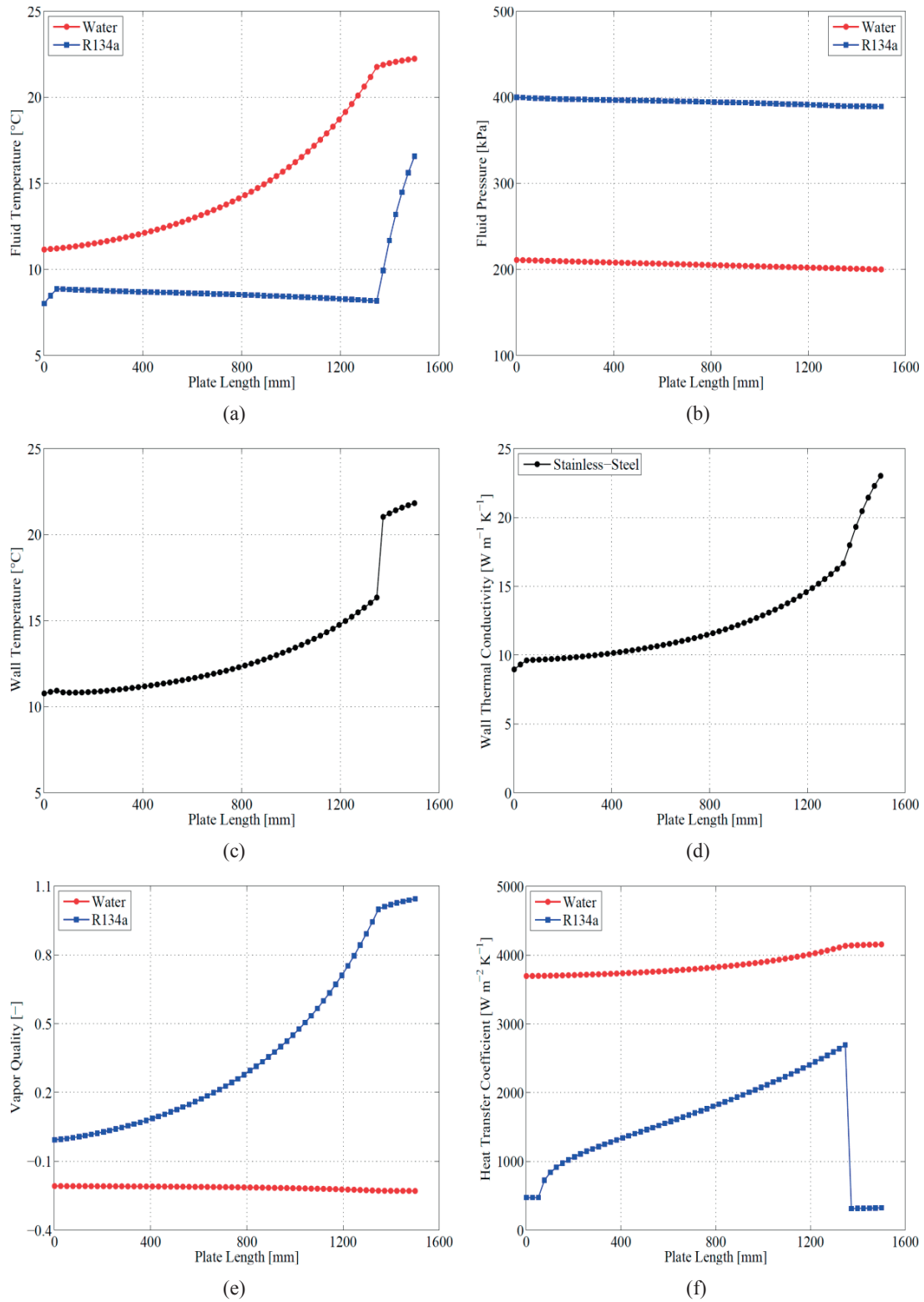


Figure 8.8: Numerical simulation of a counter-flow plate heat exchanger and local results plotted against the plate heat exchanger length: (a) fluid temperatures, (b) fluid pressures, (c) interface (wall) temperature, (d) wall thermal conductivity, (e) vapor qualities, (f) heat transfer coefficients.

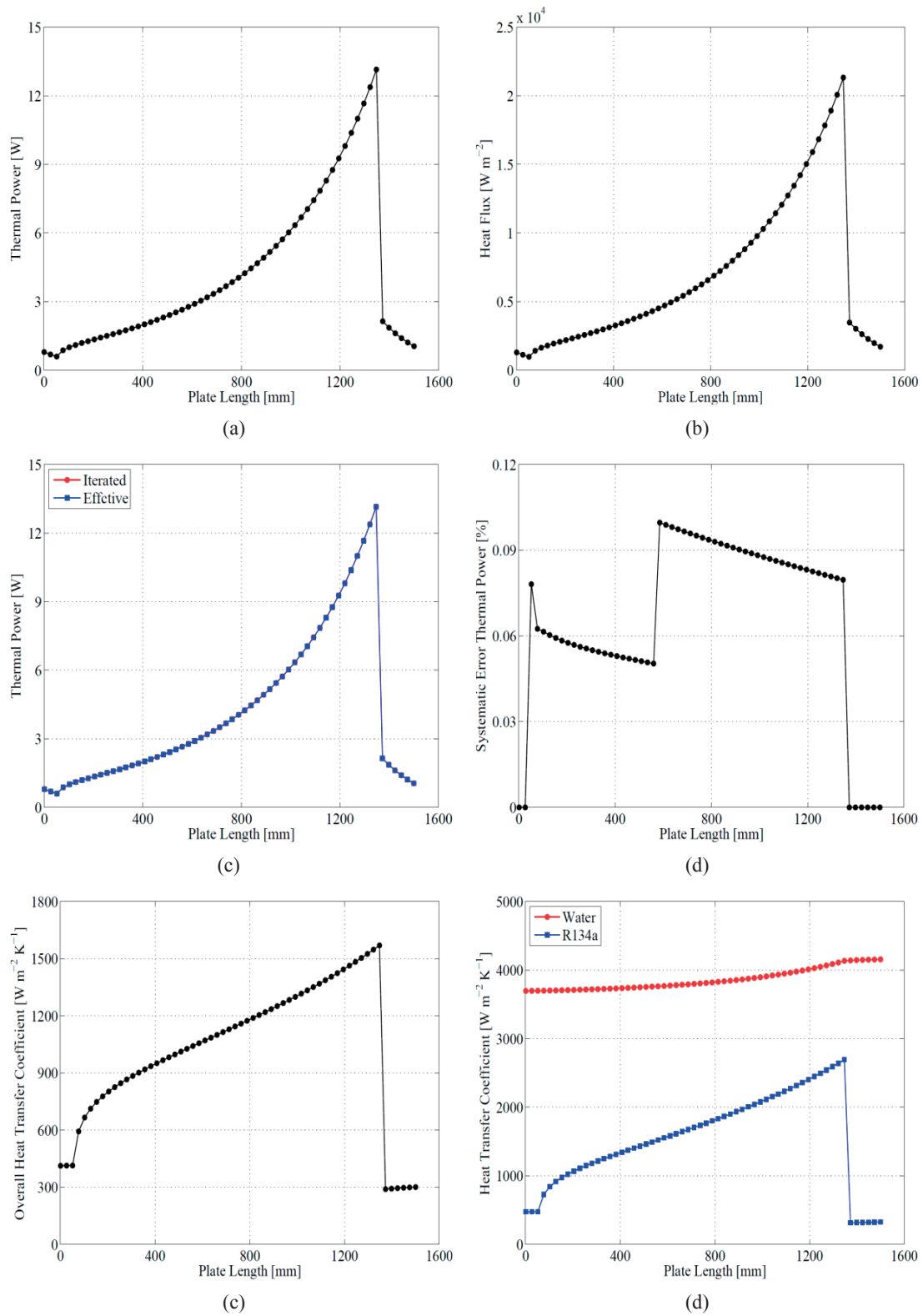


Figure 8.9: Numerical simulation of a counter-flow plate heat exchanger and local results plotted against the plate heat exchanger length: (a) thermal power, (b) heat flux, (c) convergence of the thermal power, (d) systematic error of the thermal power, (e) overall heat transfer coefficient, (f) normalized thermal resistances.

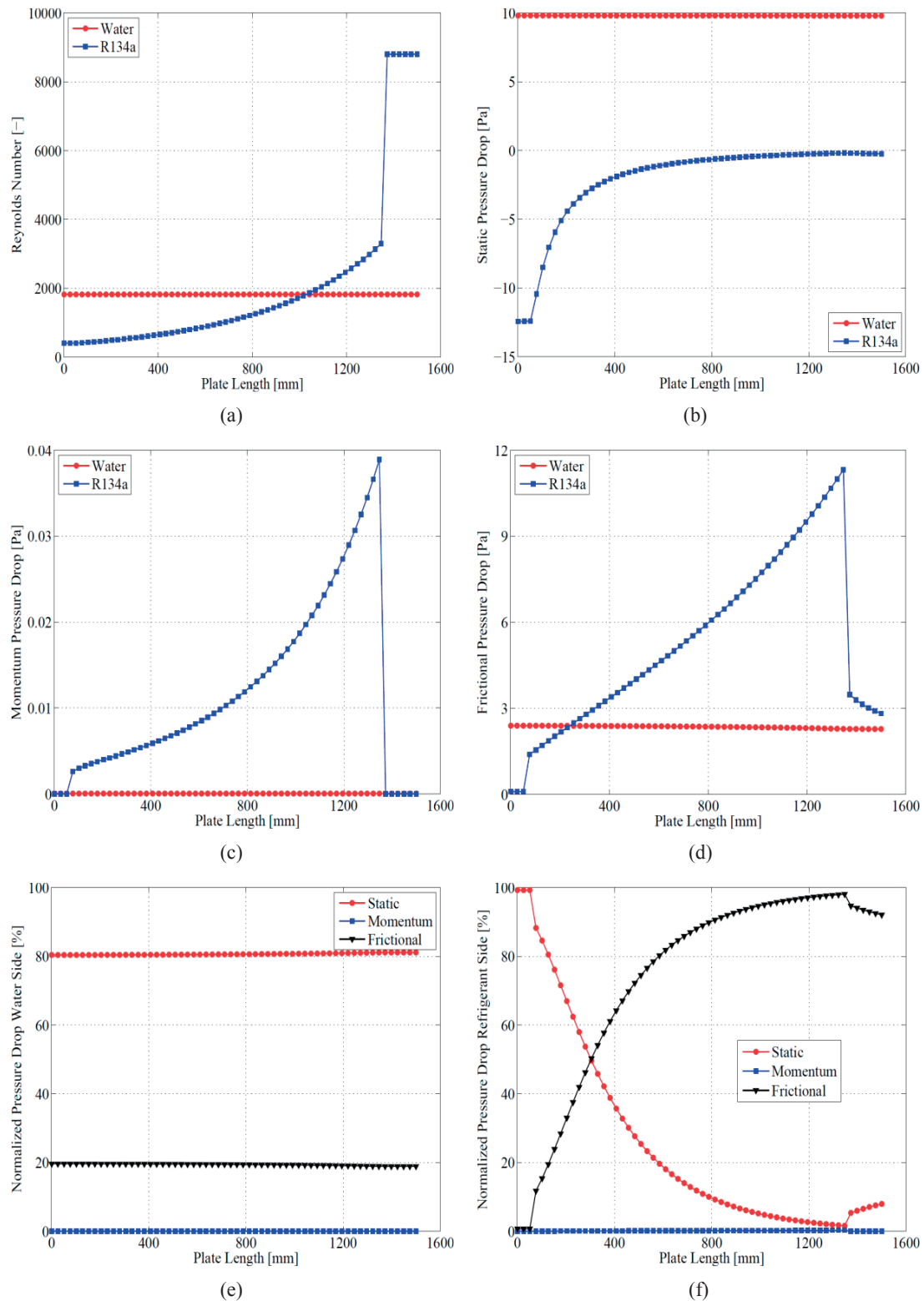


Figure 8.10: Numerical simulation of a counter-flow plate heat exchanger and local results plotted against the plate heat exchanger length: (a) Reynolds numbers, (b) static pressure drops, (c) momentum pressure drops, (d) frictional pressure drops, (e) normalized pressure drops for water side, (f) normalized pressure drops for refrigerant side.



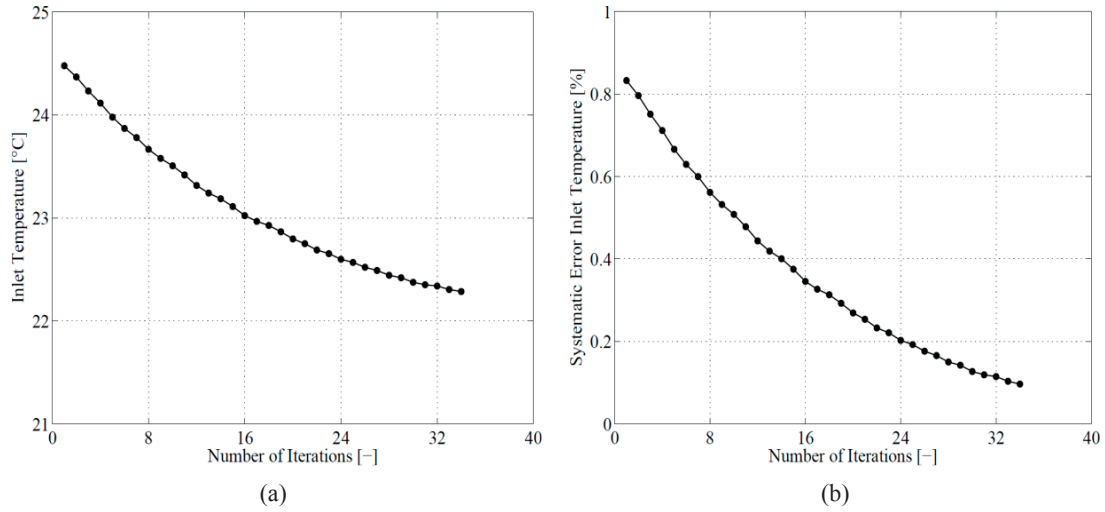


Figure 8.11: Numerical simulation of a counter-flow plate heat exchanger: (a) iterate inlet temperature for water side versus the number of iterations, (b) systematic error of the inlet temperature against the number of iterations.

In Figure 8.8, Figure 8.9, Figure 8.10 and Figure 8.11 the simulation results for a counter-flow arrangement at the same operating conditions and test geometry are reported. In this scenario, the two fluids flowed in opposite directions providing less temperature difference compared to the parallel-flow configuration and the main advantages of this arrangement are summarized below:

- More uniform temperature difference between water and refrigerant minimized the thermal stress reducing the risk of material failure and provided uniform heat transfer rate.
- The outlet temperature of the refrigerant exceeded the outlet temperature of the water-side, transferring a larger amount of heat from one fluid to the other.
- Higher log-mean temperature differences between the two streams coupled with larger overall heat transfer coefficient yielded less heat transfer area to transfer the desired heat duty, resulting in more compact plate heat exchanger design.

Finally, it has to be pointed out that, the counter-flow arrangement has been modelled assuming a possible value of the outlet temperature of the water-side (see eq. 2) and solving the simulation as a normal parallel-flow checking at the end of each calculation the residual between the calculated inlet temperature and assigned inlet temperature by the users.

For the present simulation conditions, Figure 8.11a and Figure 8.11b show that after 34 iterations the calculated inlet temperature equal to 22.2 °C converged to the input value set to 22 °C with a systematic error less than 0.1% in about 8 minutes as elapsed time.

## 8.6 Sensitivity analysis

The performances of the plate heat exchangers are strongly dependent on the geometry and dimensions of the corrugation of the plates. Therefore, in this paragraph a sensitivity analysis have been performed to highlight these influences. The present simulation code is used to assess the effect of plate geometry on thermal and hydraulic performance. The influence of the chevron angle,  $\beta$ , and corrugation aspect ratio,  $\gamma$ , on the local overall heat transfer coefficient, local thermal power, local total frictional pressure drop (water and refrigerant) and local performance index are illustrated in Figure 8.12 and Figure 8.13 respectively.

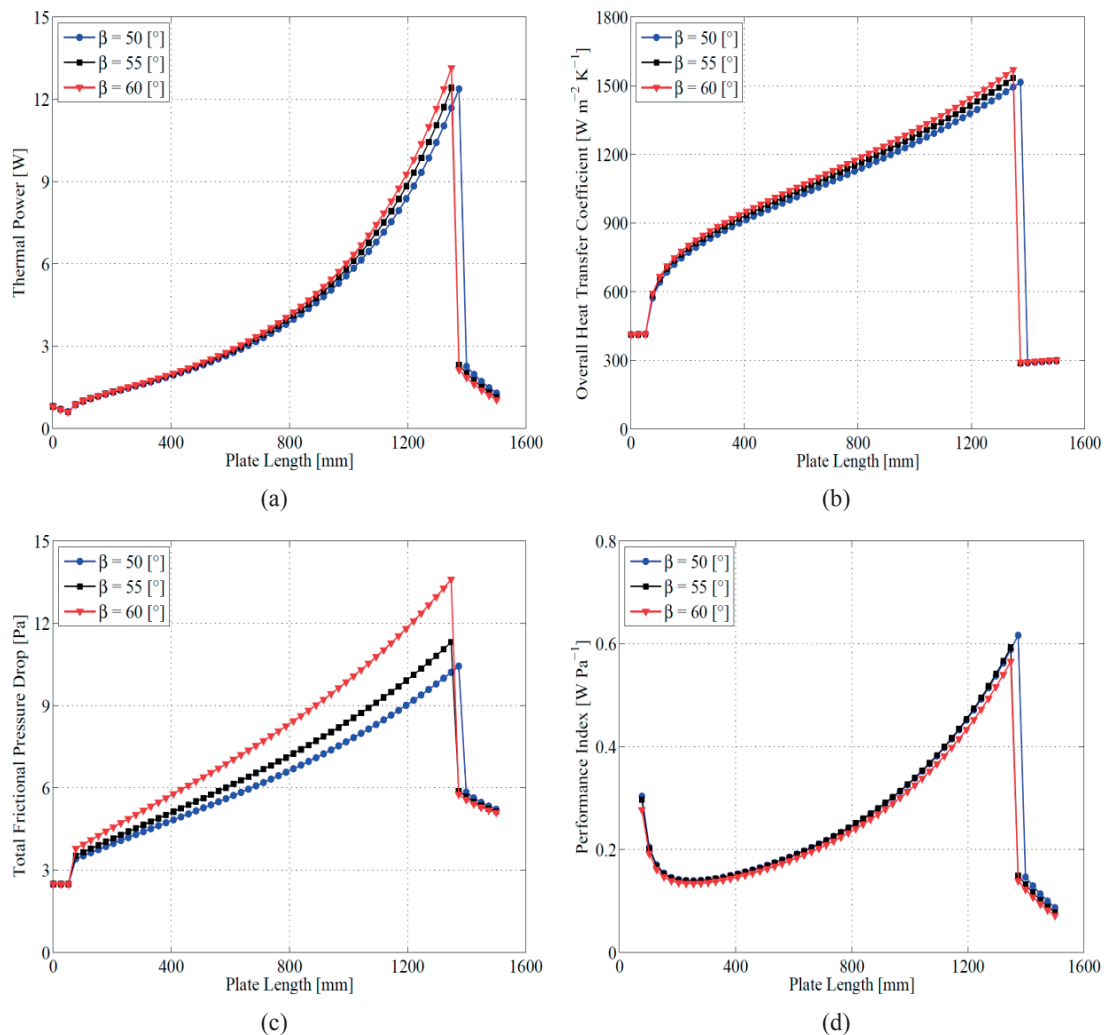


Figure 8.12: Sensitivity analysis on the effect of the chevron angle on the local thermal and local hydraulic performance plotted against the plate heat exchanger length: (a) thermal power, (b) overall heat transfer coefficient, (c) total frictional pressure drop (water plus refrigerant), (d) performance index.

For the present sensitivity analysis, the simulation results for counter-flow plate heat exchanger discussed in the previous section are used and the chevron angle was varied from  $50^\circ$  to  $60^\circ$ , while the corrugation aspect ratio was varied from 0.66 to 1.04.

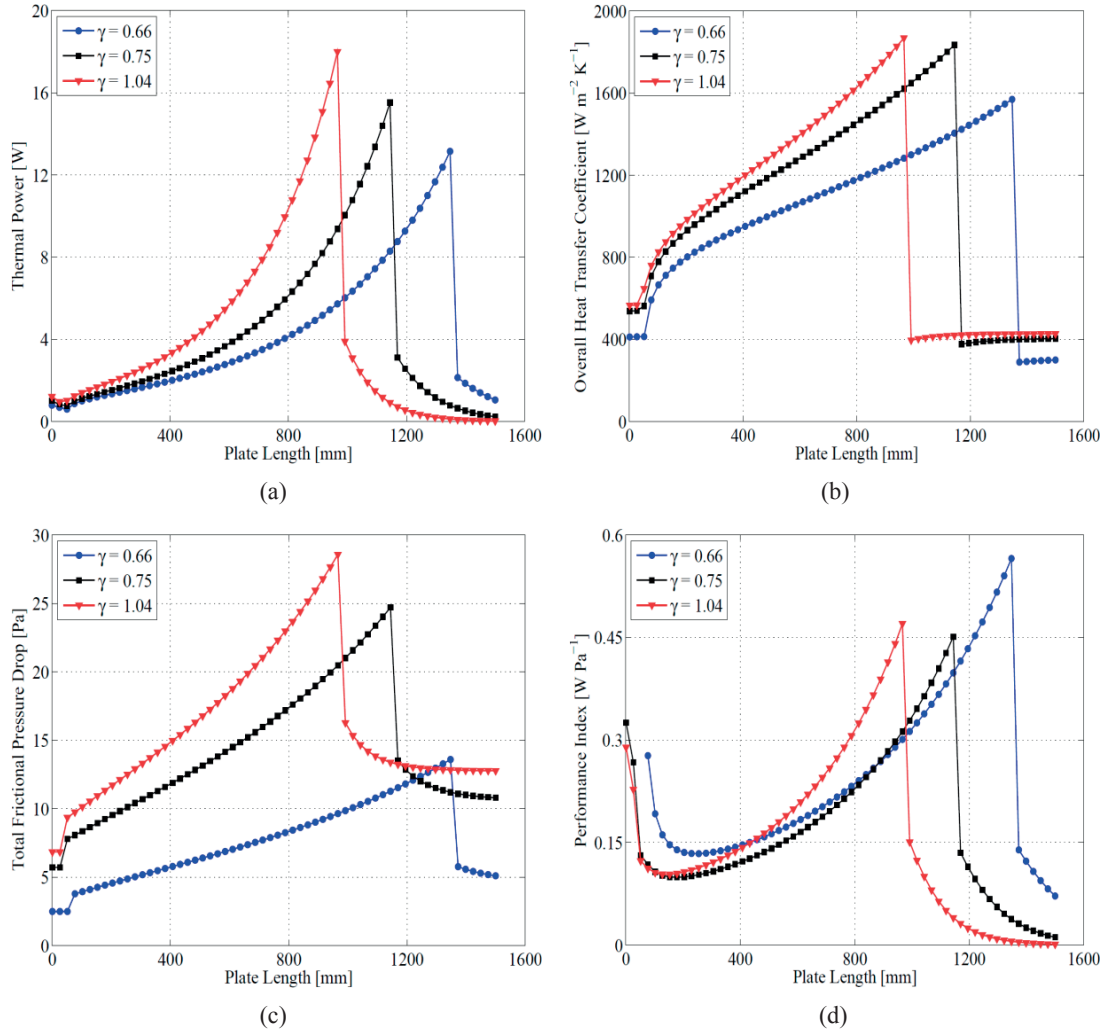


Figure 8.13: Sensitivity analysis on the effect of the corrugation aspect ratio on the local thermal and local hydraulic performance plotted against the plate heat exchanger length: (a) thermal power, (b) overall heat transfer coefficient, (c) total frictional pressure drop (water plus refrigerant), (d) performance index.

As can be observed from Figure 8.12, the thermal power, the overall heat transfer coefficient as well as the associated total frictional pressure drop increased with vapor quality going from the inlet to the outlet of the plate heat exchanger in the convective flow boiling regime. In fact, during the evaporation process the refrigerant vapor quality grows and thus the specific volume grows and consequently the fluid velocity rises. The larger velocity promotes more shear stress between the liquid and vapor phases and provides higher

turbulence; thus, the convective heat transfer coefficient is enhanced and the associated frictional pressure drop grows as well. It can be seen that at the same value of the vapor quality, the higher the plate chevron angle, the more effective the heat transfer but the higher the pressure drop. Finally, the performance index decreased in the liquid and vapor regions, while it increased within the boiling region, resulting a better trade-off between the heat exchanged and total pressure drop (water and refrigerant). Furthermore, increasing the chevron angle the performance index decreased because the gain in terms of thermal performance was less considerable than the pressure drop penalty.

In Figure 8.13 the effect of the corrugation aspect ratio, which includes the pressing depth and wavelength of the surface corrugation, on the thermal and hydraulic performance is illustrated. The heat transfer performance increased with an increase of the corrugation aspect ratio, but also the associated total frictional pressure drop rose. In this scenario, the thermal boundary layer is more frequently interrupted; also, the cross and swirl flows pass around crest of the plate and furrows to produce more turbulence, increasing the heat exchanged, overall heat transfer coefficient and total frictional pressure drop. The performance index enhanced with the corrugation aspect ratio, since the improvements of the thermal performance was more effective compared to the pressure drop penalty.

## 8.7 Conclusions

In the present chapter a novel approach to model commercial chevron plate heat exchangers and analyze their thermal and hydraulic performance have been introduced. The simulation tool has been implemented coupling a local effectiveness-NTU methods with the more general and reliable prediction methods for local heat transfer coefficients and local frictional pressure drops. Single-phase heat transfer coefficient and frictional pressure drop were predicted using the model proposed by Kumar (1984b), while the flow boiling thermal and hydraulic performance were evaluated adopting the new correlations provided by Amalfi et al. (2015b, 2015c). The parallel- and counter-flow configurations have been compared and the main simulation trends have been discussed in detail. In the counter-flow arrangement, lower and more uniform temperature difference through the plate heat exchanger were recognized, providing more uniform and higher heat transfer rate, reducing also the risk of material failure. Additionally, higher log-mean temperature difference coupled with larger overall heat transfer coefficient provided more compact plate heat exchanger design working in counter-flow rather than parallel-flow. Finally, the sensitivity analysis on the chevron

angle and corrugation aspect ratio was also performed. Based on these results, the thermal and hydraulic performance increased with the chevron angle as well as with the corrugation aspect ratio. Due to the trade-off between the thermal power exchanged and total pressure drop (water and refrigerant), the performance index decreased with chevron angle and raised with an increasing of the corrugation aspect ratio.

## **CHAPTER 9 – Conclusions**

### **9.1 Introduction**

In the final chapter of the present thesis, the research objectives achieved during these three years are highlighted and shortly explained. Next, recommendations for future research activities in the plate heat exchanger field are also summarized, that will be investigated thanks to an ongoing collaboration between LTCM (Laboratory of Heat and Mass Transfer at École Polytechnique Fédérale de Lausanne) and UMD (Phase Change Heat Transfer Laboratory at University of Maryland).

### **9.2 Main objectives and findings of the present study**

High spatial and temporal resolution infrared measurements of single- and two-phase flow in a novel compact chevron plate heat exchanger were carried out. The present plate heat exchanger prototype provided higher thermal performance and compactness (about 3-5 times) than convectional plate heat exchangers and it was tested over a wide range of operating conditions. The main objectives achieved in the current thesis are summarized below:

- A comprehensive literature survey of existing single- and two-phase flow heat transfer and pressure drops (from 1981 until 2014) within plate heat exchangers has been presented and the associated prediction methods have been analyzed in detail.
- A new experimental test facility was built in order to perform single-phase and flow boiling tests of low liquid pressure refrigerants within a novel plate heat exchanger. The data acquisition system was updated and the instrumentation was self-calibrated, including the infrared camera to reach 0.15 K accuracy, which was used to map out the local surface temperatures and obtain local (pixel-by-pixel) heat transfer coefficients and also local two-phase frictional pressure drops.
- Single-phase heat transfer and pressure drop data for R245fa and R236fa were obtained and the experimental test facility was properly validated, verifying pressure and temperature measurements against the literature prediction methods. The thermal losses

- were identified and the calibration correlations were also developed, in order to calculate the effective power (heat) delivered to the refrigerant flow during the flow boiling experiments. In particular, the heat loss due to the Joule effect was linked to the electrical current, while the heat transferred to the ambient by natural convection and radiation were correlated according to the temperature difference between the wall and ambient.
- According to the present liquid pressure drop database, the Fanning friction factor was function of Reynolds number, while it was not influenced by the Prandtl number and the imposed heat flux. The Fanning friction factor decreased with Reynolds number with different slopes according to three different flow regimes: undisturbed no swirl flow, steady swirl flow and fully turbulent flow. The prediction methods available in the open literature poorly predicted the present pressure drop database and for this reason, a novel new correlation was proposed that captured the entire database (composed of 146 points) with a mean absolute error of 8.2% and mean error of -2.6%, where 100% of the data were within a bandwidth of 20%.
- Single-phase mean heat transfer coefficients were taken for the plate heat exchanger. In particular, the Nusselt number increased with Reynolds and Prandtl numbers, while it was insensitive to the imposed heat flux. The comparison between the experimental data and the models from literature proved that, the existing correlations overestimated the present heat transfer databank (being extrapolated to this smaller pressing depth of 1 mm). A new correlation to evaluate the mean thermal performance was provided, which predicted 89.4% and 97.6% of the database (including 85 points) within bandwidths of 20% and 30%, offering a mean absolute error of 11.3% and mean error of -1.8. Performing local temperature measurements by using an infrared camera, the trends of the local heat transfer coefficient against the main involved parameters were also analyzed in this study. The local heat transfer coefficient increased with mass flux, decreased with inlet fluid temperature and it was not a function of the imposed heat flux. Higher heat transfer rates were achieved using R245fa than R236fa. Additionally, lower values of the local heat transfer coefficients were obtained close to the inlet and outlet ports due to the local flow phenomena. In the present study, the local thermal performance was also correlated to handle the inlet and outlet effects in the plate arrangement and a new model to estimate the local heat transfer coefficient was proposed. The set of correlations was developed based on 510 local experimental data points, which predicted 88.2% and 93.6% of the experimental data within a bandwidths of 20% and 30%, providing a mean absolute error of 14.8% and mean error of 0.7%.

- Next, two-phase adiabatic and flow boiling experiments employing R245fa were run and the data reduction technique was described in detail. Based on the infrared measurements, a new experimental approach to measure the local absolute pressure of the refrigerant and then obtain the local saturation temperature was also developed. A novel prediction method has then developed for evaluating the local frictional pressure drop along the test section, that captured the entire pressure drop database (composed of 122 points) in a reasonable range of  $\pm 30\%$  with a mean absolute error of 10% and mean error of 0.2%. The most quoted prediction methods extrapolated to this small pressing depth of 1 mm available in the current literature strongly overestimated the experimental results. The frictional pressure drop increased with mass flux, vapor quality and decreased with saturation temperature. The effect of the imposed heat flux on the two-phase hydraulic performance was seen to be negligible. The quasi-local heat transfer performance rose with mass flux, vapor quality, heat flux and saturation temperature. The flow instability close to the outlet port strongly influenced the heat transfer coefficient and this effect diminished with an increasing of mass flux.
- A large diversified experimental database was culled from the literature research studies, that included flow boiling heat transfer and two-phase frictional pressure drop data for many plate heat exchangers, plate geometries, operating conditions and working fluids. The leading published methods were statistically compared against this large multi-lab database. The flow boiling heat transfer coefficient were discretely predicted by the Danilova et al. (1981) and Han et al. (2003b) methods, while in the case of frictional pressure drops the best existing method was the one proposed by Khan et al. (2014a, 2012c, 2012d). Based on a dimensional analysis coupled with a multiple regression technique, general and more reliable prediction methods for local flow boiling heat transfer coefficient and local frictional pressure gradient within plate heat exchangers have been proposed here. These models were developed from 1903 heat transfer and 1513 frictional pressure drop data points, respectively, and were proven to work better than any other published method.
- The local effectiveness-NTU approach has been implemented into a MATLAB code to simulate single- and two-phase thermal and hydraulic performances of chevron plate heat exchangers in steady-state condition. The present tool was able to model several flow arrangements (parallel- and counter-flow), plate configurations and geometries over a wide range of operating conditions. The general models proposed earlier in the present thesis were implemented to evaluate the local flow boiling heat transfer coefficient and local



- frictional pressure drop. This simulation tool was first validated against independent experimental heat transfer and pressure drop database from literature. Next, the parallel- and counter-flow configurations have been compared in terms of overall heat transfer coefficient and pressure drops and the main trends have been discussed in detail. A sensitivity analysis on the chevron angle and corrugation aspect ratio was performed. Based on these results, the thermal and hydraulic performance increased with chevron angle as well as with the corrugation aspect ratio. Due to the trade-off between the thermal power exchanged and total pressure drop (water and refrigerant) the performance index decreased with chevron angle and increased with an increasing of the corrugation aspect ratio.

### 9.3 Recommendations for future work

Within the scope of the present thesis many important aspects regarding two-phase heat transfer mechanisms within plate heat exchangers have been fulfilled. However, the study generated new research questions, which will be investigated thanks to an ongoing collaboration between LTCM and UMD research labs:

- Analyzing flow patterns, flow regimes and flow distributions inside plate heat exchangers in order to understand the complex physics which is involved during the flow boiling heat transfer process.
- Providing more suitable transition criteria to define whether the heat transfer process is nucleate boiling dominated or two-phase forced convection dominated.
- Extending the current experimental database to different chevron angles and corrugation aspect ratios (that include the effect of pressing depth and wavelength of surface corrugation), combining both LTCM and UMD experimental databanks.
- Co-validating these databanks for pressure drop and heat transfer and comparing the expanded database to the methods available in the open literature.
- Advancing the new LTCM local prediction methods presented in this thesis for heat transfer coefficient and frictional pressure gradient using the new data sets, implementing these models in LTCM simulation code and validating the results.

# Bibliography

- Akers, W.W., Deans, H.A., Crosser, O.K., 1959. Condensation Heat Transfer within Horizontal Tubes. Chemical Engineering Process Symposium Series. 55, 171-176.
- Amalfi, R.L., Thome, J.R., 2015a. High Resolution Infrared Measurements of Single Phase Flow of R245fa and R236fa within a Compact Plate Heat Exchanger. Applied Thermal Engineering.
- Amalfi, R.L., Vakili-Farahani, F., Thome, J.R., 2015b. Flow Boiling and Frictional Pressure Gradients in Plate Heat Exchangers. Part 1: Review and Experimental Database. International Journal of Refrigeration.
- Amalfi, R.L., Vakili-Farahani, F., Thome, J.R., 2015c. Flow Boiling and Frictional Pressure Gradients in Plate Heat Exchangers. Part 2: Comparison of Literature Methods and New Prediction Methods. International Journal of Refrigeration.
- Ayub, Z.H., 2003a. Plate Heat Exchanger Literature Survey and New Heat Transfer and Pressure Drop Correlations for Refrigerant Evaporators. Heat Transfer Eng. 24, 3-16.
- Boccardi, G., Celata, G.P., Cumo, M., Gerosa, A., Donati, F.M., Zorzin, A., 2000a. R22 Replacement Aspects in Compact Heat Exchangers for Air Conditioning. Int. J. Heat Exchangers. 1, 77-91.
- Bogaert, R., Böles, A., 1995a. Global Performance of a Prototype Braze Plate Heat Exchanger in a Large Reynolds Number Range. Exp. Heat Transfer. 8, 293-311.
- Chen, J.C., 1966. Correlation for Boiling Heat Transfer to Saturated Fluids in Convective Flow. Ind. Eng. Chem. Process Des. Dev. 5, 322-329.
- Chisholm, D., 1967. A Theoretical Basis for the Lockhart-Martinelli Correlation for Two-Phase Flow. Int. J. Heat Mass Transfer. 10, 1767-1778
- Christensen, R., Andreasson, F., Bermhult, R., Larsoon, H., Svensson, M., 2015d. Plate Heat Exchanger. Patent 9103597, ALFA LAVAL CORPORATE AB.

## Bibliography

---

- Cicchitti, A., Lombardi, C., Silvestri, M., Soldaini, G., Zavattarelli, R., 1960a. Two-Phase Cooling Experiments: Pressure Drop, Heat Transfer and Burnout Measurements. *Energia Nucleare*. 7, 407-425.
- Cioncolini, A., Thome, J.R., 2009. Unified Macro-to-Microscale Method to Predict Two-Phase Frictional Pressure Drops of Annular Flows. *Int. J. Multiphase Flow*. 35, 1138-1148.
- Clark, D.F., 1974. Plate Heat Exchangers Design and Recent Developments. *The Chemical Engineering*. 275-279.
- Cooper, M.G., 1984a. Heat Flow Rates in Saturated Nucleate Pool Boiling-a Wide-Ranging Examination Using Reduced Properties. *Advances in Heat Transfer*. 16, 157-239.
- Danilova, G.N., Azarskov, V.M., Zemskov, B.B., 1981. Teploobmen V Plastinchatihispariteljan Razichnole Geometri - Heat Transfer in Plate Evaporators of Different Geometry. *Kholod. Tek.* 4, 25-31.
- Dittus, F.W., Boelter, L.M.K., 1930. Heat Transfer in Automobile Radiators of the Tubular Type. *Publications in Engineering*. 2, 443-461.
- Djordjevic, E., Kabelac, S., 2008. Flow Boiling of R134a and Ammonia in a Plate Heat Exchanger. *Int. J. Heat Mass Trans.* 51, 6235-6242.
- Donowski, V.D., Kandlikar, S.G., 2000b. Correlating Evaporation Heat Transfer Coefficient of Refrigerant R-134a in a Plate Heat Exchanger. *Engineering Foundation Conference on Pool and Flow Boiling*, Alaska, Paper 154.
- Dukler, A.E., Wicks, M., Cleveland, R.G., 1964. Frictional Pressure Drop in Two-Phase Flow: B. An Approach through Similarity Analysis. *AIChE J.* 10, 44-51.
- Engelhorn, H.R., Reinhart, A.M., 1990a. Investigations on Heat Transfer in a Plate Evaporator *Chem. Eng. Process*. 28, 143-146.
- Focke, W.W., Zachariades, J., Olivier, I., 1985. The Effect of the Corrugation Inclination Angle on the Thermohydraulic Performance of Plate Heat Exchangers. *Int. J. Heat Mass Transfer*. 28, 1469-1479.

- Freund, S., Kabelac, S., 2010a. Investigation of Local Heat Transfer Coefficients in Plate Heat Exchangers with Temperature Oscillation Ir Thermography and Cfd. *Int. J. Heat Mass Transfer*. 53, 3764-3781.
- Garcia-Cascales, J.R., Vera-Garcia, F., Corberan-Salvador, J.M., Gonzalvez-Macia, J., 2007a. Assessment of Boiling and Condensation Heat Transfer Correlations in the Modelling of Plate Heat Exchangers. *Int. J. Refrigeration*. 30, 1029-1041.
- Gherasim, I., Galanis, N., Nguyen, C.T., 2011a. Heat Transfer and Fluid Flow in a Plate Heat Exchanger Part 2: Assessment of Laminar and Two-Equation Turbulent Models. *Int. J. Thermal Sciences*. 1499-1511.
- Gherasim, I., Taws, M., Galanis, N., Nguyen, C.T., 2011b. Heat Transfer and Fluid Flow in a Plate Heat Exchanger. Part 1: Experimental Investigation. *Int. J. Thermal Sciences*. 1492-1498.
- Gorenflo, D., 1993a. Pool Boiling. VDI-Verlag, Düsseldorf, Germany.
- Han, D.H., Lee, K.J., Kim, Y.H., 2003b. Experiments on the Characteristics of Evaporation of R410a in Brazed Plate Heat Exchangers with Different Geometric Configurations. *Applied Thermal Eng.* 23, 1209-1225.
- Hayes, N., Jokar, A., Ayub, Z.H., 2011c. Study of Carbon Dioxide Condensation in Chevron Plate Exchangers; Heat Transfer Analysis. *Int. J. Heat Mass Transfer*. 54, 1121-1131.
- Hayes, N., Jokar, A., Ayub, Z.H., 2012a. Study of Carbon Dioxide Condensation in Chevron Plate Exchangers; Pressure Drop Analysis. *Int. J. Heat Mass Transfer*. 55, 2916-2925.
- Heavner, R.L., Kumar, H., Wanniarachchi, A.S., 1993b. Performance of an Industrial Plate Heat Exchanger: Effect of Chevron Angle. *AIChE Symposium Series*, New York, 262-267.
- Hsieh, Y.Y., Chiang, L.J., Lin, T.F., 2002a. Subcooled Flow Boiling Heat Transfer of R134a and the Associated Bubble Characteristics in a Vertical Plate Heat Exchanger. *Int. J. Heat Mass Transfer*. 45, 1791-1806.
- Hsieh, Y.Y., Lin, T.F., 2003c. Evaporation Heat Transfer and Pressure Drop of Refrigerant R410a Flow in a Vertical Plate Heat Exchanger. *J. Heat Transfer*. 125, 852-857.

## Bibliography

---

- Hsieh, Y.Y., Lin, T.F., 2002b. Saturated Flow Boiling Heat Transfer and Pressure Drop of Refrigerant R-410a in a Vertical Plate Heat Exchanger. *Int. J. Heat Mass Transfer*. 45, 1033-1044.
- Huang, J., Sheer, T., Bailey-McEwan, M., 2012b. Heat Transfer and Pressure Drop in Plate Heat Exchanger Refrigerant Evaporators. *Int. J. Refrigeration*. 35, 325-335.
- Jassim, Newell, T.A., Chato, J.C., 2006a. Refrigerant Pressure Drop in Chevron and Bumpy Style Flat Plate Heat Exchangers. *Exp. Therm. Fluid Sci.* 30, 213-222.
- Jokar, A., Hosni, M.H., Eckels, S.J., 2006b. Dimensional Analysis on the Evaporation and Condensation of Refrigerant R-134a in Minichannel Plate Heat Exchangers. *Applied Thermal Eng.* 26, 2287-2300.
- Kakaç, S., Shah, R.K., Aung, W., 1987. *Handbook of Single-Phase Convective Heat Transfer*. Wiley Interscience, New York.
- Kandlikar, S.G., 1991a. A Model for Correlating Flow Boiling Heat Transfer in Augmented Tubes and Compact Evaporators. *ASME J. Heat Transfer*. 113, 966-972.
- Kew, P.A., Cornwell, K., 1997. Correlations for the Prediction of Boiling Heat Transfer in Small-Diameter Channels. *Appl. Therm. Eng.* 17, 705-715.
- Khan, M.S., Khan, T.S., Chyu, M.C., Ayub, Z.H., 2014a. Evaporation Heat Transfer and Pressure Drop of Ammonia in a Mixed Configuration Chevron Plate Heat Exchanger. *Int. J. Refrigeration*. 41, 92-102.
- Khan, M.S., Khan, T.S., Chyu, M.C., Ayub, Z.H., 2012c. Experimental Investigation of Evaporation Heat Transfer and Pressure Drop of Ammonia in a 30° Chevron Plate Heat Exchanger. *Int. J. Refrigeration*. 35, 1757-1765.
- Khan, T.S., Khan, M.S., Chyu, M.C., Ayub, Z.H., 2012d. Experimental Investigation of Evaporation Heat Transfer and Pressure Drop of Ammonia in a 60° Chevron Plate Heat Exchanger. *Int. J. Refrigeration*. 35, 336-348.
- Khan, T.S., Khan, M.S., Chyu, M.C., Ayub, Z.H., 2010b. Experimental Investigation of Single Phase Convective Heat Transfer Coefficient in a Corrugated Plate Heat Exchanger for Multiple Plate Configurations *Applied Thermal Eng.* 30, 1058-1065.

- Kline, S., McClintock, F., 1953. Describing Uncertainties in Single-Sample Experiments. *ASME Mechanical Engineering*. 75(1), 3-8.
- Kovalenko, L.M., Maslov, A.M., 1970. Soviet Plate Heat Exchangers. *Konservnaya I Ovoshchesushil Naya Promyshlennost*. 15-17.
- Kumar, H., 1992. The Design of Plate Heat Exchangers for Refrigerants. *Proceedings of Conference of the Institute Refrigeration*. 5.1-5.2.
- Kumar, H., 1984b. The Plate Heat Exchanger: Construction and Design. *Symposium Series*, 86, 1275-1282.
- Lee, E., Kang, H., Kim, Y., 2014b. Flow Boiling Heat Transfer and Pressure Drop of Water in a Plate Heat Exchanger with Corrugated Channels at Low Mass Flux Conditions. *Int. J. Heat Mass Transfer*. 77, 37-45.
- Leuliet, J.C., Mangonnat, J.F., Laiande, M., 1990b. Flow and Heat Transfer in Plate Heat Exchangers Treating Viscous Newtonian and Pseudoplastic Products. *Canadian Journal of Chemical Engineering*. 68, 220-229.
- Lockhart, R.W., Martinelli, R.C., 1949. Proposed Correlation of Data for Isothermal Two-Phase, Two-Component Flow in Pipes. *Chem. Eng. Prog.* 45, 39-45.
- Longo, G.A., 2012e. Hydrocarbon Refrigerant Vaporization inside a Braze Plate Heat Exchanger. *J. Heat Transfer*. 134, 101801\_101801-101810.
- Longo, G.A., 2012f. Vaporisation of the Low GWP Refrigerant Hfo1234yf inside a Braze Plate Heat Exchanger. *Int. J. Refrigeration*. 35, 952-961.
- Longo, G.A., Gasparella, A., 2007b. Heat Transfer and Pressure Drop During Hfc Refrigerant Vaporisation inside a Braze Plate Heat Exchanger. *Int. J. Heat Mass Trans.* 50, 5194-5203.
- Longo, G.A., Gasparella, A., 2007c. Hfc-410a Vaporisation inside a Commercial Braze Plate Heat Exchanger. *Exp. Therm. Fluid Sci.* 32, 107-116.
- Longo, G.A., Gasparella, A., 2007d. Refrigerant R134a Vaporisation Heat Transfer and Pressure Drop inside a Small Braze Plate Heat Exchanger. *Int. J. Refrigeration*. 30, 821-830.

## Bibliography

---

- Longo, G.A., Gasparella, A., Sartori, R., 2004a. Experimental Heat Transfer Coefficients During Refrigerant Vaporisation and Condensation inside Herringbone-Type Plate Heat Exchangers with Enhanced Surfaces. *Int. J. Heat Mass Trans.* 47, 4125-4136.
- Martin, H., 1996a. A Theoretical Approach to Predict the Performance of Chevron-Type Plate Heat Exchangers. *Chem. Eng. Process. : Process Intensification*. 35, 301-310.
- Muley, A., Manglik, R.M., 1999a. Experimental Study of Turbulent Flow Heat Transfer and Pressure Drop in Plate Heat Exchanger with Chevron Plates. *J. Heat Transfer*. 121, 110-117.
- Muley, A., Manglik, R.M., Metwally, H.M., 1999b. Enhanced Heat Transfer Characteristics of Viscous Liquid Flows in a Chevron Plate Heat Exchanger. *J. Heat Transfer* 121, 1011-1017.
- Nilpueng, K., Wongwises, S., 2010c. Two-Phase Gas–Liquid Flow Characteristics inside a Plate Heat Exchanger. *Exp. Therm. Fluid Sci.* 34, 1217-1229.
- Ouazia, B., 2001a. Evaporation Heat Transfer and Pressure Drop of Hfc-R134a inside a Plate Heat Exchanger. *ASME Int. Mech. Eng. Congress and Exposition, IMECE2001/PID-25613*, New York, NY, 115-123.
- Palm, B., Claesson, J., 2006c. Plate Heat Exchangers: Calculation Methods for Single and Two-Phase Flow. *Heat Transfer Eng.* 27, 88-98.
- Palmer, S.C., Vance Payne, W., Domanski, P.A., 2000c. Evaporation and Condensation Heat Transfer Performance of Flammable Refrigerants in a Braze Plate Heat Exchanger.
- Park, J.H., Kim, Y.S., 2004b. Evaporation Heat Transfer and Pressure Drop Characteristics of R134a in the Oblong Shell and Plate Heat Exchanger. *KSME Int. J.* 18, 2284-2293.
- Rene, F., Leuliet, J.C., Lanlande, M., 1991b. Heat Transfer to Newtonian and Non-Newtonian Food Fluids in Plate Heat Exchangers: Experimental and Numerical Approaches. *Food and Bioproducts Processing*. 69, 115-126.
- Shah, M.M., 1976. A New Correlation for Heat Transfer During Boiling Flow through Pipes. *ASHRAE Trans.* 82, 66-86.

- Shah, R.K., Focke, W.W., 1988. Plate Heat Exchangers and Their Design Theory. Heat Transfer Equipment Design, Hemisphere Publishing, Washington, DC, 227-254.
- Solotych, V., Kim, J., Dessiatoun, S., 2015e. Local Heat Transfer Measurements within a Representative Plate Heat Exchanger Geometry Using Infrared (Ir) Thermography. J. Enhanced Heat Transfer.
- Stasiek, J., Collins, M.W., Ciofalo, M., Chew, P.E., 1996b. Investigation of Flow and Heat Transfer in Corrugated Passages-I. Experimental Results. Int. J. Heat Mass Transfer. 39, 149-164.
- Sterner, D., Sundén, B., 2006d. Performance of Plate Heat Exchangers for Evaporation of Ammonia. Heat Transfer Eng. 27, 45-55.
- Táboas, F., Vallès, M., Bourouis, M., Coronas, A., 2012g. Assessment of Boiling Heat Transfer and Pressure Drop Correlations of Ammonia/Water Mixture in a Plate Heat Exchanger. Int. J. Refrigeration. 35, 633-644.
- Táboas, F., Vallès, M., Bourouis, M., Coronas, A., 2010d. Flow Boiling Heat Transfer of Ammonia/Water Mixture in a Plate Heat Exchanger. Int. J. Refrigeration. 33, 695-705.
- Thonon, B., Vidil, R., Marvillet, C., 1995b. Recent Research and Developments in Plate Heat Exchangers. J. Enhanced Heat Trans. 2, 149-155.
- Tribbe, C., Müller-Steinhagen, H.M., 2001b. Gas/Liquid Flow in Plate-and-Frame Heat Exchangers - Part 1: Pressure Drop Measurements. Heat Transfer Eng. 22, 5-11.
- Tribbe, C., Müller-Steinhagen, H.M., 2001c. Gas/Liquid Flow in Plate-and-Frame Heat Exchangers - Part 2: Two-Phase Multiplier and Flow Pattern Analysis. Heat Transfer Eng. 22, 12-21.
- Troupe, R.A., Morgan, J.C., Prifiti, J., 1960b. The Plate Heater Versatile Chemical Engineering Tool. Chemical Engineering Progress. 56, 124-128.
- Vakili-Farahani, F., Amalfi, R.L., Thome, J.R., 2014c. Two-Phase Flow and Boiling of R245fa in a 1mm Pressing Depth Plate Heat Exchanger - Part 1: Adiabatic Pressure Drop. Int. J. Interfacial Phenomena and Heat Transfer. 2, 325-342.



## Bibliography

---

- Vakili-Farahani, F., Amalfi, R.L., Thome, J.R., 2014d. Two-Phase Flow and Boiling of R245fa in a 1mm Pressing Depth Plate Heat Exchanger - Part 2: Flow Boiling Heat Transfer. *Int. J. Interfacial Phenomena and Heat Transfer*. 2, 343-361.
- Vakili-Farahani, F., Amalfi, R.L., Thome, J.R., 2015f. Two-Phase Heat Transfer and Pressure Drop within Plate Heat Exchangers. *Encyclopedia of Two-Phase Heat Transfer and Flow II*. 2,
- Yan, Y.Y., Lin, T.F., 1999c. Evaporation Heat Transfer and Pressure Drop of Refrigerant R134a in a Plate Heat Exchanger. *ASME J. Heat Transfer*. 121, 118-127.
- Yan, Y.Y., Lio, H.C., Lin, T.F., 1999d. Condensation Heat Transfer and Pressure Drop of Refrigerant R134a in a Plate Heat Exchanger. *Int. J. Heat Mass Trans.* 42, 993-1006.

## Publications

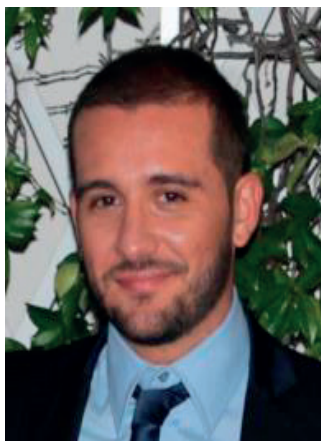
1. Vakili-Farahani F., Amalfi R.L., Thome J.R., **Two-Phase Heat Transfer and Pressure Drop within Plate Heat Exchangers**, Encyclopedia of Two-Phase Heat Transfer and Flow II, Vol. 2, Editors: Prof. J.R. Thome and J. Kim, World Scientific Publishing Company, Singapore, 2015.
2. Vakili-Farahani F., Amalfi R.L., Thome J.R., **Two-Phase Flow and Boiling of R245fa in a 1 mm Pressing Depth Plate Heat Exchanger-Part I: Adiabatic Pressure Drop**, Int. J. Interfacial Phenomena and Heat Transfer, Vol. 2, pp. 325-342, 2014.
3. Vakili-Farahani F., Amalfi R.L., Thome J.R., **Two-Phase Flow and Boiling of R245fa in a 1 mm Pressing Depth Plate Heat Exchanger-Part II: Flow Boiling Heat Transfer**, Int. J. Interfacial Phenomena and Heat Transfer, Vol. 2, pp. 343-361, 2014.
4. Amalfi R.L., Thome J.R., **Flow Boiling and Frictional Pressure Gradients in Plate Heat Exchangers: Part 1, Review and Experimental Database**, Int. J. of Refrigeration (accepted for publication), Vol. x, pp. xxx-xxx, 2015.
5. Amalfi R.L., Thome J.R., **Flow Boiling and Frictional Pressure Gradients in Plate Heat Exchangers: Part 2, Comparison of Literature Methods to Database and New Prediction Methods**, Int. J. Refrigeration (accepted for publication), Vol. x, pp. xxx-xxx, 2015.
6. Amalfi R.L., Thome J.R., **High Resolution Infrared Measurements of Single-Phase Flow of R245fa and R236fa within a Compact Plate Heat Exchanger**, Applied Thermal Engineering (accepted for publication), Vol. x, pp. xxx-xxx, 2015.
7. Amalfi R.L., Thome J.R., Solotych V., Kim J., **High Resolution Infrared Measurements of Two-phase Flow of R245fa within a Compact Plate Heat Exchanger**, Int. J. Heat and Mass Transfer (submitted), Vol. x, pp. xxx-xxx, 2015.
8. Solotych V., Lee D., Kim J., Amalfi R.L., Thome J.R., **Boiling Heat Transfer and Two-Phase Pressure Drops within Compact Plate Heat Exchangers: Experiments and**

- Flow Visualizations**, Int. J. Heat and Mass Transfer (accepted for publication), Vol. x, pp. xxx-xxx, 2015.
9. Amalfi R.L., **Two-Phase Heat Transfer and Pressure Drop within Plate Heat Exchangers**, École Polytechnique Fédérale de Lausanne (EPFL), HTRI, Texas, Lecture [https://www.htri.net/video.aspx?id=131561605&returnurl=encyclopedia-of-two-phase-heat-transfer-and-flow-ii.aspx&returnlocation=Volume2\\_Chapter4](https://www.htri.net/video.aspx?id=131561605&returnurl=encyclopedia-of-two-phase-heat-transfer-and-flow-ii.aspx&returnlocation=Volume2_Chapter4), 2014.
  10. D'Entremont B., Ong C.L., Amalfi R.L., **Boiling, Condensation and Pressure Drop for Plate Heat Exchangers**, Virtual International Research Institute of Two-Phase Flow and Heat Transfer, Interactive Tool, [http://2phaseflow.org/active:plate\\_heat\\_exchanger](http://2phaseflow.org/active:plate_heat_exchanger), 2015.
  11. Amalfi R.L., **Two-Phase Heat Transfer Mechanisms within Plate Heat Exchangers: Experiments and Modeling**, Thermal Science and Engineering Program Review, Santa Barbara, California (U.S.), Oral Presentation, June 10-11, 2015.

# Curriculum vitae

## Raffaele Luca AMALFI

---



<b>Date of birth</b>	August 19 <sup>th</sup> , 1986
<b>Birthplace</b>	Naples, Italy
<b>Civil State</b>	Single (without children)
<b>Position held</b>	Mechanical Engineer, Doctoral Assistant
<b>Personal address</b>	Av. Eglantine 24, CH-1006 Lausanne
<b>Office number</b>	Tel. +41 21 693 54 42
<b>Personal number</b>	Mob. +41 78 821 10 69
<b>Office E-mail</b>	luca.amalfi@epfl.ch
<b>Personal E-mail</b>	raffaelelucaamalfi@gmail.com
<b>Webpage</b>	<a href="http://ltdm.epfl.ch/page-87032-en.html">http://ltdm.epfl.ch/page-87032-en.html</a>

## Research activities and interests

---

Flow Boiling, Condensation and Pressure drops in Compact Plate and Fin Heat Exchangers  
On Chip-Cooling and Energy Recovery Systems (R&D)  
Heat Exchangers Thermal Design and Rating

## Education

---

- |               |   |
|---------------|---|
| 2012- Present | <b>Currently pursuing Ph.D. Degree in Energy</b><br>Fundamental research: Flow Boiling and Two-Phase Pressure Drop Mechanisms for Compact Plate Heat Exchangers<br>Applied research: Single-Phase, Flow Boiling and Condensation Heat Transfer in an Ultra-Compact Heat Exchanger<br>École Polytechnique Fédérale de Lausanne (EPFL), Switzerland<br>Supervision: Prof. John R. Thome |
| 2010 - 2011   | <b>Master in Energetics and Environmental Engineering</b><br>Federico II University, Naples, Italy<br>Final score: 110/110 summa cum laude  |
| 2006 - 2010   | <b>Bachelor in Mechanical Engineering</b><br>Federico II University, Naples, Italy  |

## Professional and research experience

---

- 2014 - Present    **Teaching Assistant**  
Heat and Mass Transfer (Bachelor), Two-Phase Heat Transfer (Master)  
École Polytechnique Fédérale de Lausanne (EPFL), Switzerland
- 2012 - 2013    **Teaching Assistant**  
Measurements Techniques (Bachelor), Heat and Mass Transfer (Bachelor)  
École Polytechnique Fédérale de Lausanne (EPFL), Switzerland
- 2012    **Internship (Master Thesis): Flow boiling of R236fa in a Novel Pin-Fin Heat Sink for Electronic Cooling Applications**  
IBM Zürich Research Laboratory, Ruschlikon, Switzerland  
Supervision: Prof. John R. Thome, Dr. Bruno Michel
- 2011    **Internship (Master Project): Flow boiling and Critical Heat Flux in a Horizontal Macrochannel**  
Laboratory of Refrigeration, Federico II University, Naples, Italy  
Supervision: Prof. Rita Maria Antonia Mastrullo
- 2010    **Internship (Bachelor Thesis): Efficiency Improvement of a Gas Turbine Plant on the Existing National Scenario**  
National Research Council (CNR), Naples, Italy  
Supervision: Prof. Renato Della Volpe

## Languages

---

- Italian**            Mother tongue
- English**            Fluent, *Trinity and EPFL Conference Skills Researchers Certificates*
- Portuguese**        Advanced
- Spanish**            Basic

## Informatics

---

- Programming**    C++, HTML, Matlab, Python
- Softwares**        Autocad, Catia, Fluent, Gambit, LabView, Microsoft Office, SolidWorks

## Additional training

---

- Sept. 8 - 13, 2014    **Micro/Nano Scale Heat Transfer and Fluid Flow**  
14<sup>th</sup> UIT Summer School, Siena, Italy
- Jun. 3 - 7, 2013    **Fundamentals of Microscale Heat Transfer**  
École Polytechnique Fédérale de Lausanne (EPFL), Switzerland

Mar. 25 - 26, 2013	<b>LabView Data Acquisition (DAQ)</b> École Polytechnique Fédérale de Lausanne (EPFL), Switzerland
Feb. 18 - 22, 2013	<b>LabView Core I and Core II</b> École Polytechnique Fédérale de Lausanne (EPFL), Switzerland
Feb. 4 - 8, 2013	<b>C++, A Comprehensive Hands-On</b> École Polytechnique Fédérale de Lausanne (EPFL), Switzerland
Apr. 6 - May 25, 2009	<b>3D Design, Modeling and Accessories</b> Osnap, Autodesk, Inc., Naples, Italy
Dec. 1 - Jan. 14, 2009	<b>Advanced Autocad and 2D Design</b> Osnap, Autodesk, Inc., Naples, Italy

## Awards

---

2010	<b>Scholarship “FEDERICO II AS”,</b> Naples, Italy
2011	<b>Scholarship “FEDERICO II AS”,</b> Naples, Italy
	<b>Master “Catia Designer”,</b> Alta Formazione Regione Campania, Naples, Italy
	<b>Internship (Master Thesis),</b> Centre Thermique de Lyon (CETHIL), France

## Additional information

---

<b>Driving license</b>	Category B license obtained on February 2005
<b>Interests</b>	Swimming, Football, Running, Table Tennis, Technology, Music

